A Musculoskeletal Model of the Human Hand to Improve Human-Device Interaction

by

Jong Hwa Lee

A Dissertation Presented in Partial Fulfillment
of the Requirements for the Degree
Doctor of Philosophy

Approved July 2014 by the
Graduate Supervisory Committee:

Devin Jindrich, Co-chair
Panagiotis Artemiadis, Co-chair
Patrick Phelan
Veronica Santos
Huei-Ping Huang

ARIZONA STATE UNIVERSITY

August 2014

ABSTRACT

Multi-touch tablets and smart phones are now widely used in both workplace and consumer settings. Interacting with these devices requires hand and arm movements that are potentially complex and poorly understood. Experimental studies have revealed differences in performance that could potentially be associated with injury risk. However, underlying causes for performance differences are often difficult to identify. For example, many patterns of muscle activity can potentially result in similar behavioral output. Muscle activity is one factor contributing to forces in tissues that could contribute to injury. However, experimental measurements of muscle activity and force for humans are extremely challenging. Models of the musculoskeletal system can be used to make specific estimates of neuromuscular coordination and musculoskeletal forces. However, existing models cannot easily be used to describe complex, multi-finger gestures such as those used for multi-touch human computer interaction (HCI) tasks. We therefore seek to develop a dynamic musculoskeletal simulation capable of estimating internal musculoskeletal loading during multi-touch tasks involving multi digits of the hand, and use the simulation to better understand complex multi-touch and gestural movements, and potentially guide the design of technologies the reduce injury risk. To accomplish these, we focused on three specific tasks. First, we aimed at determining the optimal index finger muscle attachment points within the context of the established, validated OpenSim arm model using measured moment arm data taken from the literature. Second, we aimed at deriving moment arm values from experimentally-measured muscle attachments and using these values to determine muscle-tendon paths for both extrinsic and intrinsic muscles of middle, ring and little fingers. Finally, we aimed at

exploring differences in hand muscle activation patterns during zooming and rotating tasks on the tablet computer in twelve subjects. Towards this end, our musculoskeletal hand model will help better address the neuromuscular coordination, safe gesture performance and internal loadings for multi-touch applications.

DEDICATION

I dedicate my dissertation work to my loving family, especially …

To wife, Hyung Jung Lim for opening my eyes to the real world;

To sons, Aiden J. and Jayden J. Lee for developing a sense of responsibility as a head of household;

To parents, Sung Kee and Byung Sook Lee for encouraging and pushing for tenacity ring in my ears;

To wife's parents, Jung Chul Lim and Byung Soon Min for instilling the importance of hard work and higher education;

To Jong Sang, Jong Sook and Jong Hyun Lee for encouragement;

ACKNOWLEDGMENTS

I would like to give my thanks to Professor Devin Jindrich, my advisor for his support and guidance during this work. I would like to also thank Dr. Panagiotis Artemiadis, Dr. Patrick Phelan, Dr. Veronica Santos and Dr. Huei-Ping Huang for their input and guidance as my committee members. I would like to acknowledge and thank Dr. Jack Dennerlein, Professor in Department of Physical Therapy at Northeastern University and Dr. Deanna Asakawa, Post-doctoral research fellow at California State University at San Marcos for reading and advice on my research papers. I also acknowledge the support by the National Science Foundation (NSF 0964220), Directorate for Computer & Information Science & Engineering (CISE), Human-Centered Computing (HCC).

TABLE OF CONTENTS

Page

LIST OF TABLES vii

LIST OF FIGURES viii

CHAPTER

1 INTRODUCTION 1

Research Strategy 5

2 EXTRINSIC AND INTRINSIC INDEX FINGER MUSCLE ATTACHMENTS IN AN OPENSIM UPPER-EXTREMITY MODEL 10

Abstract 10

Introduction 11

Materials and Methods 14

Results 20

Discussion 23

3 AN OBJECTIVE PROCEDURE CAN ESTIMATE ATTACHMENT LOCATIONS FOR HAND MUSCLES IN AN OPENSIM UPPER-EXTREMITY MODEL 39

Abstract 39

Introduction 41

Materials and Methods 45

Results 51

Discussion 55

4 ANALYSIS OF MUSCULOSKELETAL LOADING IN AN INDEX FINGER DURING TWO FINGER GESTURES ON A TABLET COMPUTER 81

Abstract 81

CHAPTER Page

Introduction 82

Materials and Methods 86

Results 90

Discussion 92

REFERENCES..... 97

LIST OF TABLES

Table		Page
2.1	Anthropometric Finger Dimension of Cadaveric Specimens	27
2.2	Moment Arms of Muscle Paths Discovered Through Optimization	28
2.3	Muscle-tendon Locations in the Index Finger	29
3.1	Mean Moment Arms of the Index Finger	59
3.2	Mean Moment Arms of the Middle Finger	60
3.3	Mean Moment Arms of the Ring Finger	61
3.4	Mean Moment Arms of the Little Finger	62
3.5	Anthropometic Index Finger Dimensions of Cadaveric Specimens	63
3.6	Index Finger Muscle-tendon Locations Experessed in OpenSim Frame	64
3.7	Middle Finger Muscle-tendon Locations	65
3.8	Ring Finger Muscle-tendon Locations	66
3.9	Little Finger Muscle-tendon Locations	67
4.1	Muscle Modeling Parameters	103
4.2	Joint Torque at All Joint (N-m)	104

LIST OF FIGURES

Figure		Page
2.1	All Muscle Attachment Points at the MCP, PIP and DIP Joint	31
2.2	Musculoskeletal Hand Model	32
2.3	Moment Arms for Smoothest Muscle Paths	33
3.1	Measured and Derived Moment Arms with Flex/Extension at the MCP Joint	68
3.2	Moment Arms with Flex/Extension at the MCP Joint of the All Fingers	69
3.3	Moment Arms with Add/Abduction at the MCP Joint of the All Fingers	70
3.4	Moment Arms with Flex/Extension at the PIP and DIP Joints	71
3.5	Index Finger Moment Arm Values	72
3.6	Middle Finger Moment Arm Values	73
3.7	Ring Finger Moment Arm Values	74
3.8	Little Finger Moment Arm values	75
4.1	Extrinsic Muscle Activation	105
4.2	Muscle Activity of Rotate Left and Right	106
4.3	Muscle Activation of an Index Finger during Zoom In and Zoom Out	107
4.4	Muscle Activation of an Index Finger during Rotate Left and Rotate Right	108
4.5	Joint Angle of an Index Finger during Zoom In and Zoom Out	109
4.6	Joint Angle of an Index Finger during Rotate Left and Rotate Right	110
4.7	Joint Torque of an Index Finger during Zoom In and Zoom Out	111
4.8	Joint Torque of an Index Finger during Rotate Left and Rotate Right	112
4.9	Extrinsic Muscle Force of an Index Finger during Zoom In and Out	113
4.10	Extrinsic Muscle Force of an Index Finger during Rotate Left and Right	114

CHAPTER 1

INTRODUCTION

Multi-touch tablets and smart phones are now widely used in both workplace and consumer settings. Interacting with these devices requires hand and arm movements that are potentially complex and poorly understood (Cohe and Hachet, 2012; Trudeau et al., 2013; Wagner et al., 2012; Young et al., 2013). Experimental studies have revealed differences in performance that could potentially be associated with injury risk (Lozano et al., 2011; Trudeau et al., 2013). However, underlying causes for performance differences are often difficult to identify. For example, many patterns of muscle activity can potentially result in similar behavioral output (Valero-Cuevas et al., 1998). Muscle activity is one factor contributing to forces in tissues that could contribute to injury (Norman et al., 1998). However, experimental measurements of muscle activity and force for humans are extremely challenging (Dennerlein et al., 1998, 1999).

Models of the musculoskeletal system can be used to make specific estimates of neuromuscular coordination and musculoskeletal forces. Models of the hand have helped to quantify finger mechanics and motor control in several contexts (Armstrong and Chaffin, 1978; Harding et al., 1993; Dennerlein et al., 1998; Valero-Cuevas et al., 1998). Consequently, musculoskeletal model of the hand could represent an effective tool for understanding hand and arm dynamics and control during multi-touch tasks, and contribute to interface designs that reduce the risks of injuries associated with long-term, repetitive movements.

Existing models of the hand have focused on specific fingers (typically the index finger), and have been developed using custom or proprietary software platforms (Wu et al., 2009, 2010). Therefore, existing models cannot easily be used to describe complex, multi-finger

gestures such as those used for multi-touch human computer interaction (HCI) tasks. **Consequently, we seek to develop a dynamic musculoskeletal simulation capable of estimating internal musculoskeletal loading during multi-touch tasks involving many fingers, and use the simulation to better understand complex multi-touch and gestural movements, and potentially guide the design of technologies that reduce injury risk.**

I propose to create a multi-finger hand and arm model using the OpenSim platform (Delp et al., 2007; Holzbaur et al., 2005), and to use the model to predict movements that are likely to be preferred, high-performance, and minimize injury risk. The long term goal of this research is the development of a modeling framework that allows for predictions of musculoskeletal loading associated with multi-touch gestures. The specific goal addressed in this dissertation is model development and validation. I hypothesized that the Simulated Annealing (Kirkpatrick et al., 1983) and Hooke-Jeeves (Kelley, 1999) methods could produce a set of muscle attachment points for extrinsic/intrinsic finger tendons and muscles within the context of the established, validated OpenSim arm model that results in moment arms that match experimentally-measured relationships (An et al., 1979, 1983; Armstrong and Chaffin, 1978; Chao et al., 1989; Fowler et al., 2001; Greiner, 1991; Li et al., 2008). I also hypothesized that a "partial velocity" method (Delp and Loan, 1995; Kane and Levinson, 1985) could generate continuous and realistic moment arms arising from muscle attachment points reported by An et al. (1979, 1983) and could be suitable for use as reference moment arm values for middle, ring and little fingers in an OpenSim model. I last hypothesized that extrinsic muscle activations for zooming tasks would be higher than intrinsic muscle activations for them, while

intrinsic muscle activations for rotating tasks would be higher than extrinsic muscle activations for them.

Towards this end, I propose to accomplish the following specific aims:

1. **Determine the optimal index finger muscle attachment points within the context of the established, validated OpenSim arm model using measured moment arm data taken from the literature.**

   I used Simulated Annealing (Kirkpatrick et al., 1983) and Hooke-Jeeves (Kelley, 1999) to determine the muscle paths, a series of attachments that result in the best match of modeled muscle moment arms to experimentally-measured values (An et al., 1979, 1983; Armstrong and Chaffin, 1978; Chao et al., 1989) in the index finger.

2. **Calculate moment arm values for the middle, ring and little fingers using the partial velocity method (Delp and Loan, 1995; Kane and Levinson, 1985), and use these values to determine muscle-tendon paths of attachment points for both extrinsic and intrinsic muscles.**

   I used the partial velocity method to calculate moment arm curves from anatomically-measured muscle origins and insertions that matched experimentally-measured moment arms, and used objective techniques to identify muscle attachments that resulted in accurate muscle function.

3. **Estimate hand muscle activity during two finger gestures: zoom in & out and rotate left & right on a tablet computer.**

I tested the hypothesis that intrinsic muscle activity for rotate left and right gestures would be higher than extrinsic muscle activity because extrinsic muscles control crude movements while intrinsic muscles are responsible for the fine motor functions of the hand.

RESEARCH STRATEGY

1. SIGNIFICANCE

The design of computer interfaces is one factor associated with work-related musculoskeletal disorders (MSDs) (Bergqvist et al., 1995; Kumar, 2001; Malchaire et al., 1996). However, the emergence of devices using multi-touch or gestural interfaces could fundamentally change the movements required for use. The impact of these new interfaces on risks for MSDs is unclear. Little information about the biomechanics or motor control of multi-touch or gestural device use is available, and devices are typically designed without considering the effect of interaction on the musculoskeletal system (Marcus et al., 2002; Rempel et al., 1999; Sauter et al., 1991).

Models of the musculoskeletal system can contribute to the study of neuromuscular coordination, motor performance, and be used to estimate musculoskeletal loads. Hand models have provided a basis for quantifying finger mechanics and motor control in diverse situations (Armstrong and Chaffin, 1978; Valero-Cuevas, 1998; Balakrishnan et al., 2006; Harding et al., 1993; Leijnse, 1995). While analytical musculoskeletal models are often limited to static or quasi-static analysis, computer simulations can facilitate the understanding of complex musculoskeletal systems (Zajac, 2002). However, the use of unshared or proprietary software platforms has limited the impact of musculoskeletal models. For this reason, freely-accessible models have been developed. For example, OpenSim is open-source software that allows users to study the effects of musculoskeletal geometry, joint kinematics, and muscle-tendon properties on the forces and joint moments that the muscles can produce (Delp et al, 2007). A musculoskeletal model in OpenSim consists of rigid body segments connected by joints. Muscles span these joints and generate forces and movement. The OpenSim arm model has skeletal

elements for the arm, wrist, and hand. Currently, the musculature of the shoulder, elbow, wrist, and the extrinsic finger muscles have been accurately implemented (Holzbaur et al., 2005, 2007; Saul et al., 2003). However, the intrinsic muscles of the hand, finger ligaments, and finger extensor mechanisms have not been modeled on the OpenSim platform. Implementation of intrinsic hand muscles, coupled with the shoulder and elbow model, would result in a highly detailed and powerful model of the entire upper-extremity, which would provide unprecedented opportunities for research not only in the domain of multi-touch systems, but also create a broader impact in furthering basic scientific research on musculoskeletal systems.

The discoveries resulting from the proposed study provide significant insights into how the musculoskeletal system of the human upper extremity produces multi-touch gestures.

A highly accurate musculoskeletal model of the hand could be dedicated to improve the existing biomechanical models of the hand and extend their functionality in ergonomics. In biomechanics, we could gain a deeper understanding of the causes and effects of many hand pathologies, could develop to help in medical planning and surgery for tendon transfers and could study the nervous stimulation required to restore the grasping ability for muscular dysfunction patients. In Ergonomics, the hand model could be used to simulate postures adopted while grasping hand-held devices with different postures such as the size and shape of them according to the anthropometry of the different people that have to interact.

2. INNOVATION

Experiments outlined in this study employ a novel approach to developing a new human hand model that generates gestural movements, muscle activity and motor performance to multi-touch device interactions.

Conceptual Approach. A major barrier to the study of musculoskeletal model of the hand is about how to determine muscle attachment points; many combinations of origins and insertions, or paths, could result in the same moment arm. I suggest a new approach to finding optimal muscle-tendon paths via data-driven optimization (Simulated Annealing and Hooke-Jeeves methods). Another challenge to the development of accurate hand model is regarding to reproduce moment arm values for middle, ring and little fingers. To date, no values of them have been reported yet. I seek to estimate these moment arms via the partial velocity method.

Application Domain. My approach is innovative because of the specific movements studied. Very little is known about the biomechanics and control of multi-touch gestures, and my experimental and modeling efforts not only answer specific questions about motor performance during multi-touch device use, but provide a foundation for future experimental and modeling studies.

3. APPROACH

AIM 1 – Determine a set of muscle attachment points for the tendons and intrinsic muscles of the index finger.

This Aim involves testing the working hypothesis that the Simulated Annealing (Kirkpatrick et al., 1983) and Hooke-Jeeves (Kelley, 1999) methods could determine a set of muscle attachment points for extrinsic and intrinsic index finger muscles within the context of the established, validated OpenSim arm model that results in moment arms that match experimentally-

measured relationships (An et al., 1979, 1983; Armstrong and Chaffin, 1978; Chao et al., 1989; Fowler et al., 2001; Greiner, 1991; Li et al., 2008). Successful matching was considered to be moment arms within one standard deviation of experimental measurements.

Aim 1: Hypotheses

I hypothesize that data-driven optimization method could find reasonable attachment sites for extrinsic tendons and intrinsic muscles, and predicted moment arms could be non-linear with change of joint angle.

- *Hypothesis 1.1* A Simulated Annealing algorithm could reasonably reproduce the optimized muscle-tendon paths on the index finger
- *Hypothesis 1.2* Moment arms at all joints were not constants but nonlinear as functions of joint movements

AIM 2 – Reproduce realistic finger moment arms calculated by partial velocity approach derived from anatomical attachments reported by experiments (An et al., 1979 and 1983), and determine muscle-tendon pathways for middle, ring and little fingers on the OpenSim platform.

This Aim involves testing the working hypothesis that the partial velocity method (Delp and Loan, 1995; Kane and Levinson, 1985) could generate reasonable moment arms values for middle, ring and little fingers, and these values could be used to calculate muscle attachment points for the OpenSim hand and arm model.

Aim 2: Hypotheses

I hypothesize that the partial velocity method (Delp and Loan, 1995; Kane and Levinson, 1985) could reproduce moment arms for middle, ring and little fingers, and these estimated moment

arms could be used to reference values in an optimization method that is the process of improving OpenSim model fits to experimental data via root mean square error.

- *Hypothesis 2.1* Index finger moment arms by partial velocity estimation from experimental attachment points could be similar in shape and slope to its moment arms by direct measurements on hand specimens. The partial velocity method derived from anatomical measurements (An et al., 1979, 1983) could generate moment arm values for the middle, ring and little fingers.
- *Hypothesis 2.2* A Simulated Annealing algorithm (Kirkpatrick et al., 1983) could reproduce the optimized muscle-tendon paths of the middle, ring and little fingers for the OpenSim model.

AIM 3 – Compare muscle activity during thumb and index finger gestures on a tablet.

This Aim is to quantify the differences in the joint torque, muscle forces and muscle activity using the OpenSim platform while twelve subjects performe two finger gestures: zoom in & out and rotate left & right on the tablet computer.

Aim 3: Hypotheses

I hypothesize that extrinsic muscle muscles involve more flexion/extension motion while intrinsic muscles could contribute more abduction/adduction movement.

- *Hypothesis 3.1* Extrinsic muscle activations for zoom in & out gestures could be higher than those for rotate left & right gestures.
- *Hypothesis 3.2* Intrinsic muscle activations could be higher than extrinsic muscle activations for rotate left & right gestures.

CHAPTER 2

EXTRINSIC AND INTRINSIC INDEX FINGER MUSCLE ATTACHMENTS IN AN OPENSIM UPPER-EXTREMITY MODEL

ABSTRACT

Musculoskeletal models allow estimation of muscle function during complex tasks. We used objective methods to determine attachment locations for index finger muscles in an OpenSim upper-extremity model. Data-driven optimization algorithms, Simulated Annealing and Hook-Jeeves, estimated tendon locations crossing the metacarpophalangeal (MCP), proximal interphalangeal (PIP) and distal interphalangeal (DIP) joints by minimizing the difference between model-estimated and experimentally-measured moment arms. Estimated tendon attachments resulted in variance accounted for (VAF) between calculated moment arms and measured values of 77.6% for flex/extension and 81.0% for ab/adduction at the MCP joint. VAF averaged 73.3% at the PIP joint and 53.5% at the DIP joint. VAF values at PIP and DIP joints partially reflected the constant moment arms reported for muscles about these joints. However, all moment arm values found through optimization were non-linear and non-constant. Moment arm relationships were best described with quadratic equations for all tendons at PIP and DIP joints. Sensitivity analysis revealed that multiple sets of muscle attachments with similar optimized moment arms are possible. The presence of several functionally similar solutions is consistent with the anatomical variability observed in human hands, but requires additional assumptions or data to select a single set of values when constructing anatomically-based musculoskeletal models.

INTRODUCTION

Multi-touch Human Computer Interfaces (HCIs), such as the touchscreens of many handheld devices, often involve complex multi-finger gestures or gesture sequences (Rekimoto, 2002; Rubine, 1991; Wu et al., 2003). Although the forces involved in making individual gestures may be low, long-term and repetitive interactions with touchscreen computing devices present the potential for injury (Sjoggard et al., 1998). However, the biomechanics of coordinated finger movements for touchscreen interaction are not well understood. Consequently, better understanding of finger dynamics, joint forces, and control during multi-touch tasks could lead to interface designs that reduce injury risks associated with repetitive finger movements.

External hand and finger loadings do not directly correspond to internal musculoskeletal loading, which can be difficult to determine (Radwin et al., 1999). However, anatomically-based musculoskeletal models can predict musculoskeletal loading and can help design strategies to reduce injury and improve motor function (Delp et al., 1995; Fregly et al., 2012; Lloyd and Besier, 2003; McKay and Ting, 2012; Seth et al., 2011). Anatomical studies of the elbow and shoulder enabled development of detailed arm musculoskeletal models (Ettema et al, 1998; Gerbeaux et al., 1996; Pigeon et al., 1996). Arm models can estimate torques at the shoulder and elbow, e.g. for development and user training of neural prosthesis systems (Chadwick et al., 2009; Gatti et al., 2009; Holzbaur et al., 2005; Soechting et al., 1997). Hand models have also been useful for understanding many aspects of function such as finger tapping on computer keyboards (Armstrong and Chaffin, 1978; An et al., 1979; Zajac and Gottlieb, 1989; Sancho-Bru et al., 2001; Roloff et al., 2006; Lee et al., 2009, Qin et al., 2010, 2011). Although hand models have been helpful in specific contexts, existing dynamic models of the hand often focus on

specific fingers and have not been used to understand complex, multi-finger gestures such as those used during multi-touch HCI tasks.

We therefore seek to develop a dynamic musculoskeletal model capable of estimating internal loadings during multi-touch tasks. Because multi-touch and gestural movements involve not only the fingers, but also the entire kinematic chain of the hand and arm, we chose to build upon an existing arm model available on an open access platform OpenSim (2.3.2, Simbios, Stanford, CA; Delp et al, 2007; Seth et al., 2011). The model incorporates information for muscles at the shoulder and elbow, but it does not yet model intrinsic finger muscles. OpenSim is a homeomorphic model: parameters and values correspond directly to anatomical structure and function. Therefore, appropriate muscle attachment sites within the anatomy of the OpenSim model must be determined. Detailed measurements of muscle attachments have been made for the hand (Landsmeer et al., 1961; An et al., 1979). However, muscle attachment locations are specific to the anatomical model within which they are expressed, and cannot be directly transformed to a different model such as OpenSim. For example, the model of An et al. (1979) is normalized only to the middle phalanx in a 2 dimensional (2D) sagittal plane, and scaling its attachment locations in a 3D Cartesian space (c.f. Li et al., 2008; Greiner, 1991) does not result in continuous moment arms that match experimentally-measured values (Kociolek and Kier, 2011). This poor correspondence could result from a lack of important information such as joint thickness, position and orientation of rotational axes, skeletal structure, and changes associated with transforming from 2 to 3 dimensions among other factors.

To create the most functionally useful model possible, we chose to use moment arm data for the index finger measured in vivo (Oh et al., 2007; Yoshii et al., 2009; Lopes et al., 2011) and in situ (Armstrong and Chaffin, 1978; An et al., 1983; Chao et al., 1989; Brand and

Hollister, 1993; Franko et al., 2011). However, measurements of moment arms alone cannot be directly used to develop homeomorphic models because moment arms are indeterminate: many combinations of origins and insertions, or paths could result in the same moment arm. The purpose of this study was therefore to determine a set of muscle attachment points for the tendons and intrinsic muscles of the index finger. We focused on the question: can data-driven optimization find reasonable attachment sites for extrinsic tendons and intrinsic muscles? We hypothesized that Simulated Annealing (Kirkpatrick et al., 1983) could find muscle attachment points for extrinsic and intrinsic finger tendons and muscles, resulting in moment arms that match experimentally measured relationships (An et al., 1979, 1983; Armstrong and Chaffin, 1978; Chao et al., 1989; Fowler et al., 2001; Greiner, 1991; Li et al., 2008). Successful matching was considered to be moment arms within one standard deviation (SD) of experimental measurements (An et al., 1983; Max. SD = 2.5 mm).

MATERIALS AND METHODS

We used the Holzbaur et al. (2005) upper extremity model on the OpenSim platform (2.3.2, Simbios, Stanford, CA; Delp et al, 2007; Seth et al., 2011). This model includes 15 degrees of freedom representing the shoulder, elbow, forearm, wrist, thumb, and index finger with 50 muscle compartments crossing these joints. Metacarpal and phalanx geometry and approximated positions and orientations of finger joint axes are scaled to a 50th percentile male, and axes of rotation were determined by fitting long axes of cylinders to the articular surfaces of the metacarpal and phalangeal bones (Holzbaur et al., 2005).

Musculoskeletal Model

We sought to add the following muscles or muscle groups to the index finger of OpenSim model: *terminal extensor (TE), extensor slip (ES), radial band (RB), ulnar band (UB), first dorsal interosseous or radial interosseous (RI), lumbricals (LU), first palmar interosseous or ulnar interosseous (UI), flexor digitorum profundus (FDP), flexor digitorum superficialis (FDS) and extensor digitorum communis (EDC)*. The index finger was modeled to have four degrees of freedom: ab/adduction and flex/extension at the MCP joint, and flex/extension at PIP and DIP joints. Based on experiment measurements available for comparison, we considered the following range of motion (RoM) at the MCP joint: 0° to 90° (flexion: +) as well as 0° to 30° (abduction:+). Similarly, for PIP and DIP joints we considered 0° to 90° (flexion: +) and 50° (flexion: +) respectively (An et al., 1983; Chao et al., 1989). Because specific data on muscle wrapping are not available, the wrap object set was removed from the DIP, PIP and MCP joints in the OpenSim model (Garner and Pandy, 2000).

Moment Arms

Experimentally-measured values were used as reference moment arm relationships (An et al., 1979, 1983; Armstrong and Chaffin, 1978; Chao et al., 1989). For the MCP joint, we extracted data from published relationships (An et al., 1983; Chao et al., 1989) using the GRABIT function (Matlab 2010b, Mathworks, Natick, MA), and recreated moment arm curves using Polynomial Curve Fitting function (*polyfit*; 5^{th} degree polynomial) in Matlab. For PIP and DIP joints, moment arm curves have not been reported. Therefore, constant moment arms (averaged through the RoM of 0° to 90° and 50°) were used (An et al., 1983).

To normalize for differences among data sets and reproduce finger skin surface from the bony segments in the OpenSim model, we assumed all linear dimensions scaled isometrically, as found for the ratio among the length of phalanx, the width and thickness of each joint (Fowler et al., 2001; Greiner, 1991; Li et al., 2008). We scaled measured anthropometric data to OpenSim model dimensions to describe muscle-tendon paths within the OpenSim model (Table 1), then normalized moment arms to the length of the middle phalanx (An et al., 1979).

Muscle Attachment Determination

A computational optimization method was used to determine muscle paths of moment arms matching experimentally-measured relationships. The objective function, $\mathrm{f}(\vec{\mathrm{x}})$ was defined as the root mean square (RMS) error between the experimentally-derived moment arms, $\mathrm{r_j}(\vec{\mathrm{q}}_\mathrm{i})$ and the modeled-estimate moment arms, $\hat{\mathrm{r}}_\mathrm{j}(\vec{\mathrm{q}}_\mathrm{i},\vec{\mathrm{x}})$ as follows:

$$\text{Minimize} \qquad f(\vec{x}) = \sqrt{\sum_{i=1}^{m} \frac{\left[r_j(\vec{q}_i) - \hat{r}_j(\vec{q}_i,\vec{x})\right]^2}{m}}$$

$$\text{Subject to} \qquad lb_j \le x_j \le ub_j$$

$$g_j(\vec{x}) - \varepsilon_j \leq 0$$

Where, j was each individual muscle ($j = 10$), and $\vec{x}$ was 6×1 vector (described as x, y, z origin points on the proximal side and x, y, z insertion points on the distal side) to be optimized. $\vec{q}_i$ was the joint angle with a resolution (i) of 100 increments (m) covering RoM of measured values (An et al.,1983): the 0°~90° (flexion) and 0°~30° (abduction), 0°~90° (flexion), and 0°~50° (flexion) for the MCP, PIP and DIP joints, respectively. Boundary conditions ($lb_j \leq x_j \leq ub_j$) constrained the path of muscle from violating the feasible region, expanded from bony segment (as a lower bound: lb_j, Holzbaur et al., 2005) to finger skin surface (as an upper bound: ub_j, Fowler et al., 2001; Greiner, 1991; Li et al., 2008).

Attachment points must result in moment arms appropriate for both flex/extension and ab/adduction. However, measurements for flex/extension and ab/adduction did not have equal reliability, reflected in different reported standard deviations that could reflect either measurement uncertainty or anatomical variability (An et al., 1979, 1983; Armstrong and Chaffin, 1998; Chao et al., 1989). Moreover, ab/adduction moment arm values depend on finger postures, i.e. flexion of MCP, PIP and DIP joints (Kamper et al., 2006). The specific postures used for measured ab/adduction moment arm values were not reported, contributing to uncertainty. Therefore, we did not consider both flex/extension and ab/adduction moment arm values as a same weight in the objective function. We did not have a criterion for assigning specific differential weightings for flex/extension and ab/adduction, so we used an inequality constraint $(g_j(x), \varepsilon_j)$ to weight flex/extension and ab/adduction for the objective function. The inequality constraint resulted in punishment if the RMS error of ab/adduction moment arm during flex/extension ($g_j(\vec{x})$) exceeded the bounds of the maximum standard deviation of experimental moment arms ε_j. Specifically, min. $f(\vec{x}) = \text{RMS error} + P(\vec{x})$. $P(\vec{x}) = 0$ if $g_j(\vec{x}) \leq \varepsilon_j$

and $P(\vec{x}) = \varepsilon_j \emptyset$ if $g_j(\vec{x}) > \varepsilon_{j,}$ where $\emptyset = 1000$. ε_j was 2.5 mm for extrinsic tendons and 1.7 mm for intrinsic muscles (An et al., 1983). Because extrinsic muscle ab/adduction moment arms had higher uncertainty than for intrinsic muscles, attachment points were less influenced by the ab/adduction moment arms for extrinsic muscles than for intrinsic muscles.

PIP and DIP joints are modeled to move only in flex/extension. Therefore, the inequality constraint for PIP and DIP joints favored attachments that optimized moment arms while maintaining tendon excursions within measured variance. ε_j was therefore set to the measured standard deviation (0.72~3.97 mm) of tendon excursions (An et al., 1983; Armstrong and Chaffin, 1978; Chao et al., 1989).

The objective function for each individual muscle (j) was computed for each set of parameters, then iterated by updating muscle attachment locations until an optimal set was found. We used a Simulated Annealing algorithm (Kirkpatrick et al., 1983) and Hooke-Jeeves algorithm (Kelley, 1999) for muscle path optimization because the former is suitable for discrete optimization in a global search space, and the latter is appropriate for smooth, unconstrained non-linear optimization without gradients. The Simulated Annealing algorithm used a cooling schedule with initial temperature of 1, and iterated until the average change in value of the objective function was less than 0.0001 and the maximum time limit was infinite. The maximum number of evaluations of the objective function was 18,000 (3,000 × 6 variables).

Sensitivity Analysis

Optimizations in complex search spaces can be influenced by initial parameter selection (Ackland et al., 2012; Valero-Cuevas et al., 2003). Therefore, to test the robustness of the finger model response ($\vec{x}_j$) to input ($\vec{x}_0$), we performed sensitivity analysis for all attachments

($\vec{x}_j$) by selecting starting points ($\vec{x}_0$) from 26 sets of random muscle attachments including the Holzbaur et al. (2005) OpenSim model attachments and An et al. (1979) tendon locations. Because the middle phalanx is ~25 mm (An et al., 1983), 26 increments can cover the length of the middle phalanx at 1 mm resolution. Consequently, 78,000 simulations (26 trials $\times$ 3,000 objective function evolutions) were performed for each muscle at each joint on a 3.00-GHz Intel Core2 Due with 3.25 GB of RAM.

The sensitivity analyses showed that minimizing RMS error alone resulted in multiple possible muscle paths, some of which involved sharp changes to tendon direction (Figure 2). The potential for multiple muscle attachments and paths necessitated the selection of a single set of attachment points. We therefore assumed that the most smooth muscle path was the most anatomically reasonable. We calculated curvature from three successive attachments, i.e., origin, via and insertion points and identified the attachment set with the largest curvature at each joint. We selected the path with the largest curvature for analysis and presentation.

Consequently, our procedure accomplished two objectives. The most important objective was to discover muscle attachment points that resulted in moment arms that matched experimentally-measured values in both flex/extension and ab/adduction. From the set of optimized attachment points, a single set of points was selected to satisfy the secondary objective of path smoothness. This two-step procedure ensured that the primary, functional objective of discovering the most experimentally-reasonable moment arms was not overly-influenced by the assumption that smooth muscle paths were most anatomically reasonable.

Polynomial Fitting

Finally, we determined the order and parameters of polynomial fits that could be used as simplified descriptions of calculated moment arms. We used a polynomial fitting function to regress the coefficients of a polynomial of degree n that had the fit to simulated moment arms. We tested polynomials of less than fourth degree because polynomials of order greater than four can overfit to the data and even perform worse than polynomial regressions of lower orders (Kurse et al., 2012; Murray et al., 1995).

Optimizations and data analysis were implemented in Matlab using the OpenSim Application Programming Interface (API; OpenSim 2.0 Doxygen), to compute muscle moment arms. They were performed on a 3.00-GHz Intel Core2 Due with 3.25GB of RAM.

RESULTS

Optimization Found Multiple Sets of Muscle Attachments

The optimization procedure found multiple muscle attachments (Figure 1). For some muscles, attachment points were constrained to a narrow region. For example, the standard deviation for FDS at the MCP joint was 0.6 mm (Figure 1). For other muscles, attachment points could be located in a broad region. For example, the ES at the PIP joint had a standard deviation of 1.71 mm. Still other muscles exhibited distinct alternative attachment regions. For example, RI at the MCP joint showed two alternative attachment regions, resulting in a bimodal distribution and large standard deviation of 9.03 mm. Although multiple sets of muscle attachments were possible, the different muscle attachments resulted in consistent moment arm curves. Compared to each other, the average VAF among optimized curves was of 93.7% across all attachment sets and muscles.

Optimized Moment Arms Matched Experimentally-Measured Values

The smoothest muscle paths chosen to represent the most anatomically-reasonable set of muscle attachments had moment arms that matched experimental measurements and were representative of the set of optimized moment arms (Table 2; Figure 3 A, B). At the MCP joint, all modeled moment arms, including those from the smoothest path, lay within one standard deviation of experimental measurements (max. RMS = 2.4 mm < max. experimental SD = 2.5 mm; An et al., 1983). For both flex/extension and ab/adduction motions, VAF between experimentally-measured values and smoothest-path modeled moment arms averaged 77.6% (flex/extension) and 81.0% (ab/adduction), and ranged from 48.1% to 99.5%. For most

muscles, the smoothest-path moment arms were within one standard deviation of the average calculated moment arms (Figure 3). For the EDC muscle in flex/extension, the smoothest-path moment arm differed from the average (VAF = 48.1%) but was closer to the experimentally-measured moment arm (RMS error = 0.7 mm < experiment SD = 1.6 mm).

At the PIP and DIP joints, only average moment arms have been reported. VAF between calculated and reported moment arms averaged 73.3% and 53.5% for PIP and DIP joints. Modeled moment arms from the smoothest path were located within one standard deviation of measured values (max. RMS = 0.78 mm < max. experimental SD = 2.2 mm; Figure 3).

Calculated Moment Arms at the PIP and DIP Joints Were Not Constant

Although experimental moment arms for the PIP and DIP joints were considered to be near constants (An et al., 1983), optimization did not discover constant moment arms for any muscle at the PIP and DIP joints. For example, at the PIP joint, experimentally-measured moment arms of extrinsic tendons were reported as: $\mathrm{r_{fdp}} = 7.9$, $\mathrm{r_{fds}} = 6.2$ and $\mathrm{r_{es}} = -2.8$ mm (An et al., 1983).

Calculated moment arms were non-constant and non-linear functions dependent on joint angle ($0 \leq q \leq 2.09$ rad.; Figure 3). VAF of constants fitted to calculated moment arms averaged 83.2% whereas fitting calculated moment arms with a linear function resulted in average VAF of 93.1%, quadratic of 98.6% and cubic of 99.9%. Because quadratic fits were substantially (5.5%) better than linear fits, but had only 1.3% less VAF than cubic function, we considered quadratic functions to be the lowest-degree functions that adequately fit the moment arms. Quadratic functions for the PIP were: $\mathrm{r_{fdp}} = -3.01\mathrm{q}^2 + 5.82\mathrm{q} + 5.84$, $\mathrm{r_{fds}} = -3.26\mathrm{q}^2 + 5.29\mathrm{q} + 4.75$ and $\mathrm{r_{es}} = 0.66\mathrm{q}^2 - 0.52\mathrm{q} - 3.88$. Similar reasoning led to fitted curves for intrinsic muscles

around the PIP joint of: $r_{ub} = 0.44q^2 + 1.53q - 3.24$, $r_{rb} = 0.92q^2 - 1.24q - 1.59$, and muscles about the DIP joint of: $r_{fdp} = -1.12q^2 + 3.07q + 3.09$and $r_{te} = 0.29q^2 + 1.36q - 1.56$.

DISCUSSION

The primary goal of this study was to use a data-driven optimization method to determine muscle-tendon paths for a musculoskeletal model of the index finger. Simulated Annealing and Hooke-Jeeves algorithms successfully found optimized muscle-tendon pathways, resulting in moment arms that matched experimentally-measured relationships. Optimization also suggested that moment arms at the PIP and DIP joints are primarily non-linear and non-constant.

Limitations

Several limitations of our approach should be considered when evaluating these conclusions. First, we chose not to implement complex wrapping surfaces but represented tendon paths as linear connections between via points. To our knowledge, quantitative measurements of wrapping surfaces are not generally available for finger muscles. Although including wrapping surfaces into the optimization could potentially improve modeled moment arm fits, validating the wrapping surfaces would not have been possible. Second, we modeled muscle attachment sites as single points. Muscles attach to bones and tendons with contact areas of varying size. However, point contacts can be considered equivalent systems that replace distributed loads with a simplified representation (Hibbeler, 2013), and have been successfully used in several contexts (Garner et al., 1999; Murray et al., 2002). Hand specimens used for experimental measurements are variable in size, and none precisely match the hypothetical 50th percentile male of the OpenSim model. We tried to minimize potential errors by not only normalizing by middle phalanx length, but also by MCP thickness for flex/extension moment arms and MCP width for ab/adduction values. Consequently, our model's

anthropometric dimensions lie within one standard deviation of the mean for experimental specimens (An et al., 1983; Table 1).

Moment Arms Are Reasonable Approximations of Experimentally-measured Values

Modeled moment arms fitted experimentally-measured values, lying within experimental standard deviation for joints where variances were available. These findings therefore support our hypothesis that data-driven optimization can be used to determine moment arms for musculoskeletal models.

Multiple Attachments Produced the Same Moment Arm Values

Optimization found multiple attachment points ($\vec{x}_j$) that resulted in similar moment arms. These multiple attachment sets could be related to anatomical variability among individuals commonly observed in hand and finger muscle attachments. For example, lumbrical (LU) muscles show deviations in the origins and insertions (Basu et al., 1960; Wang et al., 2014). Single tendons of extensor pollicis longus (EPL) were observed in 67.4% of hands, whereas the duplicated ones were detected in 8.3% ~ 32.6% (Abdel-Hamid et al., 2013; Caetano et al. 2004). Moment arm determines the change in musculotendon length and musculotendon velocity during joint movement (An et al., 1984; Delp and Loan 1995) and muscle contributions to joint stiffness (Hogan, 1990). Therefore, although function (i.e. moment arms) may be constrained, several anatomical configurations may be available to achieve equivalent function. Optimization based on functional objectives could therefore represent another strategy for the important goal of being able to adapt musculoskeletal models to individual differences (Arnold et al., 2000).

Modeled Moment Arms Are Non-linear and Non-constant

Experimentally-measured moment arms were reported to be nearly-constant values in flex/extension for muscles at PIP and DIP joints (An et al., 1983; Chao et al., 1989). Constant moment arms occur when the line connecting distal insertion points and proximal origin points is parallel to joint segments in a fully-extended posture. Moment arms calculated using Landsmeer's model are constants. However, muscle attachment points are not anatomically parallel to phalanx bones (An et al., 1979, 1983; Zatsiorsky, 1998). Consequently, moment arms of other models vary as a function of joint angle (Wu et al. 2010). The approximation of constant moment arms could have resulted from the projection of muscle attachment locations in the Cartesian space (3D) onto the sagittal plane (2D) during experimental measurements. The moment arms discovered by optimization were non-constants that depended on joint angle at PIP and DIP joints. Non-linear (non-constant) moment arms are consistent with simulation (Wu et al., 2010), in vitro (Franko et al., 2011), and in vivo (Fowler et al., 2001) studies at the PIP and DIP joints. Moreover, moment arms at other hand joints are also non-linear curves (An et al., 1983; Brand et al., 1975; Burford et al., 2005; Franko et al., 2011; Ketchum et al., 1978; Kociolek et al., 2011). Our findings that quadratic functions provide reasonable expressions for moment arms are consistent with studies of flexor tendons of the hand, which can be expressed with quadratic fits (Franko et al. 2011). Although we found quadratic fits to be sufficient to represent the moment arms of index fingers, more sophisticated strategies may be necessary to describe musculotendon lengths and moment arms for time-limited computational models (Rankin and Neptune 2012).

In conclusion, using optimization resulted in three primary discoveries. First, moment arm values calculated from optimization solutions match experimental values, demonstrating

that data-driven optimization approaches can be used to generate musculoskeletal models while reducing subjective judgments or estimations. Second, multiple sets of muscles attachments with similar optimized moment arms are possible, consistent with the anatomical variability observed in human hands. Third, moment arms for muscles around the PIP and DIP joints are not constant, but can be modeled with quadratic functions consistent with other muscles. Including anatomical data for finger musculature into the OpenSim arm model will result in a more complete musculoskeletal model that can be useful in many areas, including quantitative analysis of internal loading during multi-touch and HCI tasks.

Table 1. Anthropometric finger dimensions of cadaveric specimens An (1983) and OpenSim model (mm). Symbol (±) indicates standard deviation in interspecimen variation. Lengths of the phalanges in OpenSim model are calculated by the distance between the origins of two coordinate systems in 3 dimensional (3D) Cartesian space, e.g., the center of rotation at MCP and the center of rotation at PIP. Parentheses (Δ) in OpenSim bony dimensions express difference between model dimension and specimen dimension. Skin surface set is scaled in 3D to preserve the anatomical proportions of Fowler et al. (2001), Greiner (1991) and Li et al. (2008). These skin surface set (external dimensions) function as upper boundary constraints during optimization.

	Specimens bony dimensions	**OpenSim bony dimensions**	**Skin surface scaled**
Distal phalanx length	19.67±1.03	19.10 (Δ0.57)	30.65
Middle phalanx length	24.67±1.37	25.10 (Δ0.43)	27.22
Proximal phalanx length	43.57±0.98	42.60 (Δ0.97)	50.86
DIP joint thickness	5.58±0.92	4.95 (Δ0.63)	14.38
PIP joint thickness	7.57±0.45	7.31 (Δ0.26)	18.86
MCP joint thickness	15.57±0.84	17.08 (Δ1.51)	27.80

Table 2. Moment arms (MA) of muscle paths discovered through optimization (mm). Values conform to OpenSim conventions: flex(+)/extension(-) and ab(+)/adduction(-) at DIP, PIP and MCP joints. Mean MA of multiple muscle paths (top values) are represented with standard deviation (±), Mean MA of single muscle paths (bottom values) are represented with RMS error (Δ) between smoothest path and experimental values (An et al., 1983).

Joint	RoM		FDP	FDS	EDC(ES)	LU(RB)	RI	UI(UB)
MCP	Flex/	0°~90°	11.61±0.48	12.27±0.86	-6.67±0.63	2.95±0.56	4.78±0.59	3.64±1.10
	Ext		11.54(Δ0.16)	12.42(Δ0.07)	-7.44(Δ0.66)	3.82(Δ1.04)	5.49(Δ2.49)	3.31(Δ1.75)
	Ab/	0°~30°	2.88±0.64	1.66±0.64	-1.78±0.49	5.71±0.66	4.84±0.75	-6.59±0.81
	Add		2.79(Δ0.75)	1.51(Δ0.53)	-1.01(Δ0.10)	6.47(Δ2.17)	4.11(Δ0.28)	-6.92(Δ0.51)
PIP	Flex/	0°~90°	7.46±0.66	6.39±0.24	-2.78±0.09	-1.86±0.31		0.13±0.42
	Ext		7.10(Δ1.25)	6.22(Δ0.73)	-2.69(Δ0.60)	-1.86(Δ0.22)		0.13(Δ2.28)
DIP	Flex/	0°~50°	3.43±0.71		-3.29±1.89			
	Ext		4.14(Δ0.54)		-0.89(Δ0.78)			

Table 3. Muscle-tendon locations (mm) in the index finger, expressed in OpenSim frame. The coordinate system of the OpenSim model is attached to metacarpal (secondmc), proximal (proxph2), middle (midph2) and distal (distph2) phalanges respectively. x, y and z components indicate radioulnar (+ points out, perpendicular to the palm plan), axial (+ points from distal to proximal side) and dorsolar (+ points up, from palm to hand side) respectively. x, y and z values represent smoothest muscle paths, and parentheses () values of x, y and z represent minimum root mean square (RMS) difference muscle paths.

Joint	Muscles	x	y	z	x	y	z
		proximal point (secondmc)			distal point (proxph2)		
	FDP	5.006	-16.539	-3.605	2.140	-26.241	4.272
		(9.106)	(-15.997)	(-4.211)	(-0.341)	(-19.695)	(-5.031)
	FDS	5.861	-13.773	-0.659	1.324	-20.959	-1.646
		(5.861)	(-13.773)	(-0.659)	(2.088)	(-8.414)	(-12.006)
	RI	-8.032	-16.511	-12.322	0.125	-9.033	-4.359
MCP		(-8.032)	(-16.511)	(-12.322)	(0.125)	(-9.033)	(-4.359)
	LU	10.174	-26.472	-0.014	8.380	-8.291	0.043
		(10.186)	(-27.822)	(-0.335)	(10.238)	(-9.747)	(9.870)
	UI	-3.323	-29.390	-0.124	-4.312	-15.931	2.413
		(-5.096)	(-30.000)	(-0.254)	(-2.998)	(-16.573)	(-8.133)
	EDC	3.045	-29.509	12.430	3.308	-7.107	11.640
		(3.045)	(-29.509)	(12.430)	(3.308)	(-7.107)	(11.640)
		proximal point (proxph2)			distal point (midph2)		
	FDP	-1.841	-9.839	-2.703	2.742	-36.501	1.273
		(1.512)	(-36.501)	(1.273)	(-3.071)	(-9.839)	(-2.703)
	LU (RB)	13.631	-41.970	8.282	-1.060	-8.963	4.482
		(14.994)	(-39.924)	(8.360)	(1.347)	(-2.200)	(5.649)
PIP	**UI (UB)**	2.740	-38.531	9.732	3.712	-9.020	4.413
		(-0.139)	(-31.688)	(9.955)	(2.779)	(-2.025)	(5.884)
	FDS	6.345	-36.775	2.315	1.312	-9.041	-3.399
		(3.345)	(-36.775)	(2.315)	(1.312)	(-9.041)	(-3.399)
	EDC	6.342	-24.241	12.191	1.861	0.102	5.414
	(ES)	(6.881)	(-38.717)	(9.949)	(1.861)	(-0.096)	(5.414)
		proximal point (midph2)			distal point (distph2)		
	FDP	1.324	-20.959	-1.646	1.564	-10.193	-2.916
DIP		(0.173)	(-24.350)	(3.054)	(1.564)	(-10.193)	(-2.916)
	TE	2.620	-8.070	1.630	3.910	-16.534	4.132
		(0.173)	(-24.350)	(3.054)	(2.630)	(-8.070)	(1.630)

FIGURE LEGENDS

Figure 1. All muscle attachment points at the MCP, PIP and DIP joint. Red circles indicate proximal points, and blue squares indicate distal points.

Figure 2. Musculoskeletal hand model. Sagittal and transverse view. Upper two pictures represent smoothest muscle paths, and lower two pictures represent most minimum RMS error muscle paths. The x-axis (flexion-extension) is projected radially for the left hand and ulnarly for the right hand: flex(+)/extension(-), the y-axis is projected along the phalangeal or the metacarpal shaft passing from the distal to proximal side: ulnar twist(+)/radial twist(-) and the z-axis (radioulnar) is projected dorsally: ab(+)/adduction(-). The coordinate system in the OpenSim model is right-handed using homogeneous transforms.

Figure 3. Moment arms for smoothest muscle paths compared to experimental values. Solid lines represent average experimentally-measured (n=7) moment arms, with standard deviations indicated by error bars (An et al., 1983). Dotted lines represent modeled moment arms of the smoothest muscle paths. Grey bands represent one standard deviation above and below average modeled moment arms from all calculated sets of muscle attachments. Average calculated moment arms are in the center of the gray bands, but are not shown for clarity.

FIGURE 1

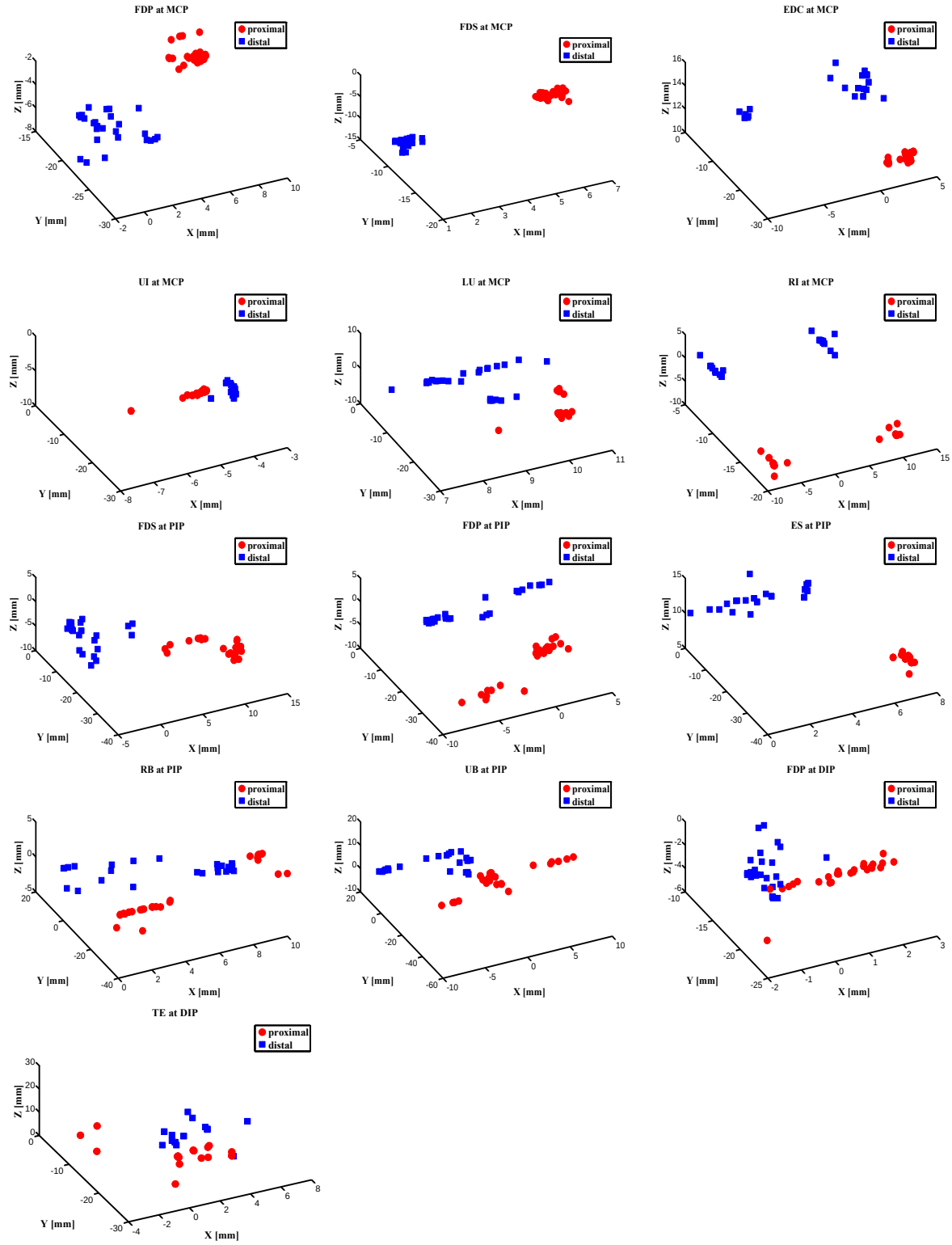
FDP at MCP
FDS at MCP
EDC at MCP
UI at MCP
LU at MCP
RI at MCP
FDS at PIP
FDP at PIP
ES at PIP
RB at PIP
UB at PIP
FDP at DIP
TE at DIP
proximal
distal
X [mm]
Y [mm]
Z [mm]

FIGURE 2

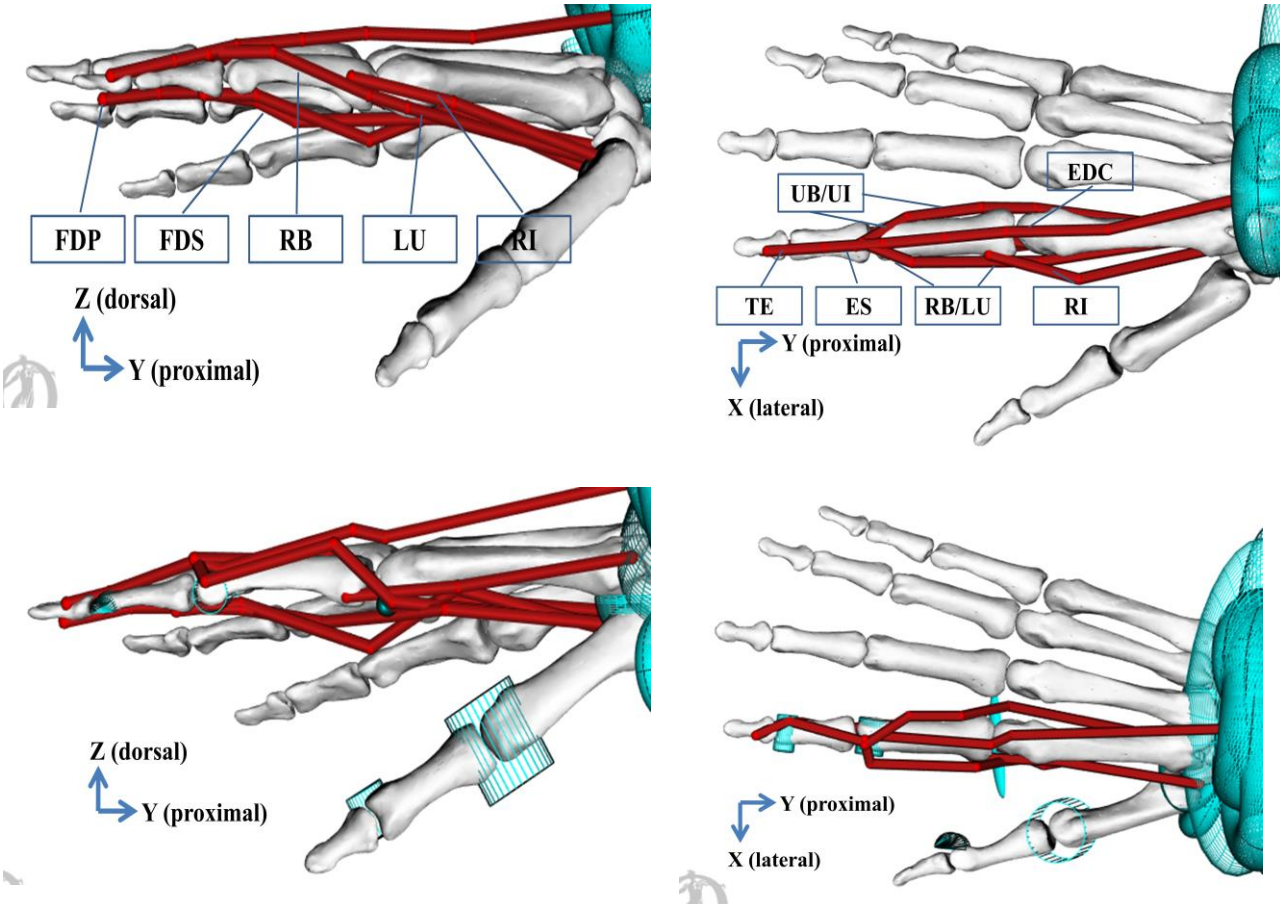
FDP
FDS
RB
LU
RI
Z (dorsal)
Y (proximal)
EDC
UB/UI
TE
ES
RB/LU
RI
Y (proximal)
X (lateral)
Z (dorsal)
Y (proximal)
Y (proximal)
X (lateral)

FIGURE 3

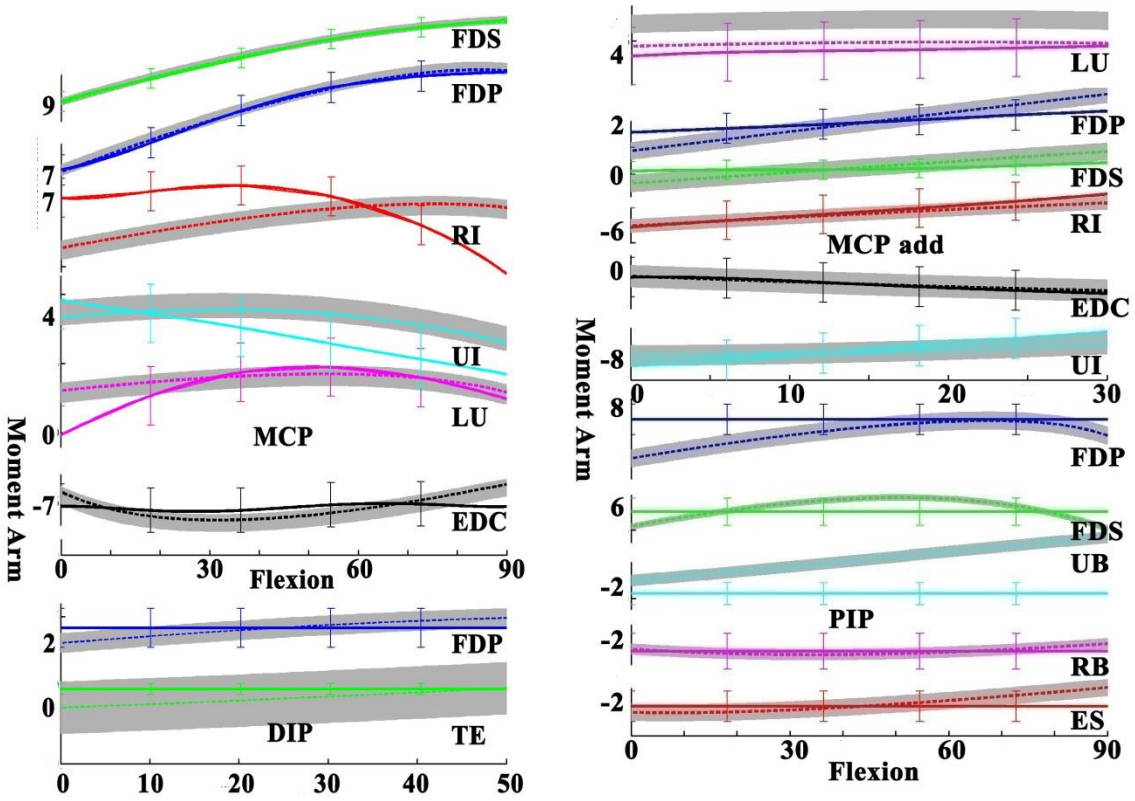
FDS
FDP
RI
UI
LU
MCP
EDC
Moment Arm
Flexion
FDP
DIP
TE
LU
FDP
FDS
RI
MCP add
EDC
UI
FDP
FDS
UB
PIP
RB
ES
Moment Arm
Flexion

REFERENCES

Abdel-Hamid, G.A., El-Beshbishy, R.A., Abdel Aal, I.H., 2013. Anatomical variations of the hand extensors. Folia Morphol 72(3), 249-257.Abarca del Rio, R., D. Gambis, and D. A. Salstein, 2000: Interannual signals in length of day and atmospheric angular momentum. *Ann. Geophys.*, **18**, 347–364.

Ackland, D.C., Lin, Y.C., Pandy, M.G., 2012. Sensitivity of model predictions of muscle function to changes in moment arms and muscle-tendon properties: A Monte-Carlo analysis. Journal of Biomechanics 45, 1461-1471.

Arnold, A.S., Salinas, S., Asakawa, D.J., Delp, S.L., 2000. Accuracy of muscle moment arms estimated from MRI-based musculoskeletal models of the lower extremity. Computer Aided Surgery 5, 108-119.

An, K.N., Chao, E.Y., Cooney, W.P., Linscheid, R.L., 1979. Normative model of human hand for biomechanical analysis. Journal of Biomechanics 12, 775-788.

An, K.N., Ueba, Y., Chao, E.Y., Cooney, W.P., Linscheid, R.L., 1983. Tendon excursion and moment arm of index finger muscles. Journal of Biomechanics 16, 419-425.

Armstrong, T.J. and Chaffin D.B., 1978. An investigation of the relationship between displacements of the finger and wrist joints and the extrinsic finger flexor tensions. Journal of Biomechanics 11, 119-128.

Arnold, A.S., Salinas, S., Asakawa, D.J., Delp, S.L., 2000. Accuracy of muscle moment arms estimated from MRI-based musculoskeletal models of the lower extremity. Computer Aided Surgery, 108-119.

Basu, S.S., Hazary, S., 1960. Variations of the lumbrical muscles of the hand. The Anatomical Record 136, 501-504.

Brand, P.W., Cranor, K.C., Ellis, J.C., 1975. Tendon and pulleys at the metacarpophalangeal joint of a finger. Journal of Bone and Joint Surgery 57, 779-784.

Brand, P.W., Hollister, A., 1993. Clinical mechanics of the hand. Mosby.

Buford Jr., W.L., Koh, S., Andersen, C.R., Viegas, S.F., 2005. Analysis of intrinsic-extrinsic muscle function through interactive 3-dimensional kinematic simulation and cadaver studies. The Journal of Hand Surgery (A) 30, 1267-1275.

Caetano, M.B.f., Albertoni, W.M., Caetano, E.B., 2004. Anatomical studies of the distal insertion of extensor pollicis longus. Acta Ortopeica Brasileira 12, 118-124.

Chao, E.Y., An, K.N., Cooney, W., Linscheid, R., 1989. Normative model of human hand, Biomechanics of the Hand. World Scientific, Singapore, pp. 5-30.

Chadwick, E.K., Blana, D., van den Bogert, A.J., Kirsch, R.F., 2009. A real-time, 3-D musculoskeletal model for dynamic simulation of arm movements. IEEE Transactions on Biomedical Engineering 56(4), 941-948.

Delp, S.L., Loan, J.P., 1995. A graphics-based software system to develop and analyze models of musculoskeletal structures. Computers in Biology and Medicine 25(1), 21-34.

Delp, S.L., Anderson, F.C., Arnold, A.S., Loan, P., Habib, A., John, C.T., 2007. Opensim: open-source software to create and analyze dynamic simulations of movement. IEEE Transactions on Biomedical Engineering 54(11), 1940-1950.

Ettema, G.J.C., Styes, G., Kippers, V., 1998. The moment arms of 23 muscles segments of the upper limb with varying elbow and forearm positions: implications for motor control. Human Movement Science 17, 201-220.

Fowler, N.K., Nicol, A.C., Condon, B., Hadley, D., 2001. Method of determination of three dimensional index finger moment arms and tendon lines of action using high resolution MRI scans. Journal of Biomechanics 34, 791-797.

Franko, O.I., Winters, T.M., Tirrell, T.F., Hentzen, E.R., Lieber, R.L., 2011. Moment arms of the human digital flexors. Journal of Biomechanics 44, 1987-1990.

Fregly, B.J., Boninger, M.L., Reinkensmeyer, D.J., 2012. Personalized neuromusculoskeletal modeling to improve treatment of mobility impairments: a perspective from European research sites. Journal of NeuroEngineering and Rehabilitation 9:18

Garner, B.A., Pandy, M.G., 2000. The obstacle-set method for representing muscle paths in musculoskeletal models. Computer Methods in Biomechanics and Biomedical Engineering 3, 1-30.

Gatti, C.J., Hughes, R.E., 2009. Optimization of muscle wrapping objects using simulated annealing. Annals of Biomedical Engineering 37, 1342-1347.

Gerbeaux, M., Turpin, E., Lensel-Corbeil, G., 1996. Musculoarticular modeling of the triceps brachii. Journal of Biomechanics 29(2), 171-180.

Greiner, T.M., 1991. Hand Anthropometry of US Army Personnel. United States Natick Research, Development and Engineering Center, Natick, MA, Document AD-A244 533.

Hibbeler, R.C., 2013. Mechanics of materials. Prentice Hall, Boston.

Hogan, N., 1990. Mechanical impedance of single- and multi-articularsystems. In: Winters, J., Woo, S. (Eds.), Multiple Muscle Systems.Springer, NewYork, pp. 149–164.

Holzbaur, K.R.S., Murray, W.M., Delp, S.L., 2005. A model of the upper extremity for simulating musculoskeletal surgery and analyzing neuromuscular control. Annals of Biomedical Engineering 33(6), 829-840.

Kamper, D.G., Fischer, H.C., Cruz, E.G., 2006. Impact of finger posture on mapping from muscle activation to joint torque. Clinical Biomechanics 21, 361-369.

Kelley, C.T., 1999. Iterative methods for optimization. SIAM, Philadelphia.

Ketchum, L.D., Brand, P.W., Thompson, D., Pocock, G.S., 1978. The determination of moments for extension of the wrist generated by muscles of the forearm. The Journal of Hand Surgery (A) 3, 205-210.

Kirkpatrick, S., Gelatt, C.D., Vecchi, M.P., 1983. Optimization by simulated annealing. Science 220(4598), 671-680.

Kociolek, A.M., Keir, P.J., 2011. Modelling tendon excursions and moment arms of the finger flexors: Anatomic fidelity versus function 44, 1967-1973.

Kurse, M.U., Lipson, H., Valero-Cuevas, F.J., 2012. Extrapolatable analytical functions for tendon excursions and moment arms from sparse datasets. IEEE Transactions on Biomedical Engineering 59 (6).

Landsmeer, J.M., 1961. Studies in the anatomy of articulation. I. The equilibrium of the "intercalated" bone. Acta Morphologica Neerlanddo – Scandinavica 3, 287-303.

Lee, S.W., Kamper D.G., 2009. Modeling of multiarticular muscles: importance of inclusion of tendon-pulley interactions in the finger. IEEE Transactions on Biomedical Engineering 56(9), 2253-2262.

Li, Z., Chang, C.C., Dempsey, P.G., Ouyang, L., Duan, J., 2008. Validation of a three-dimensional hand scanning and dimension extraction method with dimension data. Ergonomics 51(11), 1672-1692.

Lloyd D.G., Besier, T.F., 2003. An EMG-driven musculoskeletal model to estimate muscle forces and knee joint moments in vivo. Journal of Biomechanics 36, 765-776.

Lopes, M.M., Lawson, W., Scott, T., Keir, P.J., 2011. Tendon and nerve excursion in the carpal tunnel in healty and CTD wrists. Clinical Biomechanics.

McKay, J.L., Ting, L.H., 2012. Optimization of muscle activity for task-level goals predicts complex changes in limb forces across biomechanical contexts. PLoS computational biology 8(4).

Murray, W.M., Delp, S.L., Buchanan, T.S., 1995. Variation of muscle moment arms with elbow and forearm position. Journal of Biomechanics 28(5), 513-525.

Oh, S., Belohlaverk, M., Zhao, C., Osamura, N., Zobitz, M.E., An, K.N., Amadio, P.C., 2007. Detection of differential gliding characteristics of the flexor digitorum superficialis tendon and subsynovial connective tissue using color Doppler sonographic imaging. Journal of Ultrasound in Medicine: Official Journal of the American Institute of Ultrasound in Medicine 26(2), 149-155.

Pigeon, P., Yahia, L., Feldman, A., 1996. Moment arms and lengths of human upper limb muscles as functions of joint angles. Journal of Biomechanics 29(10), 1365-1370.

Qin, J., Lee, D., Li, Z., Chen, H., Dennerlein, J.T., 2010. Estimating in vivo passive forces of the index finger muscles: Exploring model parameters. Journal of Biomechanics 43, 1358-1363.

Qin, J., Trudeau, M., Katz, J., Buchholz B., Dennerlein, J.T., 2011. Biomechanical loading on the upper extremity increases from single key to directional tapping. Journal of Electromyography and Kinesiology 21, 587-94.

Radwin, R.G., Lavender, S.A., 1999. Work factors, personal factors, and internal loads: Biomechanics of work stressors. Work-related Musculoskeletal Disorders: Report, workshop summary, and workshop papers, 116-151.

Rankin, J.W., Neptune, R.R., 2012. Musculotendon lengths and moment arms for a three-dimensional upper-extremity model. Journal of Biomechanics 45, 1739-1744.

Rekimoto, J., 2002. Smartskin: An infrastructure for freehand manipulation on interactive surfaces. Proceedings of the SIGCHI conference on human factors in computing systems.

Roloff, I., Schoffl, V.R., Vigouroux L. Quaine F., 2006. Biomechanical model for the determination of the forces acting on the finger pulley system. Journal of Biomechanics 39, 915-923.

Rubine, D., 1991. Specifying gestures by example. Proceedings of the 18th annual conference on Computer graphics and interactive techniques 25(4).

Sancho-Bru, J.L., Perez-Gonzalez, A., Vergara-Monedero M., Giurintano, D., 2001. A 3-D dynamic model of human finger for studying free movements. Journal of Biomechanics 34, 1491-1500.

Seth, A., Sherman, M., Reinbolt, J.A., Delp, S.L., 2011. OpenSim: a musculoskeletal modeling and simulation framework for in silico investigations and exchange. 2011 Symposium on Human Body Dynamics, 212-232.

Sjoggard, G., Sjogaard, K., 1998. Muscle injury in repetitive motion disorders. Clinical Orthopedics and Related Research 351, 21-31.

Soechting, J.F., Flanders, M., 1997. Flexibility and repeatability of finger movements during typing: analysis of multiple degree of freedom. Journal of Computational Neuroscience 4, 29-46.

Valero-Cuevas, F.J., Johanson, M.E., Towles, J.D., 2003. Towards a realistic biomechanical model of the thumb: the choice of kinematic description may be more critical than the solution method or the variability/uncertainty of musculoskeletal parameters. Journal of Biomechanics 36, 1019-1030.

Wang, K., McGlinn, E.P., Chung, K.C., 2014. A biomechanical and evolutionary perspective on the function of the lumbrical muscle. The Journal of Hand Surgery 39(1), 149-155.

Wu, M., Balakrishna, R., 2003. Multi-finger and whole hand gestural interaction techniques for multi-user tabletop displays. Proceedings of the 16th annual ACM symposium on User interface software and technology.

Wu, J., An, K.N., Cutlip, R.G., Dong, R.G., 2010. A practical biomechanical model of the index finger simulating the kinematics of the muscle/tendon excursions. Bio-Medical Materials and Engineering 20, 89-97.

Yoshii, Y., Villarraga, H.R., Henderson, J., Zhao, C., An, K.N., Amadio, P.C., 2009. Speckle tracking ultrasound for assessment of the relative motion of flexor tendon and subsynovial connective tissue in the human carpal tunnel. Ultrasound in Medicine and Biology 35(12), 1973-1981.

Zajac, F.E., Cottlieb, G.L., 1989. Muscle and tendon: properties, models, scaling, and application to biomechancis and motor control. Critical Reviews in Biomedical Engineering 17(4), 359-411.

Zatsiorsky, V.M., 1998. Kinematics of human motion. Human Kinetics.Compo, G., and P. Sardeshmukh, 2009: Oceanic influence on recent continental warming, *Clim. Dyn.*, **32**, 333–342, doi:10.1007/s00382-008-0448-9.

https://simtk.org/project/xml/downloads.xml?group_id=660 Matlab-Opensim API

CHAPTER 3

AN OBJECTIVE PROCEDURE CAN ESTIMATE ATTACHMENT LOCATIONS FOR HAND MUSCLES IN OPENSIM UPPER-EXTREMITY MODEL

Abstract

The purpose of this study was to develop objective, quantitative techniques to determine muscle attachment points for a musculoskeletal model, and to apply the techniques to determine muscle attachment points for a non-proprietary musculoskeletal model, the OpenSim upper extremity model. The OpenSim upper extremity model includes extensive data of shoulder and elbow musculature, but does not include intrinsic muscles for most fingers of the hand. Although muscle attachments have been measured for hand muscles, the model differs in size, joint kinematics and coordinate system from source specimens. Moment arms or tendon excursions can be used for some muscles, but experimental values are not available for all intrinsic hand muscles. Therefore, we proposed a method for scaling and translating muscle attachments from one experimental or model environment to another. Our method consists of two steps. First, we sought to estimate muscle function by calculating moment arm values for all intrinsic/extrinsic muscles using the partial velocity method. We validated the technique by comparing estimated moment arms to experimentally-measured relationships where available. Second, we used an optimization method to find new attachment locations that preserved muscle function within the new model environment. Simulated Annealing and Hooke-Jeeves algorithms were used to determine muscle-tendon paths that minimized the root mean square (RMS) differences between experimentally-derived and optimally-modeled moment arms. Application of this method resulted in variance accounted for (VAF) between modeled and measured values of 80.6% on average (range from 70.1% to 94.3%) for muscles where

measured moment arm data were available. Validation of both steps of the technique, allowed for estimation of muscle attachment points for intrinsic/extrinsic muscles whose moment arms have not been measured. The resulting non-proprietary musculoskeletal model of the human hand and arm will be useful for many applications, including estimating internal musculoskeletal loading, associated with using multi-touch devices.

INTRODUCTION

Dexterous manipulation often involves complex movements of several fingers. For example, grasping or pinching can involve the coordinated activations of many hand muscles (Brochier et al., 2004). Movements similar to pinching and grasping are commonly employed by human-computer interfaces (HCIs) such as smart phones and tablet computers. The "multi-touch" interfaces of these devices often require complex, multi-finger gestures or gesture sequences on the touch screen (Rekimoto, 2002; Rubine, 1991; Wu et al., 2003). However, we have little understanding of whether the cumulative effects of long-term exposures can lead to injuries such as musculoskeletal disorders (MSDs). One way to identify exposure to potentially damaging forces is to estimate muscle and tendon forces during repetitive activities. However, individual muscle tension or stress is difficult to measure in vivo (Dennerlein et al., 1998, 1999).

Biomechanical models can help estimate internal musculoskeletal loading during movement (Cholewicki et al., 1994). Several biomechanical models of the arm or hand have been developed (An et al., 1979; Biggs and Horch, 1999; Brook et al., 1995; Li et al., 2008; Leijnse, 1995; Holzbaur et al., 2007; Valero-Cuevas et al., 1998, 2003; Tsang et al., 2005; Albrecht et al., 2003). Models have helped identify the function of the intrinsic muscles (Spoor and Landsmeer, 1976; Leijnse, 1995), movement coordination of the interphalangeal joints (Lee and Rim, 1990; Buchner et al., 1988), muscle loading during grasping (Sancho-Bru et al., 2001, 2003), and the dynamics of the index finger (Brook et al., 1995). However, existing models have four primary limitations. First, many models were developed with proprietary or commercial software, and are not generally available for use in new tasks. Second, many models are two-dimensional (2D), whereas arm movements are often three-dimensional (3D) space. Third, many models do not model the entire upper extremity, but instead focus on

specific joints or sets of joints. Finally, even models that include all of the major skeletal segments of the hand and arm do not currently include all of the muscles potentially involved in actuating complex motions.

To address these concerns, we seek to use a non-proprietary, 3D musculoskeletal model of the hand and arm that includes the intrinsic finger muscles potentially necessary for the complex finger movements associated with HCIs. We therefore chose to focus on an existing upper extremity model (2.3.2, Simbios, Stanford, CA; Holzbaur et al., 2005) on the OpenSim platform, designed to be widely-accessible (Delp et al., 2007; Seth et al., 2011). The OpenSim upper-extremity model includes detailed models of muscles at the shoulder and elbow. However, not all muscles of the hand and fingers have been included. Therefore, our specific objective is to add intrinsic muscles for the fingers of the hand and to determine intrinsic/extrinsic muscles' origins and insertions.

Muscle attachment points have been reported for both intrinsic and extrinsic muscles of the hand (An et al., 1979). However, published attachments cannot be directly used in the OpenSim model. Specimens used for experimental measurements were different from the 50^{th} percentile male used for the OpenSim model in several respects, including differences in segment size, proportion, joint center location, axis of rotation and anatomical coordinate systems. Directly adding experimentally-measured muscle attachments to the OpenSim model results in very different moment arms than those experimentally-measured for the same muscles. Muscle moment arm is an important functional measure because it determines the joint torques that result from muscle forces. Therefore, to create a musculoskeletal model capable of evaluating muscle and limb function, it is necessary to determine sets of muscle attachments that result in moment arms that are representative of human subjects.

Several studies have measured moment arm in vivo (Lopes et al., 2011; Oh et al., 2007; Yoshii et al., 2009) and in situ (An et al., 1983; Armstrong and Chaffin, 1978; Brand et al., 1993; Chao et al., 1989; Franko et al., 2011). However, to our knowledge moment arms for the middle, ring and little fingers have not been reported. Moreover, even when moment arms are known, the specific muscle attachments are unknown and indeterminate: many potential muscle attachments can result in similar moment arms (Delp et al., 2007; Seth et al., 2011).

Therefore, we sought to identify the muscle attachments for intrinsic/extrinsic hand muscles within the OpenSim arm model that resulted in the functionally important characteristic of matching experimentally-measured moment arms. Furthermore, we sought to develop an objective, data-driven procedure that can be employed to functionally transpose musculoskeletal models.

Our procedure involved two steps. First, we aimed to determine muscle function (moment arms) from experimentally-measured tendon locations (An et al., 1979). We hypothesized that partial velocity calculation (Delp and Loan, 1995; Kane and Levinson, 1985) could reproduce anatomical moment arms from experimentally-measured muscle attachment points (An et al., 1979). Successful prediction was considered to be calculated moment arms within one standard deviation (σ) of experimental measurements ($\sigma = 2.5$ mm; An et al., 1983; Biggs and Horch, 1999). Second, given this functional moment arm information, we aimed to identify muscle-tendon paths via an optimization technique. We hypothesized that data-driven optimizations: Simulated Annealing (Kirkpatrick et al., 1983) and Hooke-Jeeves (Kelley, 1999) could find origins and insertions of intrinsic/extrinsic hand muscles, resulting in optimized moment arms that fit experimentally-derived relationships (An et al., 1979, 1983; Chao et al., 1989). Successful approximation was considered to be optimized moment arms within 10% of

experimentally-derived values (Arnold et al., 2000; Rankin et al., 2012). This procedure would not only result in objectively-determined muscle attachment points for intrinsic and extrinsic muscles of each finger, but would present an objective method for customizing musculoskeletal models.

MATERIALS AND METHODS

We used an existing upper-extremity musculoskeletal model on the OpenSim platform (2.3.2, Simbios, Stanford, CA; Holzbaur et al. 2005). This model is composed of 33 segments and 15 degrees of freedom (DOFs) allowing shoulder, elbow, forearm, wrist, thumb and index finger movements in 3D. The existing model is actuated by 50 muscle compartments, including flexors and extensors of the index, middle, ring and little fingers. The rotational axes and centers for the thumb joints are based on measured values (Hollister et al., 1992, 1995), and those for the index finger joints are determined as the long axis of cylinders fit to the articular surfaces of the metacarpal and phalangeal bones. Hill-type muscle models are used (Schutte et al., 1993; Thelen et al, 2003; Zajac and Cottlieb, 1989).

Musculoskeletal Model

We appended custom joints to middle, ring and little fingers because only index finger and thumb have active joints in the existing model. Each finger was modeled to have four DOFs linking three successive phalanges: distal, middle and proximal to metacarpal bones. These four phalanges were linked with three joints: distal interphalangeal (DIP), proximal interphalangeal (PIP) and metacarpophalangeal (MCP). The DIP and PIP joints functioned in flex/extension like a hinge (1 DOF), while the MCP joint functioned flex/extension and ab/adduction like a universal joint (2 DOFs). To ensure the musculoskeletal model reflecting a physiological range of excursion, we considered the range of motion (RoM) of each joint based on experimental measurements (An et al., 1983; Chao et al., 1989). The DIP and PIP joints were modeled with a RoM of 0° to 50° (flexion: +) and 90° (flexion: +), respectively. The MCP joints also were

modeled with a RoM of $0°$ (extension: -) to $90°$ (flexion: +) as well as 0° (adduction: -) to 30° (abduction: +).

For all fingers, we modeled the following muscles: *terminal extensor (TE), extensor slip (ES), radial band (RB), ulnar band (UB), dorsal interosseous or radial interosseous (RI), lumbricals (LU), palmar interosseous or ulnar interosseous (UI), flexor digitorum profundus (FDP), flexor digitorum superficialis (FDS) and extensor digitorum communis (EDC).* Because data are not available on specific wrapping of these muscles, we removed the wrap object sets from all joints (Garner and Pandy, 2000).

Reproducing Moment Arms from Experimentally-measured Attachments

Because experimental moment arms are available only for the index finger, it was necessary to calculate their values from measured muscle attachment points for middle, ring and little fingers. We calculated moment arms from An et al. (1979)'s normative model tendon locations using the "partial velocity" method (Delp et al., 1995; Kane et al., 1985). The partial velocity method provides a consistent technique to compute the moment arms of muscles crossing all types of joints (Delp and Loan, 1995).

Muscle Attachment Determination

A data-driven optimization approach was used to identify muscle attachment sites that resulted in moment arms that most closely matched the experimentally derived relationships. Muscle attachments were expressed as distal and proximal points, $\vec{x} = [p_x^{dist}, p_y^{dist}, p_z^{dist}, p_x^{prox}, p_y^{prox}, p_z^{prox}]^T$.

An objective function was defined as the root mean square (RMS) error between the experimentally-derived moment arms, $\mathrm{r_j}(\vec{\mathrm{q}}_\mathrm{i})$ and the modeled-estimate moment arms, $\hat{\mathrm{r}}_\mathrm{j}(\vec{\mathrm{q}}_\mathrm{i}, \vec{\mathrm{x}})$. The optimization searched for the minimum values of RMS error ($f(\vec{x})$) over the domain of attachment points ($\vec{x}$) and joint angle ($\vec{q}$) that satisfy both flex/extension and ab/adduction moment arm relationships ($\mathrm{g_j(x)}$).

Minimize $\quad f(\vec{x}) = \sqrt{\sum_{i=1}^{m} \frac{[r_j(\vec{q}_i) - \hat{r}_j(\vec{q}_i, \vec{x})]^2}{m}}$

Subject to $\quad lb_j \leq x_j \leq ub_j$

$\mathrm{g_j(x)} - \varepsilon_\mathrm{j} \leq 0$

Optimization parameters and variables were defined as below:

$\vec{x}$ Muscle attachment points at the distal and proximal sides ($\vec{\mathrm{x}} \in \mathcal{R}^6$)

$\vec{\mathrm{q}}_\mathrm{i}$ Joint angle with a resolution (i) of 100 increments (m) covering RoM

$\mathrm{r_j}(\vec{\mathrm{q}}_\mathrm{i})$ Experimentally-derived moment arms

$\hat{\mathrm{r}}_\mathrm{j}(\vec{\mathrm{q}}_\mathrm{i}, \vec{\mathrm{x}})$ Modeled-estimate moment arms functioned of joint angle and muscle attachments

i Joint motions such as flex/extension or ab/adduction

j Individual muscles ($\mathrm{j} = 40$)

$\mathrm{lb_j}$ A lower bound, bony segment (internal dimension)

$\mathrm{ub_j}$ An upper bound, hand skin surface (external dimension)

ε_j Maximum standard deviation of experimental moment arms

$\mathrm{g_j(x)}$ RMS moment arm error of ab/adduction during flexion/extension movements

The boundary constraints enforced that muscle attachments were between bony segments (as a lower bound, $\mathrm{lb_j}$; Holzbaure et al., 2005) and hand skin surface (as an upper bound, $\mathrm{ub_j}$; Alexander, 2010; Fowler et al., 2001; Greiner 1991; Li et al. 2008).

Muscle-tendon paths must simultaneously satisfy moment arms for both flex/extension and ab/adduction at the MCP joint. However, measured ab/adduction moment arm values are less reliable than those for flex/extension. Ab/adduction moment arm values depend on finger postures, i.e., flexion of MCP, PIP and DIP joints (Kamper et al., 2006). However, the specific postures used for measured ab/adduction moment arm values were not reported. Ab/adduction moment arms also have substantially higher standard deviations than flex/extension, reflecting either measurement error or anatomical variability (An et al., 1979, 1983; Armstrong and Chaffin, 1998; Chao et al., 1989). Therefore, we did not consider it appropriate for both flex/extension and ab/adduction moment arm values to have the same weight in the objective function. We do not have an objective criterion for assigning specific differential weightings for bidirectional moment arms. Therefore, we chose an inequality constraint $\left(\mathrm{g_j(x)}, \varepsilon_\mathrm{j}\right)$ to encourage the discovery of solutions that maintain ab/adduction close to reported values, taking into account the measurement uncertainty. The inequality constraint resulted in punishment if the RMS error for a muscle's ab/adduction moment arm ($\mathrm{g_j}(\vec{\mathrm{x}})$) exceeded the bounds of the maximum standard deviation of experimentally-measured ab/adduction moment arms ε_j. For example, minimize (min.) $\mathrm{f}(\vec{\mathrm{x}}) = \mathrm{RMS\ error} + \mathrm{P}(\vec{\mathrm{x}})$. $\mathrm{P}(\vec{\mathrm{x}}) = 0$ if $\mathrm{g_j}(\vec{\mathrm{x}}) \leq \varepsilon_\mathrm{j}$ and $\mathrm{P}(\vec{\mathrm{x}}) = \varepsilon_\mathrm{j}\emptyset$ if $\mathrm{g_j}(\vec{\mathrm{x}}) > \varepsilon_\mathrm{j,}$ where $\emptyset = 1000$. Specifically, ε_j was 2.5 mm for extrinsic tendons and 1.7 mm for intrinsic muscles. Because extrinsic muscle ab/adduction moment arms had higher uncertainty than for intrinsic muscles, attachment points were less influenced by the ab/adduction moment arms for extrinsic muscles than for intrinsic muscles.

Global Optimization

We used Simulated Annealing (Kirkpatrick et al., 1983) and Hooke-Jeeves algorithms (Kelley, 1999). These algorithms were suitable for discrete system that do not require the gradient (Δ) of the problem to be optimized, e.g., objective function ($\mathrm{f}(\vec{\mathrm{x}})$) did not have its partial derivatives with respect to muscle attachment points ($\vec{x}$) i.e., $\Delta\mathrm{f}(\vec{\mathrm{x}}) = \mathrm{df}(\vec{\mathrm{x}})/\mathrm{d}\vec{\mathrm{x}}$. The Simulated Annealing algorithm was used with the following attributes: 1) the initial temperature was 1, 2) the algorithm iterated until the average change in value of the objective function was less than 0.0001, 3) the max. number of evaluations of the objective function was $3{,}000 \times 6$ variables and 4) the max. time limit was infinite.

Sensitivity Analysis

To determine how robust the optimization procedure was in finding attachments ($\vec{\mathrm{x}}_{\mathrm{j}}$) despite potential variability in initial conditions ($\vec{\mathrm{x}}_0$), we performed optimizations using 26 different points that included the Holzbauer et al. (2005) and An et al. (1979) attachment points, and 24 points selected to span the approximate, observed anthropometric variations (~5 mm; An et al., 1983). Sensitivity analysis was based on distribution sensitivity because determining starting points ($\vec{\mathrm{x}}_0$) was a discrete stochastic processes. Because the biggest phalanx is ~46 mm on the simulation (Grein, 1991; Alexander et al., 2010), 26 increments (1 trial = 2 mm/increment) can cover the length of biggest phalanx.

Preliminary experiments revealed that multiple sets of muscle attachments could yield similar moment arms that matched experimentally-measured values (Lee et al., 2014). The multiple solutions necessitated the selection of a criterion to select a single set of attachment points. We assumed the most smooth muscle path was most anatomically-reasonable.

Smoothness was determined as the largest curvature determined from three successive attachments, e.g., origin, via and insertion points.

Consequently, our procedure accomplished three objectives. The most important objective was to generate model parameters (i.e., muscle attachments) that best represented muscle function. The primary aspect of muscle function that we focused on was muscle moment arms, because moment arms determine the joint torques and movements that result from muscle forces. Towards this end, we estimated moment arms based on published anatomical data using the partial velocity method. We then performed optimization to discover muscle attachment points in a different modeling environment (the non-proprietary OpenSim model) that resulted in moment arms that matched experimentally-measured values in both flex/extension and ab/adduction. From the set of optimized attachment points, a single set of points was selected to satisfy the secondary objective of path smoothness that was assumed to best represent anatomy.

Optimizations were implemented in Matlab (2010b, Mathworks, Natic, MA), using the OpenSim Application Programming Interface (API; OpenSim 2.0 Doxygen), to compute moment arms. Simulations were performed on a 3.00-GHz Intel Core2 Duo with 3.25 GB of RAM.

RESULTS

The partial velocity calculation reproduced experimentally-measured moment arm values from anatomical muscle attachment points (An et al., 1979). Data-driven optimizations found muscle-tendon paths resulting in moment arms that closely matched experimental moment arms deriving from anatomical attachments.

Moment Arms Calculated From Muscle Attachments Fitted Experimentally-measured Values

To validate the partial velocity approach, we compared experimentally-measured moment arms of the index finger (An et al., 1983) with computationally-derived moment arms from anatomical muscle attachment points (An et al., 1979). Because experimentally-measured moment arms as a function of joint angle are only available for the MCP joint of the index finger, our analysis was limited to the index finger MCP joint.

Moment arms calculated using the partial velocity method fitted those measured at the MCP joint of the index finger (Figure 1; Table 1). Calculated moment arms derived from anatomical muscle attachments (An et al., 1979) lie within one standard deviation of moment arms measured by An et al. (1983). Variance accounted for (VAF) averaged 75.5% across all index finger muscles, ranging from min. 48.2% (UI) to max. 99.5% (FDS). VAF for the UI was low because of the small value for the moment arms of this muscle. However, RMS error for UI as within one standard deviation (σ) of experimental moment arms (RMS = 0.4 mm < σ = 2.1 mm) implying that the calculated moment arm is reasonable. VAF were 96.5% for extrinsic tendons and 58.7% for intrinsic muscles. Extrinsic tendons matched closer than intrinsic muscles. Standard deviations of extrinsic tendons were bigger than those of intrinsic muscles

(An et al., 1983). Overall, these results suggested that partial velocity approach is able to reproduce the moment arm values.

Calculated Moment Arms Were Reasonable for All Intrinsic/Extrinsic Finger Muscles

Moment arms calculated for muscles where no direct measured moment arm data exist were reasonable. For example, all calculated moment arms had the same ordering of magnitude as the finger dimensions, i.e., moment arms for the middle finger largest, ring/index second and little smallest (Figure 2, 3, 4). Joint thickness or phalanx lengths influenced moment arms, e.g., moment arm magnitudes increased with phalanx lengths (An et al., 1983; Armstrong and Chaffin, 1978; Kocioleck et al., 2011). Greiner (1991) and Alexander (2010) reported proportions of hand segments, e.g., proximal phalanx length (mean $\pm$ standard deviation; mm): middle (44.63 ± 3.81) > ring (41.37 ± 3.87) > index (39.78 ± 4.94) > little (32.74 ± 2.77) finger. Therefore, partial velocity calculation predicted moment arm curves consistent with phalanx sizes.

Calculated moment arms were similar in shape and in trend (Figure 2, 3, 4). Moment arms varied with joint angle. Flexors were predicted to have increasing moment arms with flexion of the joint, extensors were predicted to have moment arms that increased with extension. Experimental data indicated that moment arms for extensors (EI/EC) decreased with flexion, while these for flexors (FDP/FDS) and intrinsic muscles (RI/UI/LU) increased with flexion for the index, middle, ring and little fingers (An et al., 1979, 1983; Biggs and Horch, 1999; Chao 1989; Fowler et al., 2001; Franko et al., 2011). Moreover, many studies showed that moment arms varied with MCP joint angle (Armstrong and Chaffin, 1978; Kocioleck et al.,

2011; Kurse et al., 2012; Landsmeer, 1961; Wu et al., 2010). Therefore, the partial velocity method predicted moment arm values agreeing in trend with the experimental data.

Optimized Moment Arms Matched Calculated Values Derived from Anatomical Attachments

Model-optimized moment arms generally agreed with experimentally-derived values for index, middle, ring and little fingers at the MCP joint (Finger 5, 6, 7, 8). VAF averaged 75.5, 80.7, 74.5 and 70.9% for index, middle, ring and little finger respectively (Table 1, 2, 3, 4). At the little finger (min. VAF = 70.9%), RMS error ranged from min. 0.1 mm (FDP) to max. 6.5 mm (LU). Because measured moment arms for the little finger have not been reported, experimental standard deviations are not available. Max. RMS error (6.5 mm for LU) between optimized and experimentally-derived moment arm values differed with 66.0% error but within 1.0% of peak experimentally-derived value (An et al., 1979). Because LU experimental moment arm value was small (3 mm), error was big (66.0%): error = $(experiment - simulation)/experiment$.

Model-optimized moment arm curves for all muscles (i.e., FDP, FDS, RI, LU, UI and EDC) were continuous and nonlinear in response to the MCP flexion/extension movements, while they were linear in accordance with ab/adduction motions. A polynomial fitting function (polyfit, Matlab 2010b) was used to classify into linear ($ax + b$; two degree) and nonlinear ($ax^2 + bx + c$; three degree). For example, we considered nonlinear function if moment arms were fitted to a polynomial of degree three with VAF over 99%, or linear function if they were fitted to a polynomial of degree two with VAF over 99%.

For the PIP joints, model-optimized moment arms reasonably matched experimentally-derived data. VAF averaged 75.1, 73.7, 85.7 and 95.8% for index, middle, ring and little finger respectively. At the middle finger (min. VAF = 73.7%), RMS error ranged from min. 0.3 mm (FDP) to max. 2.6 mm (ES). Max. difference (RMS error =2.6 mm for ES) was 26.4% of experimentally-derived moment arm value (An et al., 1979). Because ES moment arm averaged -0.25 mm over RoM, error was bigger than 10.0%. Overall errors of all PIP joints were within 10.0% of experimentally-derived moment arm values (An et al., 1979).

For the DIP joints, model-optimized moment arms reasonably fitted experimentally-derived values. VAF averaged 78.5, 78.5, 84.2 and 90.8% across all muscles for index, middle, ring and little finger respectively. At the index finger (min. VAF=78.5%), RMS error ranged from min. 0.5 mm (FDP) to max. 0.8 mm (TE). Because experimentally-derived moment arm of TE was close to zero, its error was big (76.8% of experimental value).

DISCUSSION

The primary goal of this study was to develop an objective, quantitative method for transforming experimentally-measured muscle attachments to a 3D musculoskeletal model while faithfully modeling muscle function. The method we developed involved 1) deriving moment arm curves from experimentally-measured muscle attachments, and 2) using a data-driven optimization to identify muscle-tendon paths in the 3D musculoskeletal model. Muscle moment arms are important functional targets because they relate muscle forces to joint moments (Murray et al., 1995). We used the method to estimate moment arms and muscle attachments of middle, ring and little fingers in an OpenSim arm model. Moment arms calculated from muscle attachments were validated by comparison to available experimental measurements.

Limitations

Our approach had several limitations. First, we did not model muscle-wrapping. Muscle-wrapping, potentially over multiple surfaces, can result in high accurate muscle paths (Starness et al., 2012). However, to our knowledge quantitative, experimental data for wrapping surfaces are not available. Therefore, muscles were connected to single points at each joint, consistent with published data (An et al., 1979). Second, compiling data drawn from different reference frame and sources into a common model could introduce errors. We attempted to mitigate these potential sources of error by not only normalizing by middle phalanx length for flex/extension moment arms at the PIP and DIP joints, but also normalizing by MCP thickness for flex/extension moment arms and MCP width for ab/adduction values. Our model's

anthropometric dimensions lie within one standard deviation of the mean for experimental specimens (Table 5).

Calculated Moment Arms Derived from Anatomic Attachments are Reasonable Approximations of Experimentally-measured Values of the Index Finger.

This study tested whether the partial velocity method could calculate moment arm curves from anatomically-measured muscle origins and insertions that matched experimentally-measured moment arms. Calculated moment arms, derived from muscle attachment locations of An et al. (1979) agreed with experimental values measured by An et al. (1983). For most muscle, RMS errors were substantially less than the experimental standard deviation for MCP joint. The partial velocity method may provide a consistent technique to compute the moment arms of muscles crossing many types of joints. The same algorithm could potentially be used to calculate the moment arm of muscles about the knee, hip, elbow and shoulder, even though the mechanics of these joints differ considerably (Delp and Loan, 1995).

Optimization Found Muscle Attachments That Maintained Muscle Function

We hypothesized that objective techniques, Simulated Annealing and Hook-Jeeves optimization, could find muscle attachments that resulted in accurate muscle function. Optimized moment arms matched experimentally-derived values within 10% error of experimental values (RMS errors = 0.07~6.88 mm) supporting the hypothesis. Although previous studies have compared moment arms with experimental data, similarity is often not quantitatively assessed (Wu et al., 2010; Biggs and Horch 1999). The optimization technique

allows for modeling of both intrinsic and extrinsic muscles for index, middle, ring, and little fingers

This procedure helps translate data from one musculoskeletal model to another

This procedure, deriving moment arm values from anatomical attachments and using a data-driven optimization to identify muscle-tendon paths, is capable of helping translate data from one musculoskeletal model to another. Scaling is typically performed based on body segment lengths or limb circumferences. For example, An et al. (1979) scaled hand muscle attachment measured in 10 hand specimens by normalizing middle phalanx length. An et al. (1981) scaled elbow muscle moment arms by the cross-sectional area of the dissected forearm. Murray et al. (2002) scaled peak moment arms of elbow muscles with the shorter distance between the elbow flexion axis and a muscle's origin and insertion. However, previous approaches have limitations to apply for hand muscles. Intrinsic hand muscles have not reported yet, moment arms at PIP and DIP joints reported not continuous values but average constant values (An et al., 1983), and to represent endpoint forces we need accurate axes of rotation but do not have their orientations (Wohlman et al., 2013). To translate functional and anatomical data, previous studies need continuous moment arm values, muscle attachment points and coordinate system including Euler angle describing the orientation of segments and the axes of rotation. Our approach enables anatomical data to be translated to another musculoskeletal model without measured data: moment arm curves and joint kinematics.

In conclusion, partial velocity method successfully derived moment arms from anatomic muscle/tendon attachments measured by An et al. (1979), and our data-driven optimizations discovered muscle-tendon paths for the highly accurate musculoskeletal model of the human

hand that resulted in moment arms that fitted experimental values estimated from anatomic muscle/tendon locations. Moment arms derived anatomic muscle attachments were non-constants that changed with angle in a non-linear fashion. This complete musculoskeletal model of the hand can be dedicated to more accurate analysis of internal musculoskeletal loading during multi-touch tasks involving many fingers, and use the simulation to better understand complex multi-touch and gestural movements, and potentially guide the design of technologies that reduce injury risk.

Table 1. Mean moment arms (MA) of the index finger. All are expressed in millimeters (mm) in OpenSim: flexion(+)/extension(-) and abduction(+)/adduction(-) for MCP, PIP and DIP joints. Parentheses indicate RMS error (Δ) between OpenSim model and experimentally-measured values (An et al., 1983). VAF represents Variance Accounted For, and Error represents percentage erro

Joint	RoM		FDP	FDS	EDC(ES)	LU(RB)	RI	UI(UB)
MCP 2	0°~90° Flex/Ext	MA	11.54	12.42	-7.44	3.46	6.61	1.96
		(VAF)	(98.7%)	(99.5%)	(91.2%)	(73.0%)	(54.9%)	(48.1%)
		RMS	Δ0.16	Δ0.07	Δ0.66	Δ0.85	Δ0.27	Δ0.31
		(Error)	(1.23%)	(0.50%)	(7.73%)	(19.70%)	(45.79%)	(53.40%)
	0°~30° Ab/Add	MA	2.79	1.51	-1.01	4.30	-4.07	-6.85
		(VAF)	(75.3%)	(68.0%)	(90.1%)	(66.4%)	(84.5%)	(55.8%)
		RMS	Δ0.70	Δ0.53	Δ0.10	Δ0.55	Δ0.24	Δ0.36
		(Error)	(24.08%)	(32.21%)	(8.67%)	(50.61%)	(4.35%)	(6.90%)
PIP 2	0°~90° Flex/Ext	MA	8.51	6.22	-2.47	-1.82		0.80
		(VAF)	(82.4%)	(89.1%)	(78.1%)	(47.7%)		(78.1%)
		RMS	Δ0.31	Δ0.73	Δ0.43	Δ0.19		Δ1.32
		(Error)	(16.28%)	(9.52%)	(63.83%)	(14.25%)		(36.25%)
DIP 2	0°~50° Flex/Ext	MA	4.14		-0.88			
		(VAF)	(93.1%)		(63.8%)			
		RMS	Δ0.54		Δ0.78			
		(Error)	(7.94%)		(76.77%)			

Table 2. Mean moment arms (MA) of the middle finger. All are expressed in millimeters (mm) in OpenSim: flexion(+)/extension(-) and abduction(+)/adduction(-) for MCP, PIP and DIP joints. Parentheses indicate RMS error (Δ) between OpenSim model and experimentally-derived values (An et al., 1979). VAF represents Variance Accounted For, and Error represents percentage error

Joint	RoM		FDP	FDS	EDC(ES)	LU(RB)	RI	UI(UB)
MCP3	0°~90° Flex/Ext	MA	13.05	17.07	-8.56	3.75	7.20	2.94
		(VAF)	(98.7%)	(99.5%)	(91.2%)	(73.0%)	(98.0%)	(48.2%)
		RMS	Δ0.39	Δ0.44	Δ0.42	Δ1.02	Δ0.34	Δ1.49
		(Error)	(2.36%)	(2.16%)	(4.39%)	(6.51%)	(3.19%)	(24.16%)
	0°~30° Ab/Add	MA	-0.18	1.54	-0.37	5.90	6.93	-3.86
		(VAF)	(75.3%)	(68.0%)	(90.1%)	(66.4%)	(66.8%)	(92.1%)
		RMS	Δ0.72	Δ0.86	Δ0.09	Δ3.86	Δ2.30	Δ0.91
		(Error)	(87.18%)	(1.65%)	(7.80%)	(7.50%)	(24.20%)	(24.15%)
PIP3	0°~90° Flex/Ext	MA	7.63	6.07	-0.25	-2.97		-1.06
		(VAF)	(90.1%)	(87.1%)	(44.1%)	(47.7%)		(99.6%)
		RMS	Δ0.28	Δ0.40	Δ2.64	Δ2.14		Δ1.34
		(Error)	(1.40%)	(5.68%)	(26.40%)	(92.89%)		(82.82%)
DIP3	0°~50° Flex/Ext	MA	4.11		-2.38			
		(VAF)	(93.1%)		(63.8%)			
		RMS	Δ0.58		Δ0.60			
		(Error)	(12.43%)		(6.32%)			

Table 3. Mean moment arms (MA) of the ring finger. All are expressed in millimeters (mm) in OpenSim: flexion(+)/extension(-) and abduction(+)/adduction(-) for MCP, PIP and DIP joints. Parentheses indicate RMS error (Δ) between OpenSim model and experimentally-derived values (An et al., 1979). VAF represents Variance Accounted For, and Error represents percentage error

Joint	RoM		FDP	FDS	EDC(ES)	LU(RB)	RI	UI(UB)
MCP4	0°~90° Flex/Ext	MA	11.73	12.40	-6.78	3.77	6.37	2.39
		(VAF)	(96.4%)	(92.8%)	(96.5%)	(76.3%)	(76.4%)	(78.5%)
		RMS	Δ0.43	Δ0.91	Δ0.25	Δ0.91	Δ1.51	Δ0.59
		(Error)	(3.56%)	(4.16%)	(0.24%)	(4.98%)	(4.28%)	(14.86%)
	0°~30° Ab/Add	MA	1.18	1.15	1.03	4.64	6.45	-2.58
		(VAF)	(46.3%)	(48.2%)	(64.3%)	(98.8%)	(95.5%)	(22.8%)
		RMS	Δ0.91	Δ0.88	Δ0.40	Δ0.06	Δ0.29	Δ0.85
		(Error)	(32.70%)	(15.13%)	(4.09%)	(1.10%)	(4.52%)	(44.03%)
PIP4	0°~90° Flex/Ext	MA	6.88	5.63	-1.80	-1.64		-0.86
		(VAF)	(95.5%)	(94.2%)	(93.4%)	(77.7%)		(67.9%)
		RMS	Δ0.33	Δ0.33	Δ0.35	Δ1.14		Δ0.31
		(Error)	(4.42%)	(4.63%)	(4.80%)	(71.13%)		(10.78%)
DIP4	0°~50° Flex/Ext	MA	4.92		-2.06			
		(VAF)	(80.9%)		(87.4%)			
		RMS	Δ0.96		Δ0.32			
		(Error)	(18.76%)		(6.75%)			

Table 4. Mean moment arms (MA) of the little finger. All are expressed in millimeters (mm) in OpenSim: flexion(+)/extension(-) and abduction(+)/adduction(-) for MCP, PIP and DIP joints. Parentheses indicate RMS error (Δ) between OpenSim model and experimentally-derived values (An et al., 1979). VAF represents Variance Accounted For, and Error represents percentage error.

Joint	RoM		FDP	FDS	EDC(ES)	LU(RB)	RI	UI(UB)
MCP5	0°~90° Flex/Ext	MA	9.55	10.10	-1.98	8.95	6.02	-8.66
		(VAF)	(98.9%)	(94.8%)	(90.2%)	(90.2%)	(56.3%)	(91.1%)
		RMS	Δ0.11	Δ0.57	Δ0.23	Δ0.88	Δ2.66	Δ0.59
		(Error)	(0.22%)	(18.48%)	(0.93%)	(8.44%)	(21.38%)	(0.78%)
	0°~30° Ab/Add	MA	2.00	2.59	1.36	9.87	10.01	-8.76
		(VAF)	(55.7%)	(27.1%)	(77.7%)	(33.9%)	(37.2%)	(97.6%)
		RMS	Δ3.47	Δ0.39	Δ1.40	Δ6.54	Δ6.31	Δ0.21
		(Error)	(92.70%)	(80.49%)	(67.72%)	(66.03%)	(91.97%)	(1.14%)
PIP5	0°~90° Flex/Ext	MA	7.00	7.92	-1.29	-1.02		-0.06
		(VAF)	(93.1%)	(97.2%)	(90.6%)	(98.6%)		(99.5%)
		RMS	Δ0.49	Δ0.22	Δ0.25	Δ0.13		Δ0.25
		(Error)	(6.21%)	(0.02%)	(13.01%)	(5.37%)		(137.92%)
DIP5	0°~50° Flex/Ext	MA	5.43		-2.16			
		(VAF)	(98.2%)		(83.4%)			
		RMS	Δ0.10		Δ0.38			
		(Error)	(1.54%)		(3.53%)			

Table 5. Anthropometric index finger dimensions of cadaveric specimens An (1983) and OpenSim model (mm). Symbol (±) indicates standard deviation in interspecimen variation. Lengths of the phalanges in OpenSim model are calculated by the distance between the origins of two coordinate systems in three-dimensional (3D) Cartesian space, e.g., the center of rotation at MCP and the center of rotation at PIP. Parentheses (Δ) in OpenSim bony dimensions express difference between model dimension and specimen dimension. Skin surface set is scaled in three-dimensions to preserve the anatomical proportions of Fowler et al. (2001), Greiner (1991) and Li et al. (2008). These skin surface (external dimensions) function as upper boundary constraints during optimization.

	Specimens bony dimensions	**OpenSim bony dimensions**	**Skin surface scaled**
Distal phalanx length	19.67±1.03	19.10 (Δ0.57)	30.65
Middle phalanx length	24.67±0.98	25.10 (Δ0.43)	27.22
Proximal phalanx length	43.57±0.98	42.60 (Δ0.97)	50.86
DIP joint thickness	5.58±0.92	4.95 (Δ0.63)	14.38
PIP joint thickness	7.57±0.45	7.31 (Δ0.26)	18.86
MCP joint thickness	15.57±0.84	17.08 (Δ1.51)	27.80

Table 6. Index finger muscle-tendon locations, expressed in OpenSim frame (mm). The coordinate system of the OpenSim model is attached to metacarpal (secondmc), proximal (proxph2), middle (midph2) and distal (distph2) phalanges. x, y and z components indicate radioulnar (+ points out, perpendicular to the palm plan), axial (+ points from distal to proximal side) and dorsolar (+ points up, from palm to hand side) respectively.

Joint	**Muscles**	**x**	**y**	**z**	**x**	**y**	**z**
		proximal point (secondmc)			distal point (proxph2)		
MCP2	FDP	5.006	-16.539	-3.605	2.144	-26.237	-4.267
	FDS	5.861	-13.773	-0.659	2.088	-8.414	-12.006
	RI	9.556	-19.964	-4.924	8.517	-7.082	0.193
	LU	10.174	-26.472	-0.014	8.380	-8.291	0.043
	UI	-3.323	-29.390	-0.124	-4.312	-15.931	2.413
	EDC	3.045	-29.509	12.430	3.308	-7.107	11.640
		proximal point (proxph2)			distal point (midph2)		
PIP2	FDP	2.742	-36.501	1.273	-1.841	-9.839	-2.703
	LU (RB)	13.074	-33.051	11.192	2.001	-6.120	4.701
	UI (UB)	1.053	-35.973	7.612	2.921	-7.730	4.621
	FDS	6.345	-36.775	2.315	1.312	-9.041	-3.399
	EDC (ES)	6.342	-24.241	12.191	1.861	-0.102	5.414
		proximal point (midph2)			distal point (distph2)		
DIP2	TE	3.910	-16.534	4.132	2.620	-8.070	1.630
	FDP	1.324	-20.959	-1.646	1.564	-10.193	-2.916

Table 7. Middle finger muscle-tendon locations, expressed in OpenSim frame (mm).

Joint	Muscles	x	y	z	x	y	z
		proximal point (thirdmc)			distal point (proxph3)		
MCP3	FDP	-0.973	-8.368	-6.185	1.545	-15.019	-7.646
	FDS	2.236	-10.874	-13.446	2.437	-19.191	-8.006
	RI	9.094	-4.311	1.481	7.988	-2.016	-8.019
	LU	10.252	-23.168	-0.825	6.840	-21.962	7.261
	UI	-6.721	-24.631	-2.008	-6.164	-23.125	8.369
	EDC	0.858	-35.104	14.174	1.738	-14.787	7.915
		proximal point (proxph3)			distal point (midph3)		
PIP3	FDP	-0.746	-37.000	2.350	-3.638	-6.369	-7.129
	LU (RB)	3.002	-39.747	10.070	2.511	-5.104	6.554
	UI (UB)	-0.400	-39.940	10.535	-1.100	-9.913	7.009
	FDS	2.551	-39.274	0.581	0.532	-12.210	-1.923
	EDC (ES)	-2.116	-36.999	2.917	1.994	-14.148	11.986
		proximal point (midph3)			distal point (distph3)		
DIP3	TE	0.735	-20.531	7.520	1.865	-11.051	3.480
	FDP	-1.000	-19.568	-0.998	0.122	-13.402	-1.352

Table 8. Ring finger muscle-tendon locations, expressed in OpenSim frame (mm).

Joint	Muscles	x	y	z	x	y	z
		proximal point (fourthmc)			distal point (proxph4)		
MCP4	FDP	-0.470	-10.548	-8.319	1.794	-19.902	-4.000
	FDS	-0.541	-10.446	-8.941	1.925	-19.967	-4.937
	RI	7.876	-14.419	0.313	3.129	-24.336	0.110
	LU	6.012	-5.433	-6.720	4.941	-10.520	5.294
	UI	-5.096	-22.187	-4.160	2.998	-16.573	-7.492
	EDC	-1.264	-19.347	8.177	-0.480	-9.395	14.182
		proximal point (proxph4)			distal point (midph4)		
PIP4	FDP	-2.926	-33.255	-5.816	1.178	-8.730	-6.849
	LU (RB)	1.711	-30.448	5.939	0.466	-4.916	4.801
	UI (UB)	-8.570	-40.061	4.472	-2.204	-6.159	2.273
	FDS	1.143	-33.076	-6.319	-0.875	-14.713	-2.067
	EDC (ES)	-4.742	-42.431	8.620	1.822	-14.258	9.945
		proximal point (midph4)			distal point (distph4)		
DIP4	TE	-4.150	-22.180	5.650	-1.950	-7.800	2.750
	FDP	-1.921	-18.052	-3.237	0.180	-13.954	-2.164

Table 9. Little finger muscle-tendon locations, expressed in OpenSim frame (mm).

Joint	Muscles	x	y	z	x	y	z
		proximal point (fifthmc)			distal point (proxph5)		
MCP5	FDP	2.607	-0.022	-3.540	-0.005	-14.639	-5.003
	FDS	4.451	-0.952	-4.962	1.823	-14.312	-5.462
	RI	9.017	-16.218	-4.985	8.052	-37.892	0.202
	LU	8.512	-0.091	-0.923	6.690	-18.142	0.471
	UI	0.512	7.871	-2.212	-9.492	-11.443	0.712
	EDC	-0.044	-18.404	5.227	-2.683	-19.037	4.025
		proximal point (proxph5)			distal point (midph5)		
PIP5	FDP	-3.06	-25.941	-9.280	0.095	-8.958	-6.143
	LU (RB)	-4.944	-33.359	0.265	-3.059	-8.338	4.124
	UI (UB)	-8.452	-34.267	-1.186	-6.429	-8.501	4.996
	FDS	1.103	-26.254	-12.262	1.109	-18.248	-4.588
	EDC (ES)	-7.601	-34.002	1.304	-3.234	-10.233	2.193
		proximal point (midph5)			distal point (distph5)		
DIP5	TE	-3.603	-19.040	0.220	-2.071	-7.242	0.210
	FDP	-2.355	-15.238	-4.663	-0.028	-13.925	-4.752

Figure 1. Measured and derived moment arms (mm) with flexion (+)/ extension (-) at the MCP joint of the index finger. Dotted moment arm values are derived from experimental muscle attachments (An et al., 1979), and solid moment arm values are those directly-measured by An et al., 1983 (n=7 specimens with mean and standard deviation (error bar)). Positive values indicate flexion moment arms, negative values indicate extension moment arms, and 0° flexion is full extension.

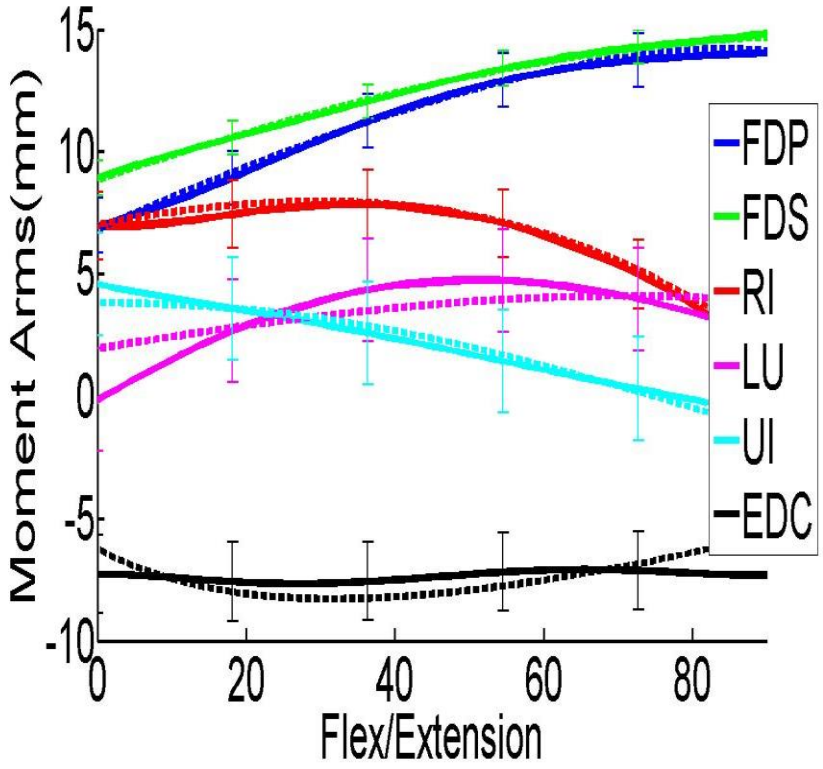

Figure 2. Moment arms (mm) with flexion (+)/ extension (-) at the MCP joint of the all fingers. Dotted moment arm values are derived from experimentally-measured muscle attachments (An et al., 1979), and solid moment arm values are those directly measured by An et al., 1983 (n=7 specimens with mean and standard deviation). Positive values indicate flexion moment arms, negative values indicate extension moment arms, and 0° flexion is full extension.

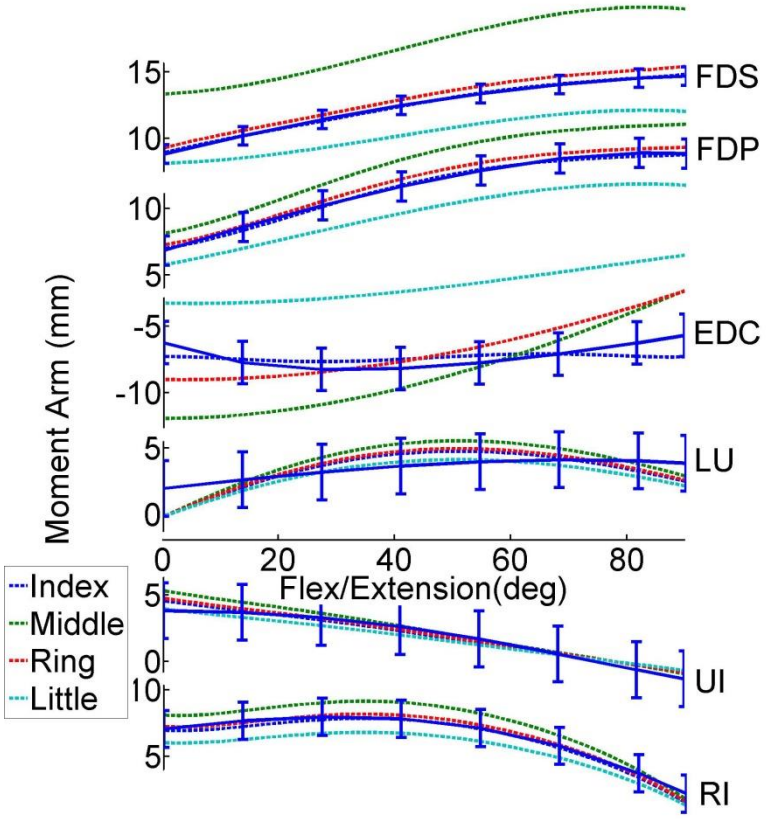

Figure 3. Moment arms (mm) with adduction (+)/ abduction (-) at the MCP joint of the all fingers

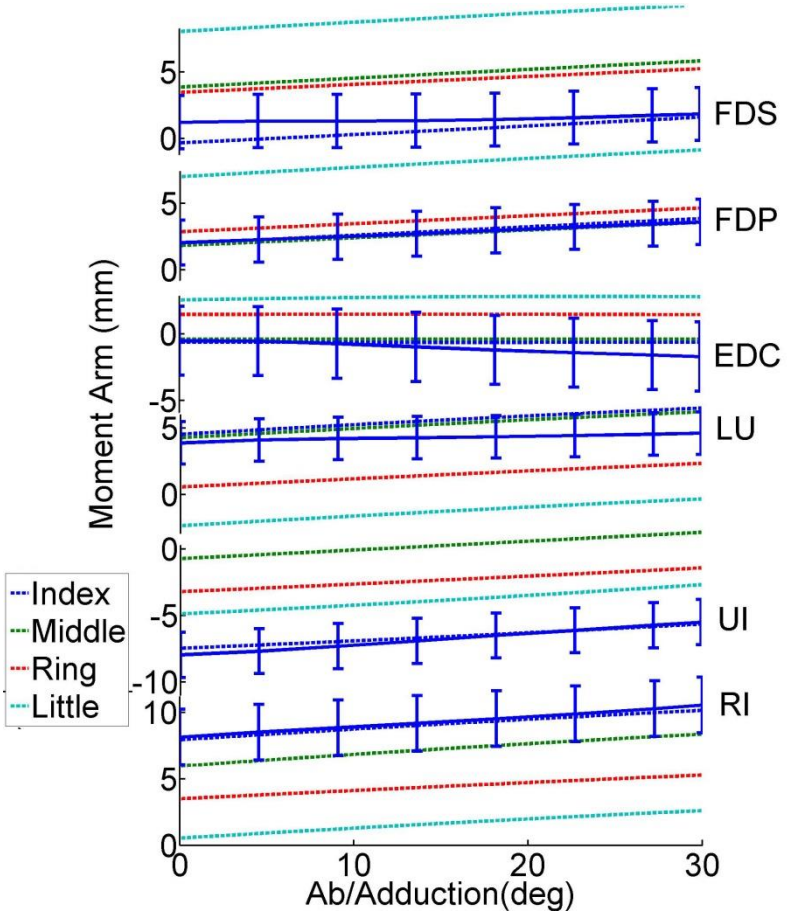

Figure 4. Moment arms (mm) with flexion (+)/ extension (-) at the PIP and DIP joint of the all fingers

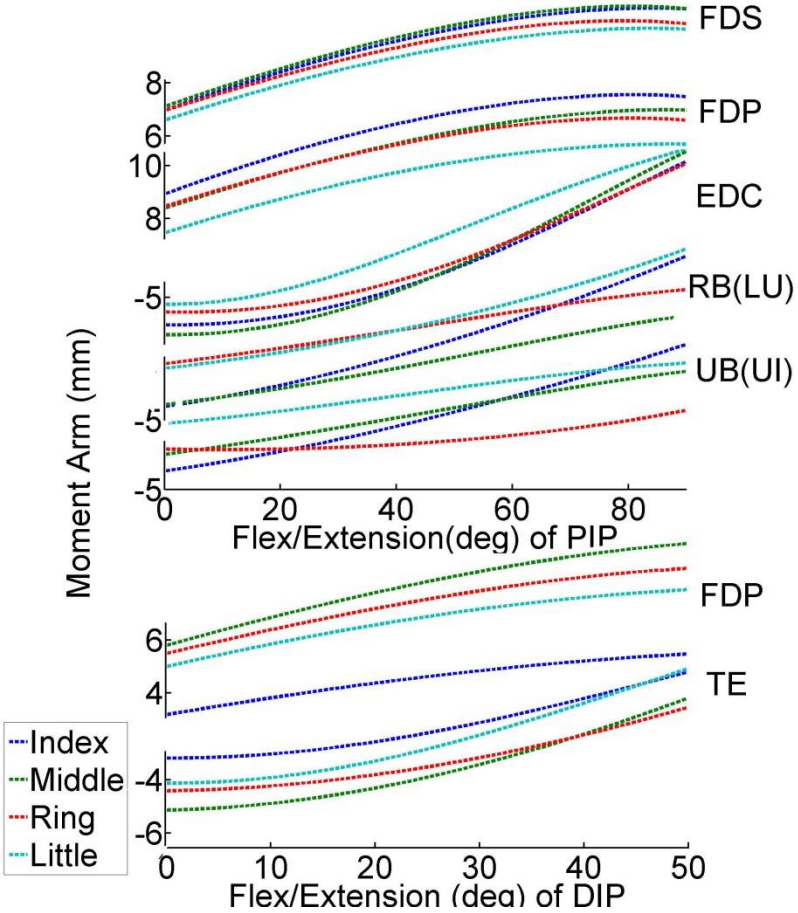

Figure 5. Index finger moment arm values (in millimeters). Solid moment arms are calculated values using partial velocity method, and dotted moment arms are optimized values using a data-driven method. Positive values indicate flexion moment arms, negative values indicate extension moment arms, and 0° flexion is full extension.

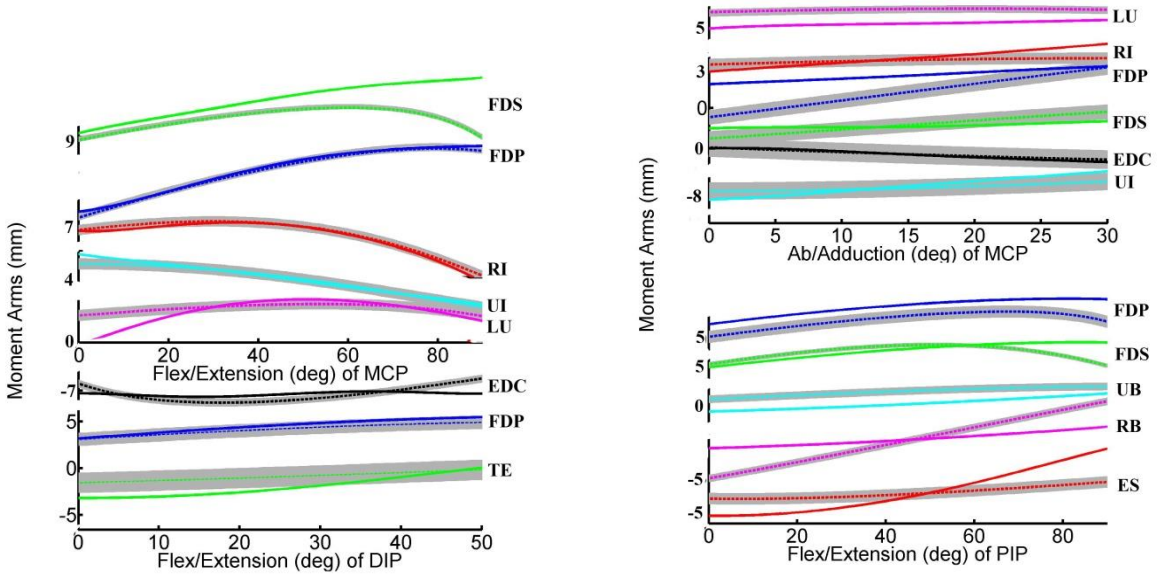

Figure 6. Middle finger moment arm values (mm).

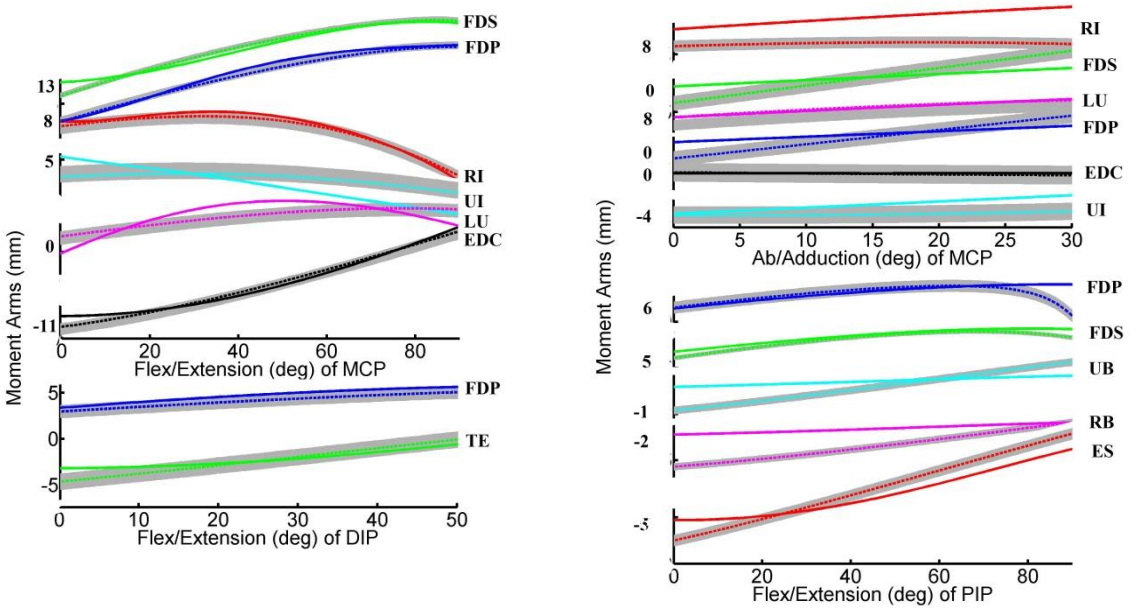

Figure 7. Ring finger moment arm values (mm).

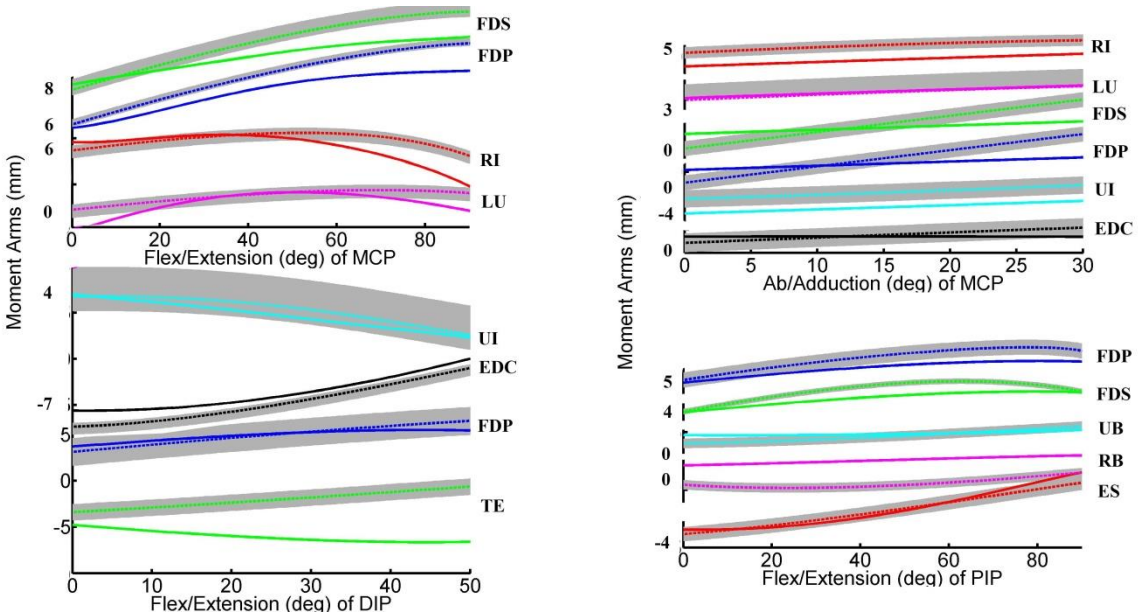

Figure 8. Little finger moment arm values (mm).

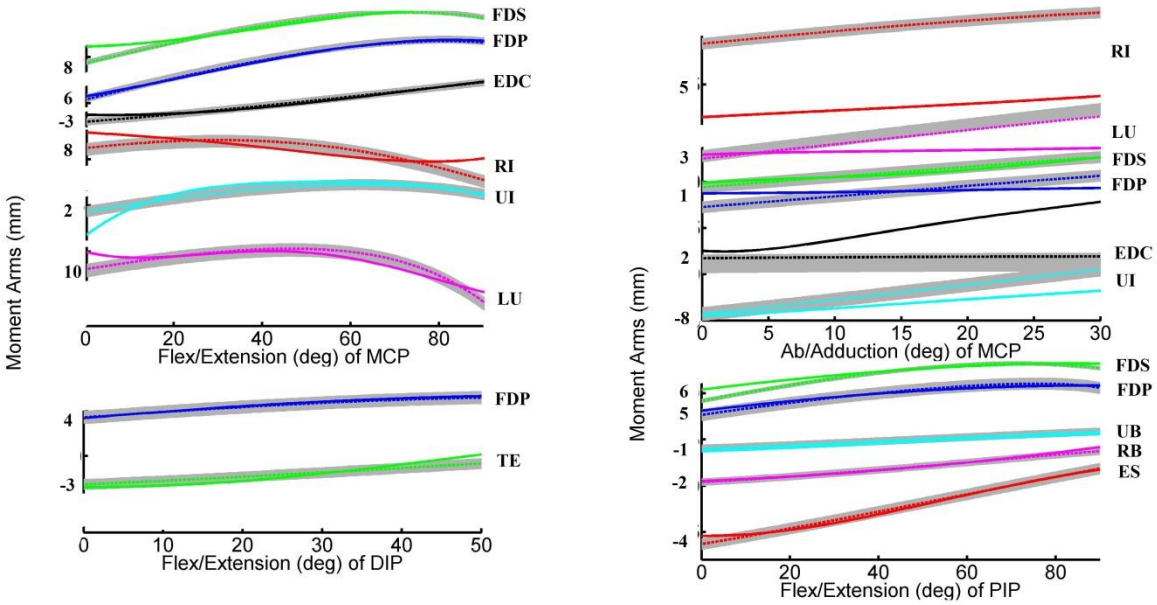

REFERENCES

Albrecht I, Haber J, Seidel HP, et al. (2003) Construction and animation of anatomically based human hand models. ACM SIGGRAPH/EG Symposium on Computer Animation (SCA'03), 98-109.

Alexander B, Viktor K, et al. (2010) Proportions of hand segments. International Journal of Morphology, 28(3):755-758.

An KN, Chao EY, Cooney WP, Linscheid RL, et al. (1979) Normative model of human hand for biomechanical analysis. Journal of Biomechanics 12, 775-788.

An KN, Hui FC, Morrey BF, Linscheid RL, Chao EY, et al. (1981) Muscles across the elbow joint: a biomechanical analysis. Journal of Biomechanics 14, 659-669.

An KN, Ueba Y, Chao EY, Cooney WP, Linscheid RL, et al. (1983) Tendon excursion and moment arm of index finger muscles. Journal of Biomechanics 16, 419-425.

Armstrong TJ and Chaffin DB, et al. (1978) An investigation of the relationship between displacements of the finger and wrist joints and the extrinsic finger flexor tensions. Journal of Biomechanics 11, 119-128.

Arnold AS, Salinas S, Asakawa DJ, Delp SL, et al. (2000) Accuracy of muscle moment arms estimated from MRI-based musculoskeletal models of the lower extremity. Computer Aided Surgery, 108-119.

Biggs J, Horch K, et al. (1999) A three-dimensional kinematic model of the human long finger and the muscles that actuate it. Medical Engineering & Physics 21, 625-639.

Brand PW, Cranor KC, Ellis JC, et al. (1975) Tendon and pulleys at the metacarpophalangeal joint of a finger. Journal of Bone and Joint Surgery, 57, 779-784.

Brand PW, Hollister A, et al. (1993) Clinical mechanics of the hand. Mosby.

Brochier T, Spinks RL, Umilta MA, Lemon RN, et al. (2004) Patterns of muscle activity underlying object-specific grasp by the macaque monkey. Journal of Neurophysiology 92, 1770–1782.

Brook N, Mizrahi J, Shoham M, Dayan J, et al. (1995) A biomechanical model of index finger dynamics. Medical Engineering & Physics 17(1): 54-63.

Buchner HJ1, Hines MJ, Hemami H, et al. (1988) A dynamic model for finger interphalangeal coordination. Journal of Biomechanics, 21(6):459-68.

Buford Jr. WL, Koh S, Andersen CR, Viegas SF, et al. (2005) Analysis of intrinsic-extrinsic muscle function through interactive 3-dimensional kinematic simulation and cadaver studies. The Journal of Hand Surgery (A) 30, 1267-1275.

Chao EY, An KN, Cooney W, Linscheid R, et al. (1989) Normative model of human hand, Biomechanics of the Hand. World Scientific, Singapore, pp. 5-30.

Cholewicki J1, McGill SM, et al. (1994) EMG assisted optimization: a hybrid approach for estimating muscle forces in an indeterminate biomechanical model, Journal of Biomechanics. Oct;27(10):1287-9.

Delp SL, Loan JP, Hoy MG, Zajac FE, Topp EL, Rosen JM, et al. (1990) An interactive graphics-based model of the lower extremity to study orthopaedic surgical procedures, IEEE Transactions on Biomedical Engineering 37, 757-767.

Delp SL, Loan JP, et al. (1995) A graphics-based software system to develop and analyze models of musculoskeletal structures. Computers in Biology and Medicine 25(1), 21-34.

Delp SL, Anderson FC, Arnold AS, Loan P, Habib A, John CT, et al. (2007) Opensim: open-source software to create and analyze dynamic simulations of movement. IEEE Transactions on Biomedical Engineering 54(11), 1940-1950.

Dennerlein JT, Mote CD, Jr. Rempel DM, et al. (1998) Control strategies for finger movement during touch-typing: The role of the flexor and extensor muscles. Experimental Brain Research, 121:1-6.

Dennerlein JT1, Diao E, Mote CD Jr, Rempel DM, et al. (1999) In vivo finger flexor tendon force while tapping on a keyswitch. Journal of Orthopaedic Research Mar;17(2):178-84.

Fowler NK, Nicol AC, Condon B, Hadley D, et al. (2001) Method of determination of three dimensional index finger moment arms and tendon lines of action using high resolution MRI scans. Journal of Biomechanics 34, 791-797.

Franko OI, Winters TM, Tirrell TF, Hentzen ER, Lieber RL, et al. (2011) Moment arms of the human digital flexors. Journal of Biomechanics 44, 1987-1990.

Garner BA, Pandy MG, et al. (2000) The obstacle-set method for representing muscle paths in musculoskeletal models. Computer Methods in Biomechanics and Biomedical Engineering 3, 1-30.

Greiner TM, (1991) Hand Anthropometry of US Army Personnel. United States Natick Research, Development and Engineering Center, Natick, MA, Document AD-A244 533.

Hollister A1, Buford WL, Myers LM, Giurintano DJ, Novick A, et al. (1992) The axes of rotation of the thumb carpometacarpal joint. Journal of Orthopaedic Research. 10(3):454-60.

Hollister A1, Giurintano DJ, Buford WL, Myers LM, Novick A, et al. (1995) The axes of rotation of the thumb interphalangeal and metacarpophalangeal joints. Clinical Orthopedics and Related Research, (320):188-93.

Holzbaur KRS, Murray WM, Delp SL, et al. (2005) A model of the upper extremity for simulating musculoskeletal surgery and analyzing neuromuscular control. Annals of Biomedical Engineering 33(6). 829-840.

Kamper DG, Fischer HC, Cruz EG, et al. (2006) Impact of finger posture on mapping from muscle activation to joint torque. Clinical Biomechanics 21. 361-369.

Kane TR, Levinson DA, et al. (1985) Dynamics: Theory and applications, New York, McGraw-Hill.

Kelley CT, (1999) Iterative methods for optimization. SIAM, Philadelphia.

Ketchum LD, Brand PW, Thompson D, Pocock GS, et al. (1978) The determination of moments for extension of the wrist generated by muscles of the forearm. The Journal of Hand Surgery (A) 3, 205-210.

Kirkpatrick S, Gelatt CD, Vecchi MP, et al. (1983) Optimization by simulated annealing. Science 220(4598), 671-680.

Kociolek AM, Keir PJ, et al. (2011) Modelling tendon excursions and moment arms of the finger flexors: Anatomic fidelity versus function. Journal of Biomechanics 44, 1967-1973.

Kurse MU, Lipson H, Valero-Cuevas FJ, et al. (2012) Extrapolatable analytical functions for tendon excursions and moment arms from sparse datasets. IEEE Transactions on Biomedical Engineering, 59 (6) 1572-1581.

Landsmeer JM, (1961) Studies in the anatomy of articulation. I. The equilibrium of the "intercalated" bone. Acta Morphologica Neerlanddo – Scandinavica 3, 287-303.

Lee JH, Asakawa DS, Dennerlein JT, Jindrich DL, et al. (2014) Using optimization to determine attachment points for extrinsic and intrinsic muscles of the index finger on an OpenSim model of the hand. Journal of Biomechanics, In press.

Lee JW, Rim K, et al. (1990) Maximum finger force prediction using a planar simulation of the middle finger. Proceedings of the Institution of Mechanical Engineers, Part H: Journal of Engineering in Medicine. 204(3):169-78.

Leijnse JN, Kalker JJ, et al. (1995) A two-dimensional kinematic model of the lumbrical in the human finger. Journal of Biomechanics, 28(3):237-49.

Li Z, Chang CC, Dempsey PG, Ouyang L, Duan J, et al. (2008) Validation of a three-dimensional hand scanning and dimension extraction method with dimension data. Ergonomics 51(11), 1672-1692.

Lopes MM, Lawson W, Scott T, Keir PJ, et al. (2011) Tendon and nerve excursion in the carpal tunnel in healty and CTD wrists. Clinical Biomechanics.

Murray WM, Delp SL, Buchanan TS, et al. (1995) Variation of muscle moment arms with elbow and forearm position. Journal of Biomechanics 28, 513-525.

Murray WM, Buchanan TS, Delp SL, et al. (2002) Scaling of peak moment arms of elbow muscles with upper extremity bone dimensions. Journal of Biomechanics 35, 19-26.

Oh S, Belohlaverk M, Zhao C, Osamura N, Zobitz ME, An KN, Amadio PC, et al. (2007) Detection of differential gliding characteristics of the flexor digitorum superficialis tendon and subsynovial connective tissue using color Doppler sonographic imaging. Journal of Ultrasound in Medicine: Official Journal of the American Institute of Ultrasound in Medicine 26(2), 149-155.

Rankin JW, Neptune RR, et al. (2012) Musculotendon lengths and moment arms for a three-dimensional upper-extremity model. Journal of Biomechanics 45, 1739-1744.

Rekimoto J, (2002) Smartskin: An infrastructure for freehand manipulation on interactive surfaces. Proceedings of the SIGCHI conference on human factors in computing systems.

Rubine D, (1991) Specifying gestures by example. Proceedings of the 18th annual conference on Computer graphics and interactive techniques 25(4).

Sancho-Bru JL, Perez-Gonzalez A, Vergara-Monedero M, Giurintano D, et al. (2001) A 3-D dynamic model of human finger for studying free movements. Journal of Biomechanics 34, 1491-1500.

Sancho-Bru JL, Perez-Gonzalez A, Vergara M, Giurintano DJ, et al. (2003) A 3d biomechanical model of the hand for power grip. Journal of Biomechanical Engineering 125 (1), 78-83.

Schutte LM, Rodgers MM, Zajac FE, Glaser RM, et al. (1993) Improving the efficacy of electrical stimulation-induced leg cycle erometry: an analysis based on a dynamics musculoskeletal model. IEEE Transactions on Rehabilitation Engineering 1(2), 109-125.

Seth A, Sherman M, Reinbolt JA, Delp SL, et al. (2011) OpenSim: a musculoskeletal modeling and simulation framework for in silico investigations and exchange. 2011 Symposium on Human Body Dynamics, 212-232.

Spoor CW, Landsmeer JMF, et al. (1976) Analysis of the zigzag movement of the human finger under the influence of the extensor digitorum and the deep flexor tendon. Journal of Biomechnaics 9, 561-566.

Thelen DG, (2003) Adjustment of muscle mechanics model parameters to simulate dynamics contractions in older adults. Journal of Biomechanical Engineering 125(1), 70-77.

Tsang W, Singh K, Fiume E, et al. (2005) Helping hand: An anatomically accurate inverse dynamics solution for unconstrained hand motion. In SCA'05: Proc 2005 ACM SIGGRAPH/EG Symposium on Computer Animation, 319-328.

Valero-Cuevas FJ1, Zajac FE, Burgar CG, et al. (1998) Large index-fingertip forces are produced by subject-independent patterns of muscle excitation. Journal of Boimechanics 31(8):693-703.

Valero-Cuevas FJ, (2005) An integrative approach to the biomechanical function and neuromuscular control of the fingers. Journal of Boimechanics 38 (4), 673-684.

Valero-Cuevas FJ, Johanson ME, Towles JD, et al. (2003) Towards a realistic biomechanical model of the thumb: the choice of kinematic description may be more critical than the solution method or the variability/uncertainty of musculoskeletal parameters. Journal of Biomechanics 36, 1019-1030.

Wohlman SJ, Murray WM, et al. (2013) Bridging the gap between cadaveric and in vivo experiments: A biomechanical model evaluating thumb-tip endpoint forces. Journal of Biomechanics 46(5) 1014-1020.

Wu M, Balakrishna R, et al. (2003) Multi-finger and whole hand gestural interaction techniques for multi-user tabletop displays. Proceedings of the 16th annual ACM symposium on User interface software and technology.

Wu J, An KN, Cutlip RG, Dong RG, et al. (2010) A practical biomechanical model of the index finger simulating the kinematics of the muscle/tendon excursions. Bio-Medical Materials and Engineering 20, 89-97.

Yoshii Y, Villarraga HR, Henderson J, Zhao C, An KN, Amadio PC, et al. (2009) Speckle tracking ultrasound for assessment of the relative motion of flexor tendon and subsynovial connective tissue in the human carpal tunnel. Ultrasound in Medicine and Biology 35(12), 1973-1981.

Zajac FE, Cottlieb GL, et al. (1989) Muscle and tendon: properties, models, scaling, and application to biomechancis and motor control. Critical Reviews in Biomedical Engineering 17(4), 359-411.Ackland, D.C., Lin, Y.C., Pandy, M.G., 2012. Sensitivity of model predictions of muscle function to changes in moment arms and muscle-tendon properties: A Monte-Carlo analysis. Journal of Biomechanics 45, 1461-1471.

https://simtk.org/project/xml/downloads.xml?group_id=660 Matlab-Opensim API.

CHAPTER 4

ANALYSIS OF INDEX FINGER MUSCLE ACTIVITY DURING TWO FINGER GESTURES ON A TABLET COMPUTER

Abstract

Predicting neuromuscular activations during multi-touch interacting with a tablet computer is still challenging questions. Estimates of musculoskeletal loading, i.e., joint torque, muscle force and activity help understand the cumulative effects of long-term exposures that can lead to injuries. The objective of this study was to compare joint torque, muscle force and activity of the index finger during gestural tasks: zoom in & out, and rotate left & right on the tablet computer. We hypothesized that zooming motion could arouse greater extrinsic muscle activations, whereas rotating motion could arouse greater intrinsic muscle activations because extrinsic muscles control crude movements along with the sagittal (vertical) plane, while intrinsic muscles are responsible for the fine motor functions on the transverse (horizontal) plane. A three-dimensional musculoskeletal model of the upper extremity was used to calculate intrinsic/extrinsic muscle force and activity of twelve subjects while they performed two finger gestures: thumb and index finger for zooming and rotating with interacting multi-touch tablet technology. On the OpenSim platform, we used Computed Muscle Control (CMC) to evaluate a set of muscle excitations (or, more generally, actuator controls) that drive a dynamic musculoskeletal model to track a set of subjects desired kinematics in the presence of two finger gestures. We observed that extrinsic muscle activations of zoom in & out were higher than those of rotate left & right, and intrinsic muscle activations were higher than extrinsic ones for rotate left & right. This study suggests that gestural tablet interaction can alter muscle activation: intrinsic muscles get more involved in rotate gestures on the tablet.

INTRODUCTION

With the advent of multi-touch technology, we often use handheld devices such as tablets and smart phones in our daily life. There is no hardware keyboard or mouse. Instead, we communicate with these devices through some hand gestures, e.g., tapping, scrolling, panning, rotating and zooming (Wang et al., 2012). Technology has tried to provide a concise set of touch interactions that are used throughout a touch-screen surface. During interactions with multi-touch devices, people often touch with more than one finger as an input device (Develop Center – Windows, 2014). Although many researchers constantly strive for successful user inputs, interaction with these handheld devices controlled by fingers and thumb has little understood.

Gestural interface, i.e., particularly zoom in & out and rotate left & right on the tablet, is a significant part of handheld devices. While these zoom and rotation tasks, the index finger and thumb are involved with various postures, finger forces and muscle activities. Long-term and repetitive exposures to these conditions, e.g., awkward postures, finger forces and muscle activities may lead to musculoskeletal disorders (MSDs; Gerr et al., 2002). To avoid causing these side effects, several studies were performed to improve the ergonomic design of keyboard and determine optimal upper limb posture.

Experimental studies have explored the effect of computer keyboard keyswitch design on force-travel curves, keyswitch design guidelines, biomechanical outcomes, single keyswitch tapping, tactile and auditory feedback and motor control strategies. Typing on keyboards with higher activation forces (or make force) were associated with larger typing forces (Armstrong et al., 1994; Gerard et al., 1999; Rempel et al., 1997), hand and forearm muscle activities (Gerard et al., 1999; Rempel et al., 1997), muscle fatigue (Gerard et al., 1996; Radwin and Ruffalo,

1999), and a greater risk of hand/arm musculoskeletal symptoms and disorders for keyboards with key activation forces greater than 0.47N (Marcus et al., 2002). Key travel (or displacement) also affects applied fingertip force in that longer key travel designs are associated with smaller applied key forces (Radwin and Jeng, 1997; Radwin and Ruffalo, 1999). However, these studies have been limited to generalize the effect on tablet computers; the force-displacement characteristics are greatly different between each physical keyboard and touch screen that many are now using.

Electromyography (EMG) studies are used to evaluate muscle activity because measuring exact muscle force and excitation during performing tasks is not currently possible (Zajac and Gordon, 1989). For example, Gerard et al. (1999) have examined EMG activity to access the effects of typing force and keypad stiffness on musculoskeletal disorders (MSDs). Woods and Babski-Reeves (2005) analyzed the EMG of the hand-arm to identify the effects of posture on MSDs. The relationships among tendon force, contact force at the fingertip, and finger posture have been studied by using a force transduces mounted directly onto the flexor digitorum superficialis (FDS) and flexor digitorum profundus (FDP) tendons of the fingers (Schuind et al., 1992; Dennerlein et al., 1999; Kursa et al., 2005). Dennerlein et al. (1998) compared the experimentally measured tendon force with that calculated using an inverse dynamic approach and found that the measured tendon force is consistently greater than that predicted by the model with the muscle in an isometric contraction. The dynamic force distribution in the finger muscles during multi-touch gestures has not been investigated either experimentally or theoretically (Wu et al., 2008).

Although previous researches have contributed to reveal important information, we are still facing a lack of knowledge concerning the mechanisms of pathologic conditions associated

with multi-touch interactions. For example, how the fingers' muscle forces coordinate flexor muscles including both extrinsic and intrinsic muscles on the touch screen surface because it is not required to high forces (over 350 N) such as power grip (Monsabert et al., 2012; Vigouroux et al., 2011). Why extensor muscles are highly activated during power grip task; it is not extension but flexion task (Monsabert et al., 2012). Then, how about multi-touch tasks on the tablet? The activation of extensor as well as flexor muscles for the multi-touch tasks should be studied.

However, conducting experiments: joint torque, hand muscle tension, and muscle excitation pattern on the tablet is confronted with two major challenges. First, the measurements of the external forces exerted at the fingertip on the tablet are experimentally difficult because on-screen keys are activated even if fingers slightly contact or swipe a button on the screen (Lai et al., 2012; OSK-Windows, 2014). Second, the repartition of internal muscle tension and joint torque from external force is extremely challenging because direct measurement of hand joint forces in vivo is ethically infeasible (Zajac and Gordon, 1989). Individual muscle forces evaluated from experimental motions analysis may be useful in mathematical simulation, but require additional musculoskeletal and mathematical modeling (Blazkiewicz, 2013).

We therefore use OpenSim, an open access software package enabling to model musculoskeletal structures and dynamic simulation of movement (2.3.2, Simbios, Stanford, CA; Delp et al., 2007; Holzbaur et al., 2005; Seth et al., 2011). The developed optimization method calculates optimal forces during multi-touch tasks, given a specific performance criterion, using kinematics and kinetics from multi-touch analysis together with muscle architectural data (Blazkiewicz 2013). Because multi-touch and gestural movements involve not only the fingers,

but also the entire kinematic chain of the hand and arm, we chose to build upon ax existing upper extremity model (Holzbaur et al., 2005).

The purpose of this study was to compare muscle activity during zooming and rotating tasks on the tablet computer in twelve subjects. We hypothesized that extrinsic muscle activations for zooming tasks would be higher than intrinsic muscle activations for them, while intrinsic muscle activations for rotating tasks would be higher than extrinsic muscle activations for them. This is possibly because extrinsic muscles act as primary mover along with flex/extension movements, and intrinsic muscles act as stabilizer along with ab/adduction movements (Chao et al., 1976; Clavero et al., 2003; Darling et al., 1994; Long et al., 1970). Specifically, we conducted a series of two finger gestures experiments to test these hypotheses and estimated dynamic joint torques, muscle tensions and activations using the OpenSim model. All measurements and calculations were performed in the 27 DOFs (shoulder, elbow, wrist and multi-digit of the hand) in 3D Cartesian space. Our results show how intrinsic/extrinsic hand muscles involve in neuromuscular activation to generate finger gestures on the tablet computer. This study could provide a better understanding of hand muscle activity and its connection to finger and thumb movements on the handheld environments.

MATERIALS AND METHODS

Twelve healthy volunteers (6 males and 6 females, ages 20-30) participated in the experiments. All subjects were right-handed and free of upper extremity musculoskeletal disorders (MSDs). They have experience of a tablet computer with mean self-estimated usage times more than 40 hours per a week, which eliminated gesture/interaction familiarization time. The consent forms and procedures were approved by the Institutional Review Board of Arizona State University and were in accordance with the declaration of Helsinki.

Experimental procedure

Subjects repeated two-finger right-handed gestures on an iPad for 20 second (s) trials, while the right arm was not supported. The two-finger (thumb and index) gestures were: rotating to the right and left, zooming in and out. All gestures were performed on 2 contextual scenarios (non-contextual, when device was off; contextual, when device was on and subjects interacted with the Google Earth Globe) and 2 device position (exocentric, fixed at 15° in front of the subject while non-dominant hand was resting on the side; egocentric, held by the subject with non-supported non-dominant hand). Subjects were instructed on perform gestures on the center of the device, while looking at it and as if it was on. Each condition was presented 3 times for a total of 48 trials (4 gestures $\times$ 2 contexts $\times$ 2 device conditions $\times$ 3 replicates). The order of the gestures was randomized within set and the order of the device conditions (contextual/device position) among participants were presented in a complete counterbalance for immediate sequential effects order. We included rests between trials (20s), set of trials (5 min.) and changes of device conditions (at least 5 min.) to minimize mental/physical fatigue.

Data acquisitions

A wireless CyberGlove (CyberGlove Ⅱ, CyberGlove Systems LLC, San Jose, CA) was used for collecting joint angles of the all joint: metacarpohpalangeal (MCP), proximal interphalangeal (PIP) and distal interphalangeal (DIP) joints of the index finger, and carpometacarpal (CMC), metacarpophalangeal (MCP), and interphalangeal (IP) of the thumb. These joint angles were transformed to describe the index finger and thumb movements for Computed Muscle Control estimation on the OpenSim platform. Continuous recordings of finger motions for each experimental trial included: 5s of rest followed by 20 s of the gesture repetition.

Musculoskeletal model of the upper extremity

The Holzbaur et al. (2005) upper extremity model and Lee et al. (2014) hand model were used on the OpenSim (2.3.2, Simbios, Stanford, CA) platform because many muscles of the upper extremity crossed over multiple finger joints. This model incorporated 33 segments and 11 joints which enabled shoulder, elbow, forearm, wrist, thumb and index finger to movements in 3 dimensional (3D) Cartesian spaces. It had 15 DOFs and was actuated by 37 muscle compartments. We added intrinsic muscle on the index finger and ensured intrinsic and extrinsic hand muscles resulted in moment arm values to be matched with experimental data (Lee et al., 2014 in progress). We added mass properties and segment inertia values based on the full body model and publications (Bundhoo et al., 2005; Hamner et al., 2010; Kuo et al., 2006; Lee and Yoon, 2014; Leva, 1996; Saul et al., 2014; Wu et al., 2008). We used The Scale Tool on OpenSim to alter the anthropometry of a model so that it matches a particular subject as closely as possible. Scaling is performed based on a comparison of experimental kinematic data with virtual makers placed on a upper extremity model.

Hill type muscle model and parameters

Hill-type musculotendon model (Zajac, 1989; Winters, 1990) was implemented in OpenSim model. The force producing properties of muscle are complex, highly nonlinear and can have substantial effects on movement (McMaho, 1984). So, Hill type muscle model, lumped-parameter dimensionless muscle model capable of representing a range of muscles with different architectures, is commonly used in the dynamics simulation of movement (Zajac, 1989). The magnitude of the muscle force depends on its activation level and its force-generation properties: passive and active force–length, series elasticity, force–activation, force–velocity, maximum isometric muscle force, optimal muscle fiber length, tendon slack length and pennation angle. We adapted these physiological parameters from Holzbaure et al., (2005), Hu et al., (2011), Wu et al. (2008).

The maximum isometric muscle force is considered to proportional to the physiologic cross-section area (PCSA), i.e., $F^{max} = S \cdot PCSA$ with $\mathrm{S} = 30\mathrm{N}/cm^2$ (Epstein and Herzog, 1998). The PCSA and the optimal fiber length of the muscles are adopted from the experimental data reported by Brand and Hollister (1999) and the pennation angle of the muscles is taken from the experimental data by Lieber et al. (1990, 1992), Jacobson et al. (1992) and Wang et al. (2014) (Table 1). A tendon slack length was calculated from musculotendon excursion (Garner and Pandy, 2003; Vilimek, 2005). The ratio of fast to slow muscle fibers is considered to be 1:4 for all muscles (We et al., 2008).

Computed muscle control

Computed Muscle Control (CMC) tool on the OpenSim was used to compute a set of muscle excitations that drive a dynamic musculoskeletal model to track a set of desired kinematics measured from CyberGlove. CMC tool combined proportional-derivative (PD) control and static optimization (Thelen et al., 2006). For stable fingertip control (critically damped fashion: no over-shooting or over-damping), the velocity gains were selected using the following relation: $\vec{k}_v = 2\sqrt{\vec{k}_p}$, where $\vec{k}_v = 20$ and $\vec{k}_p = 100$. Static optimization performed on distributing the load across synergistic muscle excitations.

The activation dynamics of muscle was modeled with a first-order differential equation. This equation relates the rate of change of muscle activation (i.e., the concentration of calcium ions within the muscle) to the muscle excitation (i.e., the firing of motor units): $^{da}/_{dt} = {}^{u-a}/_{\tau(a,u)}$. Where *u* and *a* are the excitation and activation signals, respectively. In the model, activation is allowed to vary continuously between 0 (no contraction) and 1 (full contraction). In the body, the activation of a muscle is a function of the number of motor units recruited and the firing frequency of these motor units. Some models of excitation–contraction coupling distinguish these two control mechanisms (Hatze, 1976), but it is often not computationally feasible to use such models when conducting complex dynamic simulations. In a simulation, the muscle excitation signal is assumed to represent the net effect of both motor neuron recruitment and firing frequency. Like muscle activation, the excitation signal is also allowed to vary continuously between 0 (no excitation) and 1 (full excitation). The activation and deactivation time constants can be assumed to be 10 and 40 ms, respectively (Zajac, 1989; Winters, 1990).

RESULTS

Finger joint torques, muscle forces and activities for the index finger were predicted in the OpenSim platform while twelve subjects performed two finger gestures on the tablet computer. Joint torques, muscle forces and activities differ in tasks: zoom in & out and rotate left & right as shown in Figure 1- 10. Positive values of the joint angle correspond to flexion or abduction of the index finger. Flexor excursions decrease during the finger flexion, while extensor excursions increase. Muscle activation was represented between 0 (no excitation) and 1 (full excitation).

Extrinsic muscle activity for zooming was greater than intrinsic one for it.

Extrinsic muscle activations for zoom in & out were higher than those of rotate left & right (Figure 1, 3, 4). For zooming motions, activity of extrinsic muscles: flexor digitorum superficialis (FDS), flexor digitorum profundus (FDP) and extensor digitorum communis (EDC) averaged 0.4281 ranged from 0.3605 (FDS for zoom in) to 0.5506 (EDC for zoom in). For rotating movements, activity of extrinsic muscles averaged 0.2359 ranged from 0.2051 (FDS for rotate right) to 0.2955 (EDC for rotate right). Extrinsic muscle activity for zooming was 19.22% (0.1922) bigger than that for rotating.

Intrinsic muscle activations were higher than extrinsic muscle activations for rotate left & right (Figure 2, 3, 4). For rotate left & right gestures, activity of intrinsic muscles: lumbricals (LU), ulnar interosseous (UI) and radial interosseous (RI) averaged 0.5107 ranged from 0.2765 (UI for rotate right) to 0.6099 (LU for rotate right). Intrinsic muscle activity was 27.48% (0.2748) bigger than extrinsic muscle activity. Moreover, coupled activities between the intrinsic muscles and the extrinsic tendons were repeatedly observed among all simulations.

Joint torque was not proportional to range of joint angles.

Joint torque was not proportional to range of joint angles. Range of joint angles for PIP joint was bigger than range of joint angle for other joints, but joint torque for MCP joint was bigger than joint torques for other joints. Peak range of joint angles was 69.9, 88.5 and 19.8° for MCP, PIP and DIP joints respectively (Figure 5, 6). Peak joint torque was 0.0220, 0.0138 and 0.0027 N-m for MCP, PIP and DIP joints (Table 2; Figure 7, 8).

Joint torques for rotate left and right bigger than those for zoom in and out. Max. joint torque was 0.0904 N-m for rotate left at MCP add joint (Table 2).

FDP muscle operated with greatest active force for two finger gestures.

FDP forces were greater than other tendons' forces for all simulations (Figure 9, 10). Muscle tensions averaged 1.0404 N of range of motion (RoM), ranged from 0.6047 N for EDC (rotate left) to 1.5160 N for FDP (zoom in). Across all tasks, FDP tensions were higher than FDS tensions.

PIP joint had max. flexion angle, while DIP joint had min. flexion angle during gestures.

Proximal interphalangeal (PIP) joints were highly flexed. Among all gestural tasks, peak flexion angles were 69, 8.8, 88 and 20° for metacarpophalangeal (MCP), MCP add, PIP and DIP joints. Distal interphalangeal (DIP) joint range of joint angle for zoom out was lower its for zoom in (Figure 5, 6). Maximum (max.) joint angles of DIP joint flexed 19.8 and 2.3° for zoom in and zoom out interactions.

DISCUSSION

An increasing number of devices: smart phones, tablets, laptops or desktop computers features functions triggered by multi-touch gestures (LogiGEAR MAGAZINE, 2014). During multi-touch gestures, forces that hand muscles produce act directly on the bone segments. These forces influence movement, as ground reactions cause the effects of muscle force to be transmitted to segments remotely from the muscular contraction (Blazkewicz, 2013). However, this complex mechanism interacting with multi-touch technology remains unclear.

The main goal of this study was to quantify the difference in the joint torque, muscle force and muscle activity patterns during two finger gestures: zoom in & out, and rotate left & right on the tablet computer using an OpenSim upper limb model. Our results showed that high extrinsic muscle activations were associated with zooming motions, whereas high intrinsic muscle activations were associated with rotating motions. We also found that max. joint torque occurred at the metacarpophalangeal (MCP) joint, Flexor digitorum profundus (FDP) muscle operated with greatest active force, and range of joint angle for the proximal interphalangeal (PIP) joint was higher than that for the MCP joint. While this study did not compare through the EMG activities, these findings give us fascinating insights, i.e., neuromuscular activation patterns have been predicted in order to better understand underlying motor control during multi-touch gestures.

Limitations

Drawing a conclusion from these results is limited by several factors. First, our model parameters were taken from the literature, and not matched to our subjects. Compiling data

from diverse sources into a common model could introduce measure errors. Moreover, hand kinematics used for experimental measurements are variable in size, and none precisely match the hypothetical 50th percentile male on which the OpenSim model is based. We accounted for these potential sources of error by the Scaling function that is performed based on a combination of measured distances between x-y-z marker locations and manually-specified scale factors. The dimensions of each segment in the model are scaled so that the distances between the virtual markers match the distances between the experimental markers. Second, we did not compare simulation results with experimental data such as electromyography (EMG). To our knowledge, evaluating and recording the muscle activity are not available during hand gestures on the tablet computer because it is not feasible to measure fingertip force and intrinsic muscle activity on the tablet. Consequently, predicted peak values, i.e., joint torque, muscle force and activity may be greater or smaller than what directly measures. However, these predicted value patterns may be retained between computational simulations and direct measurements. Drawing a conclusion from these results is limited by several factors. First, our model parameters were taken from the literature, and not matched to our subjects. Compiling data from diverse sources into a common model could introduce measure errors. Moreover, hand kinematics used for experimental measurements are variable in size, and none precisely match the hypothetical 50th percentile male on which the OpenSim model is based. We accounted for these potential sources of error by the Scaling function that is performed based on a combination of measured distances between x-y-z marker locations and manually-specified scale factors. The dimensions of each segment in the model are scaled so that the distances between the virtual markers match the distances between the experimental markers.

Second, we did not compare simulation results with experimental data such as electromyography (EMG). To our knowledge, evaluating and recording the muscle activity are not available during hand gestures on the tablet computer because it is not feasible to measure fingertip force and intrinsic muscle activity on the tablet. Consequently, predicted peak values, i.e., joint torque, muscle force and activity may be greater or smaller than what directly measures. However, these predicted value patterns may be retained between computational simulations and direct measurements due to a residual elimination algorithm (REA) in OpenSim package (Thelen et al., 2006).

Third, thumb model does not include intrinsic muscles. Intrinsic muscles are normally independent (Hager-Ross et al., 2000; Tubiana, 1981). The thumb moves differently from the other fingers due to its unique bone structure and dedicated set of muscles (Shultz, 2014). These muscles enable to use out thumb independently and make it able to oppose the position of the fingers (Shultz, 2014). This exercises minor influence on the muscle activation patterns that we predicted for the index finger.

Finally, the finger extensor mechanism in the OpenSim model has not modelled yet. Passive tissues, e.g., the extensor hood, affect the translation of muscle forces to the finger (Lee et al., 2008). Lee et al. (2008) demonstrated two different types of tendon force transmission: the tendon force distribution into two tendon slips with in the extensor apparatus, and the dissipation of tendon force into surrounding structure through the connective tissues. The force distribution ratio between two tendon slips was found to remain relatively constant across different postures within each specimen (Lee et al., 2008). Wu et al. (2010) found that simplified modeling of the extensor mechanism in an index finger had difference in muscle forces and tendon excursions within 10~20% range. Moreover, the effects of the extensor

mechanism on the flexors are relatively small when the location of force application is distal to the PIP joint (Li et al., 2001). Although the detailed assessments with extensor mechanism leave for the next step, the neuromuscular activation patterns maintain consistency with force distribution ratio between two tendon slips in the extensor apparatus.

Zooming movements led to high extrinsic muscle activities, while rotating ones led to high intrinsic muscle activities

Extrinsic muscle activations for zoom in & out were higher than those of rotate left & right. This is because each extrinsic muscle crossing over the wrist produces movement in the sagittal plane, i.e., extrinsic muscle flexes the fingers at each joint. Higher flexion (range of joint angle at all joints) for zoom in & out compared with rotate left & right observed in subjects performing tasks. Previous works also have shown that EMG increased as joint angle increased in the shoulder (Sigholm et al., 1984; Valero-Cuevas et al., 1998; Mathiassen and Winkel, 1990; Jarvholm et al., 1991).

Intrinsic muscle activations were higher than extrinsic ones for rotate left & right. Extrinsic muscles flex the fingers at each joint, while intrinsic muscles adduct the fingers at the MCP joint. So, intrinsic muscles were involved in rotate left & right gestures. Lower range of ab/adduction (0° ~ 8.8°) than range of flex/extension (-4.8° ~ 69.9°) at the MCP joints was observed in subjects during rotate left & right tasks. Although MCP ab/adduction had short range of joint angle, the high intrinsic muscle activation in rotate left & right tasks was observed due to intrinsic muscles linking the extensors and flexors. Intrinsic muscles: radial interosseous (RI) and ulnar interosseous (UI) predominantly adduct/abduct the MCP joint and also extend the distal interphalangeal (DIP) joint when the interphalangeal (IP) joints are extended (Kamper

et al., 2006). These findings support our hypothesis that zooming motion cause extrinsic muscles greater activations, whereas rotating motion cause intrinsic muscles greater activations.

Max. joint torque occurred at the MCP joint

Although peak flexion angle observed at the PIP joint, joint torques at the MCP joint was greater than that at the PIP joint. During both zooming and rotating motions, PIP range of joint angle is higher than MCP flex/extension and ab/adduction range of joint angle. However, for zooming MCP flex/extension joint torque was greater than PIP flex/extension joint torque, and for rotating MCP ab/adduction joint torque was also greater than PIP one. Joint torque was proportional to more moment arm than range of joint angle. When the point of force application was on the distal phalanx, the moment arm of the load increased from the DIP joint to the PIP joint, and to the MCP joint (Li et al., 2000). Multi-touch gestures on the tablet seem to be free movements without consideration for resistance or reaction force with the touch screen surface. However, our result was consistent with other studies, i.e., tapping on the physical keyboard. Joint torque exerted an more influence on DIP, MCP add, PIP and MCP for zooming motion, and DIP, PIP, MCP and MCP add for rotating motion in consecutive order.

In conclusion, index finger interactions on the tablet was characterized in terms of joint torque, muscle force and muscle activation. Our results demonstrate the influence of external factors such as finger posture, finger loading and dynamic exertion on hand muscle activity. This study provides insight into the relationship between internal (i.e., muscle activity) and external (i.e., finger posture, fingertip force or joint torque) loadings of the finger joint on the multi-touch technology, and into information concerning muscle activity patterns in the index finger muscles, which are used by subjects to perform a number of daily multi-touch activities.

REFERENCES

Armstrong, T.J., Foulke, J.A., Martin, B.J., 1994. Investigation of applied forces in alphanumeric keyboard work. American Industrial Hygiene Association Journal 55(1) 30-35.

Asatryan, D.G., Feldman, A.G., 1965. Functional tuning of the nervous system with control of movement or maintenance of a steady posture. I. Mechanographic analysis of the work the joint or execurtion of a postural task. Biofizika 10, 925-935.

Balakrishnan, A.D., Jindrich, D.L., Dennerlein, J.T., 2006. Keyswitch orientation can reduce finger joint torques during tapping on a computer keyswitch. Human Factors, 48, 121-129

Bergqvist, U., Wolgast, E., Nilsson, B., Voss, M., 1995. Musculoskeletal disorders among visual display terminal workers: individual, ergonomic, and work organizational factors. Ergonomics, 38, 763-776.

Bizzi, E., Hogan, N., Mussa-Ivaldi, F.A., Giszter, S., 1992. Does the nervous system use equilibrium-point control to guide single and multiple joint movements?. Behavioral and Brain Science 15, 603-613.

Blazkiewicz, M., 2013. Muscle force distribution during forward and backward locomotion. Acta of Bioengineering and Biomechancis, 15(3), 3-9.

Brand, P.W., Hollister, A.M., 1999. Clinical Mechanics of the Hand, third ed. Mosby, Inc., St. Louis, Blatimore, Boston.

Bundhoo, V., Park, E.J., 2005. Design of an artificial muscles actuated finger towards biomimetic prosthetic hands. 12th International Conference on Advanced Robotics, ICAR'05.

Chao, E.Y., Opagrande, J.D., Axmear, F.E., 1976. Three dimensional force analysis of finger joints in selected isometric hand function. Journal of Biomechanics 19(6), 387-396.

Cohe, A., Hachet, M., 2012. Beyond the mouse: Understanding user gestures for manipulating 3D objects from touchscreen inputs. Computers & Graphics-UK, 36(8) 1119-1131.

Clavero, J.A., Golano, P., Farinas, O., Alomar, X., Monill, J.M., Esplugas, M., 2003. Extensor mechanism of the fingers: MR imaging-anatomic correlation. Radiographics, 23(3) 593-611.

Darling, W.G., Cole, K.J., Miller, G.F., 1994. Coordination of index finger movements. Journal of Biomechanics 27(4), 479-491.

Dennerlein, J.T., Diao, E., Mote Jr., C.D., Rempel, D.M., 1998. Tensions of the flexor digitorum superficialis are higher than a current model predicts. Journal of Biomechanics 31(4), 295-301.

Dennerlein, J.T., Diao, E., Mote Jr., C.D., Rempel, D.M., 1999. In vivo finger flexor tendon force while tapping on a keyswitch. Journal of Orthopaedic Research 17(2), 178-184.

Develop center – Windows, 2014. Touch interactions for Windows, <msdn.microsoft.com/en-us/library/windows/apps>

Garner, B.A., Pandy, M.G., 2003. Estimation of musculotendon properties in the human upper limb. Annals of Biomedical Engineering 31 207-220.

Gerard, M.J., Armstrong, T.J., Foulke, J.A., 1996. Effects of key stiffness on force and the development of fatique while typing. American Industrial Hygiene Association Journal, 57(9) 849-854.

Gerard, M.J., Armstrong, T.J., Franzblau, A., 1999. The effects of keyswitch stiffness on typing force, finger electromyography, and subjective discomfort. American Industrial Hygiene Association Journal, 60(6) 762-769.

Gerr, F., Marcus, M., Ensor, C., 2002. A prospective study of computer users: I. Study design and incidence of musculoskeletal symptoms and disorders. American Journal of Industrial Medicine (4) 221-235.

Hager-Ross, C., Schieber, M.H., 2000. Quantifying the independence of human finger movement: Comparisons of digits, hands, and movement frequencies. Journal of Neuroscience, 20(22) 8542-8550.

Hamner, S.R., Seth, A., Delp, S.L., 2010. Muscle contributions to propulsion and support during running. Journal of Biomechanics (43) 2709-2716.

Hatze, H., 1976. A method for describing the motion of biological system. Journal of Biomechanics 9(2), 101-104.

Holzbaur, K.R.S., Murray, W.M., Delp, S.L., 2005. A model of the upper extremity for simulating musculoskeletal surgery and analyzing neuromuscular control. Annals of Biomedical Engineering 33(6). 829-840.

Harding, D.C., Brandt, K.D., Hilberry, B.M., 1993. Finger joint force minimization in pianists using optimization techniques. Journal of Biomechanics, 26, 1403-1412.

Jacobson, M.D., Raab, R., Fazeli, B.M., Abrams, R.A., Botte, M.J., Lieber, R.L., 1992. Architectural design of the human intrinsic hand muscles. Journal of Hand Surgery 17(5), 804-809.

Jarvholm, U. Palmerud, G., Karlsson, D., Herberts, P., Kadfors, R., 1991. Intramuscular pressure and electromyography in four shoulder muscles. Journal of Orthopedic Research (9), 609-619.

Kumar, S., 2011. Theories of musculoskeletal injury causation. Ergonomics, 44, 17-47.

Kuo P.L., Lee, D.L., Jindrich, D.L., Dennerlein, J.T., 2006. Finger joint coordination during tapping. Journal of Biomechanics 39, 2934-2942.

Kursa, K., Diao, E., Lattanza, L., Rempel, D., 2005. In vivo forces generated by finger flexor muscles do not depend on the rate of fingertip loading during an isometric task. Journal of Biomechancis 38(11), 2288-2293.

Lai, C.C, Wu, C.F., 2012. Size effects on the touchpad, touchscreen, and keyboard tasks of netbooks. Percept Motor Skills Journal 115(2) 481-501.

Lee, J.H., Asakawa, D.S., Dennerlein, J.T., Jindrich, D.J., 2014. Extrinsic and intrinsic index finger muscle attachments in an OpenSim upper-extremity model. Annals of Biomedical Engineering in Progress.

Lee, S.J., Yoon, H.M., 2014. OpenSim Project Website. Simple dynamic arm model with muscles.

Lee, S.W., Chen, H., Towles, J.D., Kamper, D.G., 2008. Effect of finger posture on the tendon force distribution within the finger extensor mechanism. Journal of Biomechanical Engineering 130(5).

Leijnse, J.N.A.L., 1995. A two-dimensional kinematic model of the lumbrical in the human finger. Journal of Biomechanics, 28, 237-249.

Leva, P.D., 1996. Adjustments to zatsiorsky-seluyanov's segment inertia parameters. Journal of Biomechanics (29) 1223-1230.

Lieber, R.L., Fazeli, B.M., Botte, M.J., 1990. Architecture of selected wrist flexor and extensor muscles. Journal of Hand Surgery, 15(2) 244-250.

Lieber, R.L., Jacobson, M.D., Fazeli, B.M., Abrams, R.A., Botte, M.J., 1992. Architecture of selected muscles of the arm and forearm: anatomy and implications for tendon transfer. Journal of Hand Surgery, 17(5) 787-798.

LogiGEAR MAGAZINE, 2014. Test tools and automation: Mobile testing, <www.logigear.com/magazine/issue/glossary-mobile-testing>.

Long, C., Conrad, P.W., Hall, E.A., Furler, S.L., 1970. Intrinsic-extrinsic muscle control of the hand in power grip and precision handing. Journal of Bone and Joint Surgery 52-A (5), 853-867.

Lozano, C., Jindrich, D., Kahol, K., 2011. The impact on musculoskeletal system during multitouch tablet interactions. Proceedings of the SIGCHI Conference on Human Factors in Computing Systems, 825-828.

Malchaire, J.B., Cock, N.A., Robert, A.R., 1996. Prevalence of musculoskeletal disorders at the wrist as a function of angles, force, repetitiveness and movement velocities. Scandinavian Journal of Work, Environment & Health, 22, 176-181.

Marcus, M., Gerr, F., Monteilh, C., 2002. A prospective study of computer users: II. Postural risk factors for musculoskeletal symptoms and disorders. American Journal of Industrial Medicine, 41(4) 236-249.

Mathiassen, S.E., Winkel, J., 1990. Electromyographic activity in the shoulder-neck region according to arm position and glenohumeral torque. European Journal of Applied Physiology and Occupational Physiology 61, 370-379.

McIntyre, J., Mussa-Ivaldi, F.A., Bizzi, E., 1996. The control of stable postures in the multijoint arm. Experimental Brain Research 110: 248-264.

McMahon, T.A., 1984. Muscles, reflexes, and locomotion. Princeton University Press, Princeton, NJ.

Monsabert, B.G.D., Rossi, J., Berton, E., Vigouroux, L., 2012. Quantification of hand and forearm muscle forces during a maximal power grip task. Medicine & Science in Sports & Exercise, 44(10), 1906-1916.

Mussa-Ivaldi, F.A., Hogan, N., Bizzi, E., 1985. Neural mechanical and geometric factors subserving arm posture in humans. Journal of Neuroscience 5, 2732-2743.

Norman, R., Wells, R., Neumann, P., Frank, J., and Kerr, M., 1998. A comparison of peak vs. cumulative physical work exposure risk factors for the reporting of low back pain in the automotive industry. Clinical Biomechanics 13, 561-573.

OSK Windows, 2014. Use the on-screen keyboard to type, <windows.microsoft.com/en-us/windows-8/type-with-the-on-screen-keyboard>.

Radwin, R.G., Jeng, O.J., 1997. Activation force and travel effects on overexertion in repetitive key tapping. Human Factors 39(1), 130-140.

Radwin, R.G., Ruffalo, B.A., 1999. Computer key switch force-displacement characteristics and short-term effects on localized fatique. Ergonomics 42(1), 160-170.

Rempel, D., Serina, E., Klinenberg, E., 1997. The effect of keyboard keyswitch make force on applied force and finger flexor muscle activity. Ergonomics 40(8) 800-808.

Saul, K.R., Hu, X., Goehler, C.M., Vidt, M.E., Daly, M., Velisar, A., Murray, W.M., 2014. Benchmarking of dynamic simulation predictions in two software platforms using an

upper limb musculoskeletal model. Computer Methods in Biomechancis and Biomedical Engineering 1-14.

Sauter, S.L., Schleifer, L.M., Knutson, S.J., 1991. Work posture, workstation design, and musculoskeletal discomfort in a VDT data entry task. Human Factors 33, 151-167.

Schuind, F., Garcia-Elias, M., Cooney III, W.P., An, K.N., 1992. Flexor tendon forces: in vivo measurements. Journal of Hand Surgery 17(2), 291-298.

Sigholm, G., Herberts, P., Almstrom, C., Kadefors, R., 1984. Electromyograhic analysis of shoulder muscle load. Journal of Orthopedic Research 1, 379-386.

Thelen, D.G., Anderson, F.C., 2006. Using computed muscle control to generate forward dynamics simulations of human walking from experimental data. Journal of Biomechanics 39(6):1107-1115.

Trudeau, M., Catalano, P.J., Jindrich, D.L., Dennerlein, J.T., 2013. Tablet keyboard configuration affects performance, discomfort and task difficulty for thumb typing in a two-handed grip. PLoS ONE 8(6).

Tubian, R., 1981. The hand. Interdependent and independent action of the fingers. W B Saunders.

Valero-Cuevas, F.J., Zajac, F.E., Burgar, C.G., 1998. Large index-fingertip forces are produced by subject-independent patterns of muscle excitation. Journal of Biomechanics 31, 696-703.

Valero-Cuevas, F.J., 2000. Predictive modulation of muscle coordination pattern magnitude scales fingertip force magnitude over the voluntary range. Journal of Neurophysiology 83(3) 1469-1479.

Valero-Cuevas, F.J., 2005. An integrative approach to the biomechanical function and neuromuscular control of the fingers. Journal of Biomechanics 38: 673-684.

Valero-Cuevas, F.J., 2009. A mathematical approach to the mechanical capabilities of limbs and fingers. Advances in Experimental Medicine and Biology (629) 619-633.

Vigouroux, L., Rossi, J., Foissac, M., Grelot, L., Berton, E., 2011. Finger force sharing during an adapted power grip task. Neuroscience Letters 504(3), 290-294.

Wagner, J., Huot, S., Mackay, W.E., 2012. BiTouch and biPad: Designing bimanual interaction for hand-held tablets. CHI 12-30th International Conference on Human Factors in Computing Systems.

Wang, K., McGlinn, E.P., Chung, K.C., 2014. A biomechanical and evolutionary perspective on the function of the lumbrical muscle. American Society for Surgery of the Hand, 39(1) 149-155.

Wang, Y., Williamson, K.E., Kelley, P.J., James, J.A., Hamilton, P.W., 2012. SurfaceSlide: a multitouch digital pathology platform. PLoS one 7(1):e30783.

Winter, J.M., 1990. Hill-based muscle models: a systems engineering perspective In: Winters, J.M., Woo, S.L. (Eds), Multiple Muscle Systems: Biomechanics and Movement Organization. Springer, New York, 69-93.

Wood, M., Babski-Reeves, K., 2005. Effects of negatively sloped keyboard wedges on risk factors for upper extremity work-related musculoskeletal disorders and user performance. Ergonomics 48(15), 1793-1808.

Wu, J.Z., An, K.N., Cutlip, R.G., Krajnak, K., Welcome, D., Dong, R.G., 2008. Analysis of musculoskeletal loading in an index finger during tapping. Journal of Biomechanics 41, 668-676.

Wu, J.Z., An, K.N., Cutlip, R.G., Andrew, M.E., Dong, R.G., 2009. Modeling of the muscle/tendon excursions and moment arms in the thumbs using the commercial software anybody. Journal of Biomechanics 42, 383-388.

Wu, J.Z., An, K.N., Cutlip, R.G., Dong, R.G., 2010. A practical biomechanical model of the index finger simulating the kinematics of the muscle/tendon excursions. Biomedical Materials and Engineering 20(20), 89-97.

Young, J.G, Trudeau, M.B., Odell, D. Marinelli, K., Dennerlein, J.T., 2013. Wrist and shoulder posture and muscle activity during touch-screen tablet use: Effects of usage configuration, tablet type, and interacting hand. Work-A Journal of Prevention Assessment & Rehabilitation, 45(1), 59-71.

Zajac, F.E., 1989. Muscle and tendon-properties, models, scaling, and application to biomechanics and motor control. Critical Reviews™ in Biomedical Engineering 17, 359-411.

Zajac, F.E., Gordon, M.E., 1989. Determining muscle's force and action in multi-articular movement. Exercise and Sport Science Reviews 17, 187-230.

Table 1. Muscle modeling parameters

Muscle	PCSA (cm^2)	Max. isometric Force (N)	Optimal fiber length (cm)	Tendon slack length (cm)	Pennation (degree)
FDP	1.5	68.3	7.5	29.4	7
FDS	1.4	61.2	8.4	27.5	6
RI	1.5	68.6	3.2	29.6	9.2
UI	0.8	36.6	2.5	24.9	6.3
LU	0.1	4.6	5.5	22.8	1.2
EDC	0.4	18.3	7.0	32.2	3

Table 2. Joint Torque at all joint (N-m)

	MCP	**MCP add**	**PIP**	**DIP**
Zoom In	0.0220	0.0056	0.0138	0.0027
Zoom Out	0.0221	0.0050	0.0139	0.0018
Rotate Left	0.0608	0.0904	0.0099	0.0031
Rotate Right	0.0771	0.0814	0.0105	0.0018

Figure 1. Extrinsic muscle activation. X components represent extrinsic muscles, and y components represent activation level.

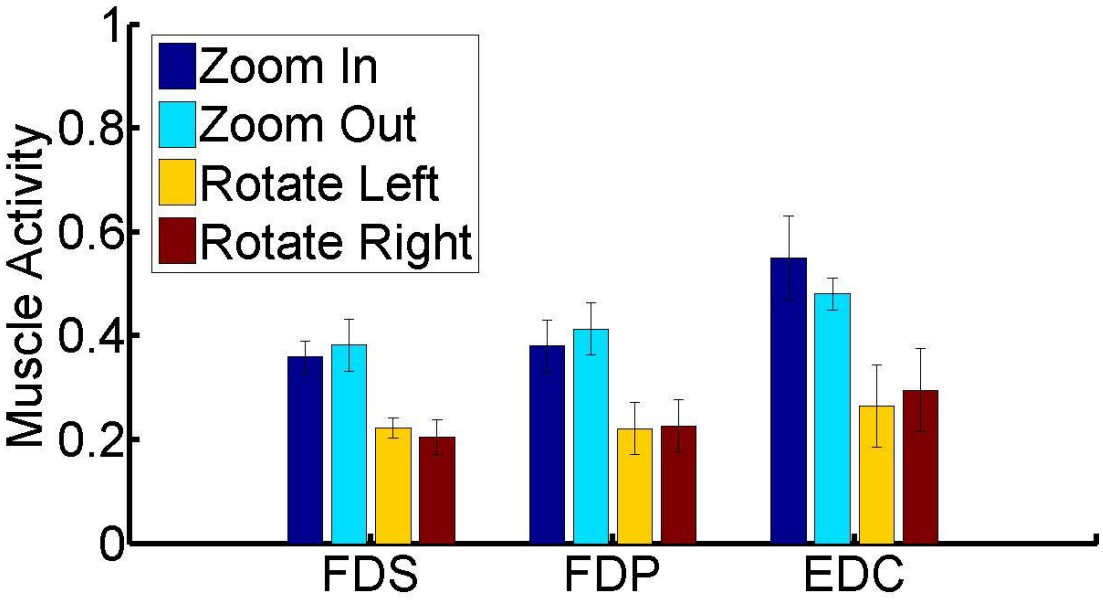

Figure 2. Muscle activity of rotate left and right. X components represent extrinsic & intrinsic muscles, and y components represent activation level.

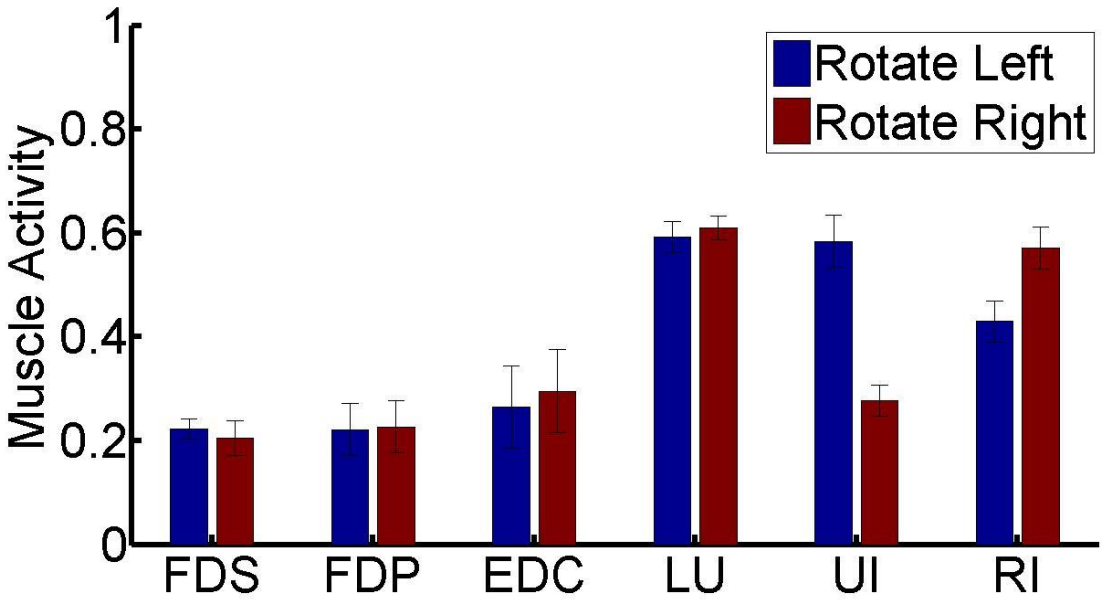

Figure 3. Muscle activation of an index finger during zoom in (top) and zoom out (bottom). x component indicates scaled time histories (not real time), and y component indicates muscle activation.

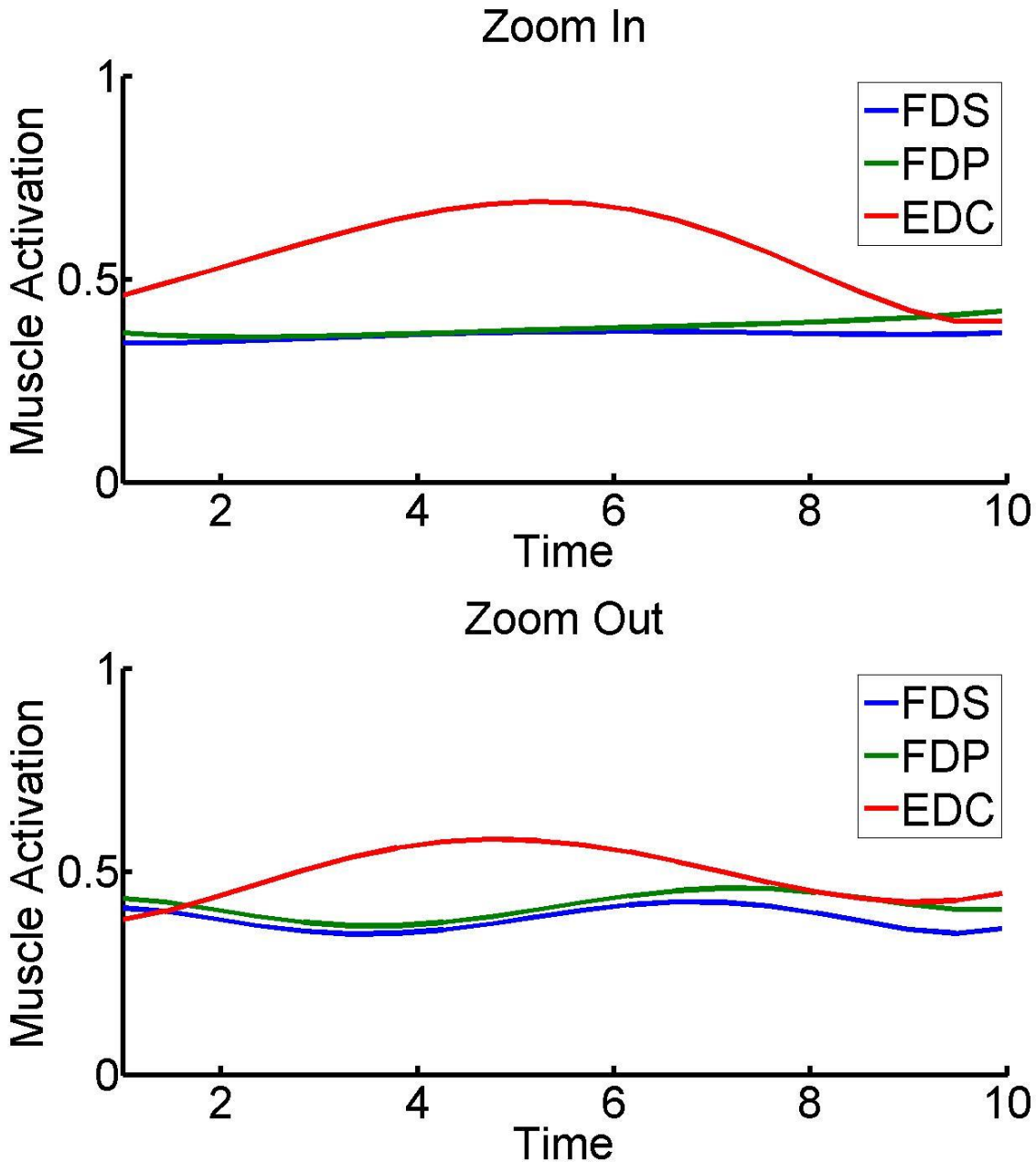

Figure 4. Muscle activation of an index finger during rotate left (top) and rotate right (bottom). x component indicates scaled time histories (not real time), and y component indicates muscle activation.

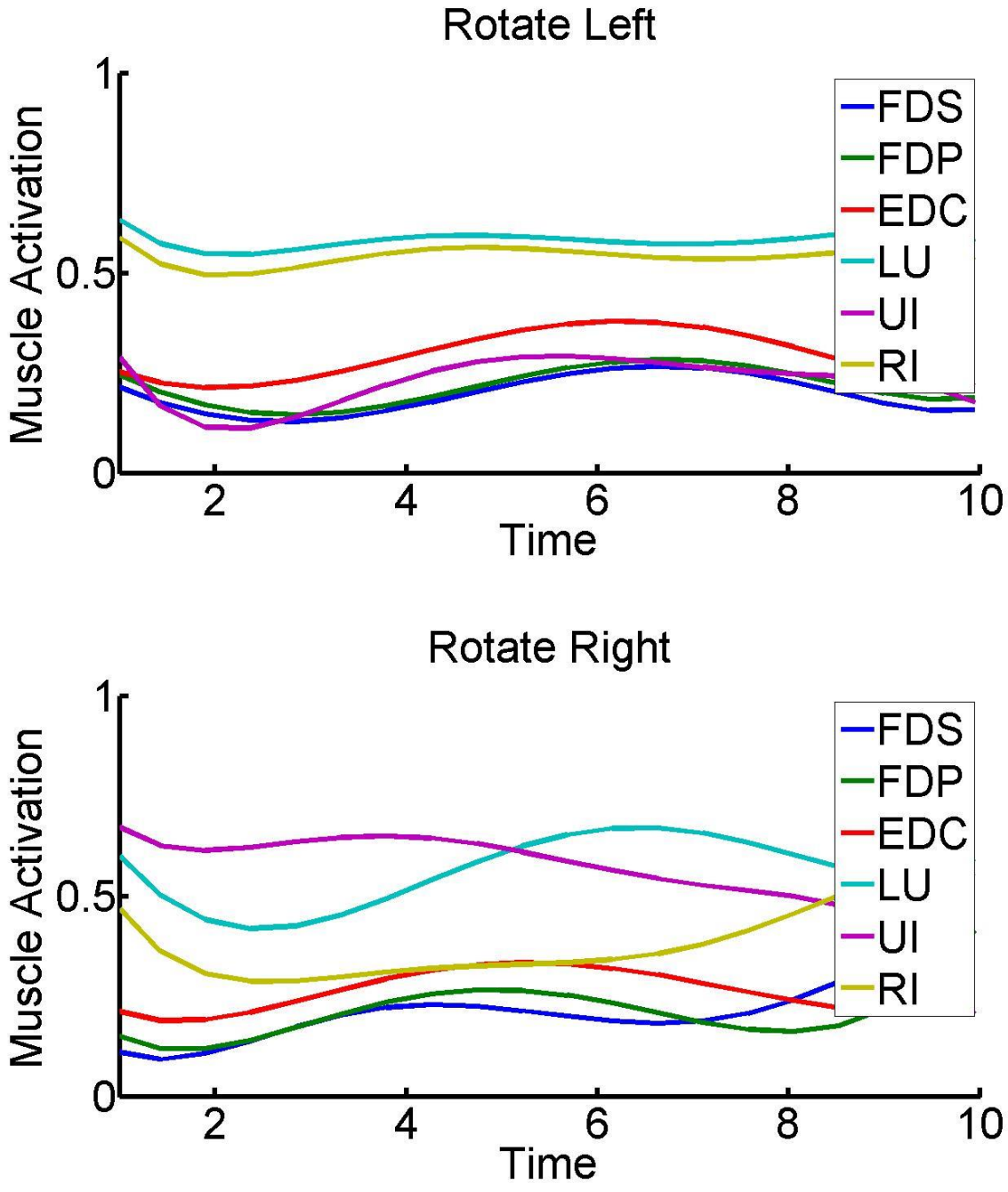

Figure 5. Joint angle of an index finger during zoom in (top) and zoom out (bottom). x component indicates scaled time histories (not real time), and y component indicates joint angle (degree).

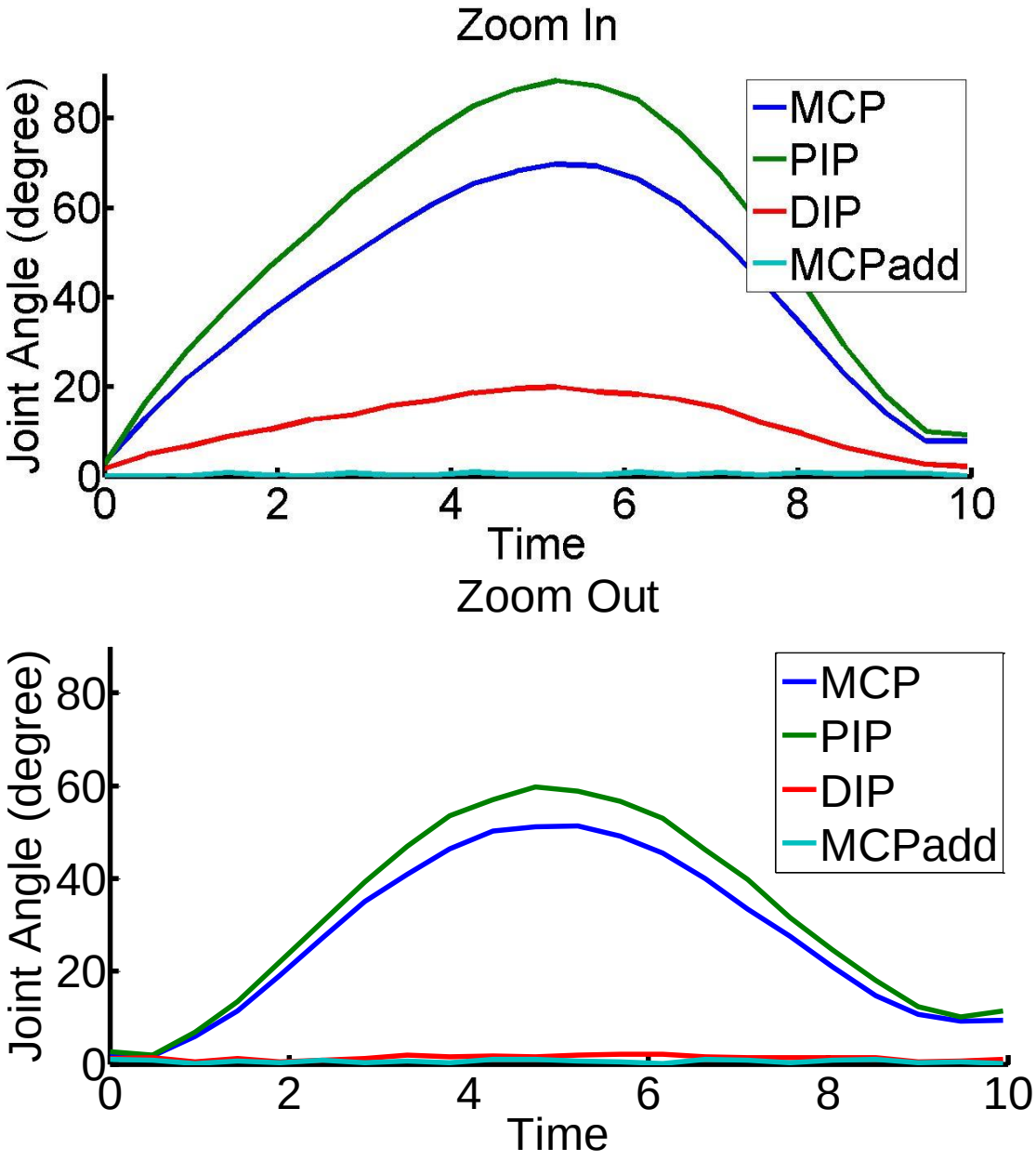

Figure 6. Joint angle of an index finger during rotate left (top) and rotate right (bottom). x component indicates scaled time histories (not real time), and y component indicates joint angle (degree).

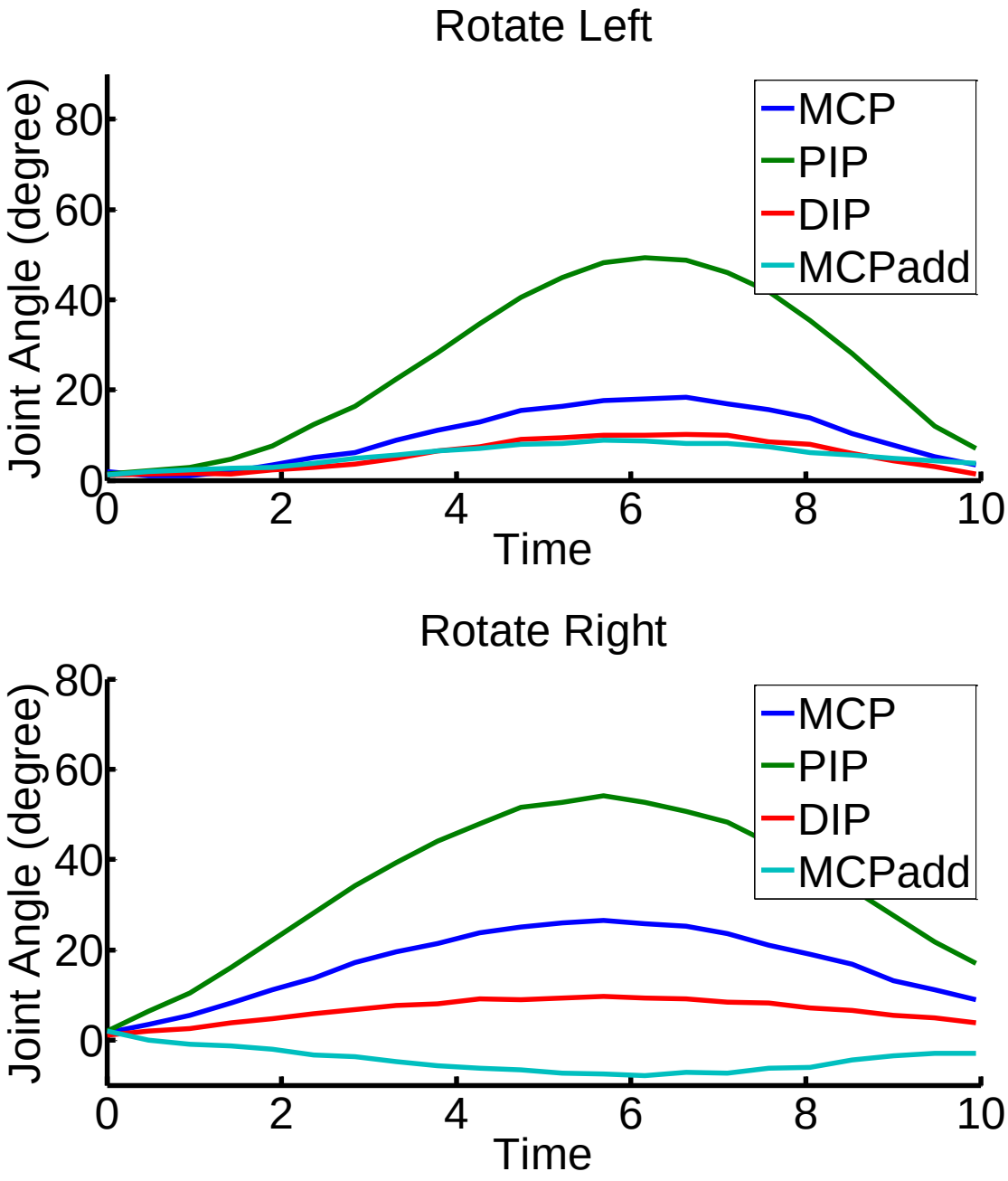

Figure 7. Joint Torque of an index finger during zoom in (top) and zoom out (bottom). x component indicates scaled time histories (not real time), and y component indicates joint torque (N-m).

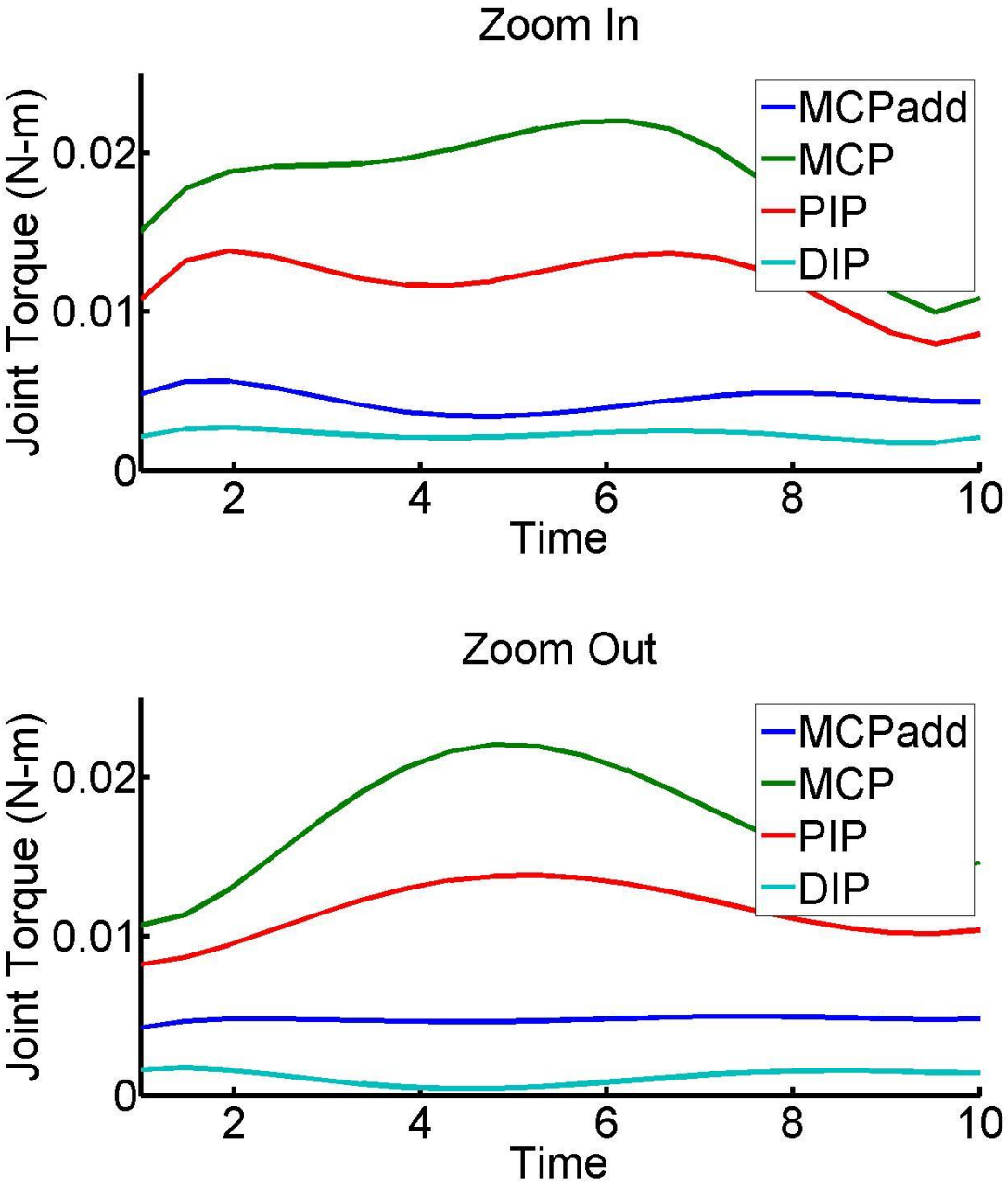

Figure 8. Joint Torque of an index finger during rotate left (top) and rotate right (bottom). x component indicates scaled time histories (not real time), and y component indicates joint torque (N-m).

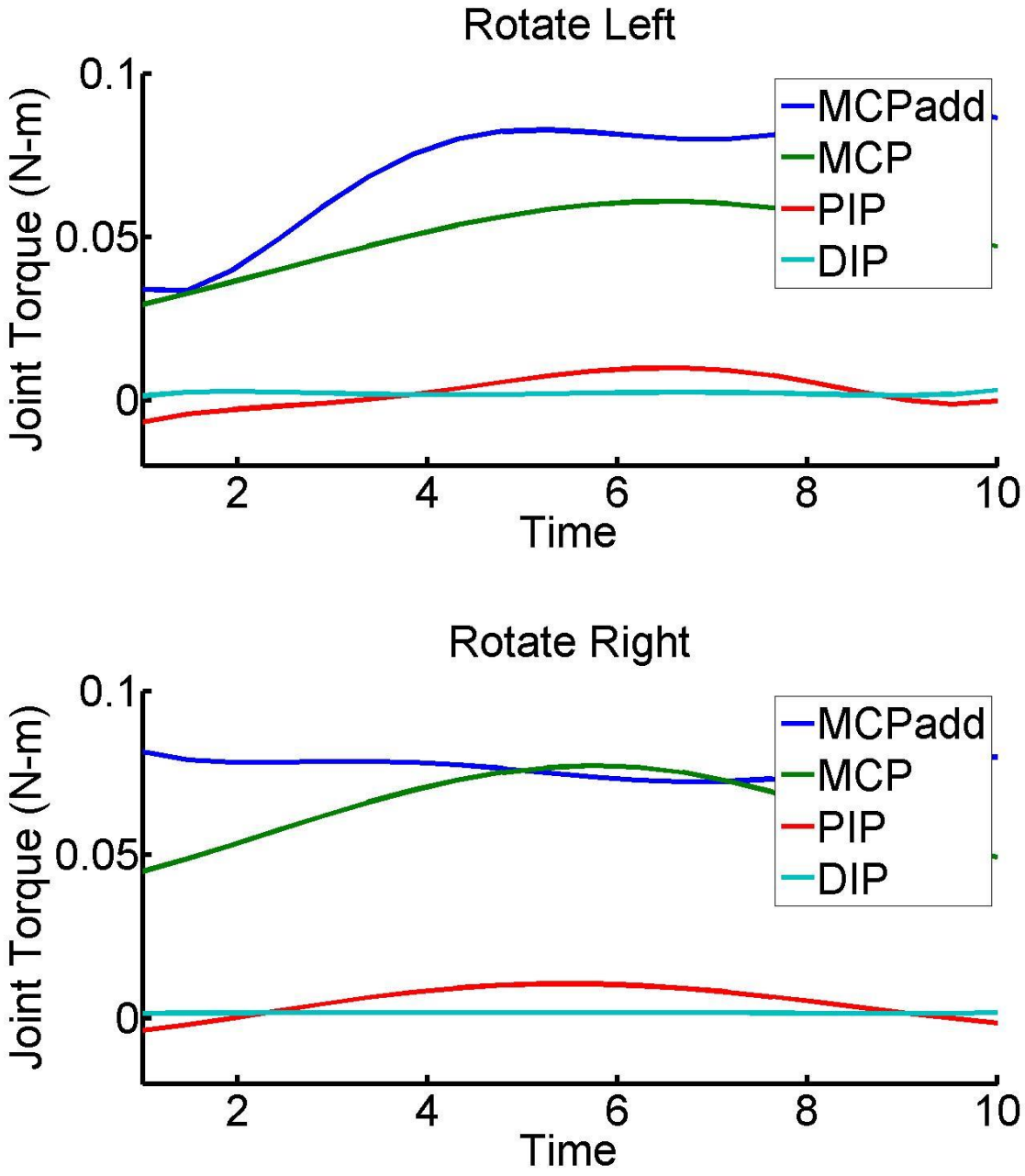

Figure 9. Extrinsic muscle force of an index finger during zoom in (top) and zoom out (bottom). x component indicates scaled time histories (not real time), and y component indicates joint torque (N).

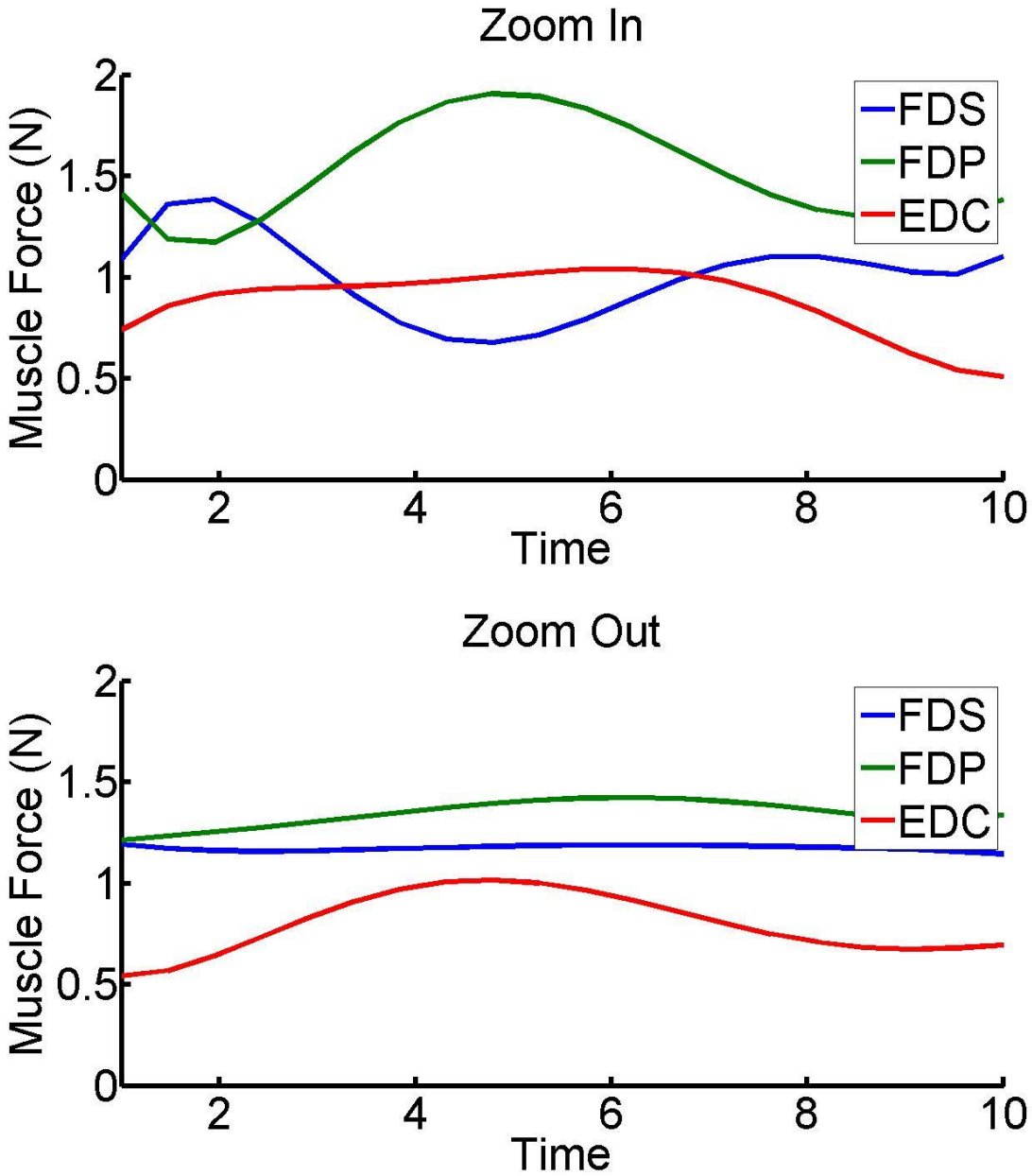

Figure 10. Extrinsic muscle force of an index finger during rotate left (top) and rotate right (bottom). x component indicates scaled time histories (not real time), and y component indicates joint torque (N).